STATIONARY AND NON–STATIONARY STOCHASTIC ANALYSIS OF GROUND WATER FLOW THROUGH HETEROGENEOUS POROUS MEDIA

by

TONGYING SHUN

Submitted in Partial Fulfillment

of the Requirements for the Degree of

MASTER OF SCIENCE IN GEOSCIENCES

Department of Geosciences

New Mexico Institute of Mining and Technology

Socorro, New Mexico

May, 1995

ABSTRACT

Recently, the use of conditional simulation has been developed for the prediction of transport, groundwater flow path and groundwater travel time. Since the auto–covariances and cross–covariances of the random processes take on very important roles in conditional simulation for groundwater flow and transport, it's important to derive the stochastic structure of spatial variables in groundwater flow.

For stationary log hydraulic conductivity, the auto–covariance and cross–covariance of the random fields in groundwater flow were derived by the numerical spectral method and compared with the solutions of theoretical analysis and Monte Carlo simulation. We present the characteristics of the auto–covariance and cross–covariance functions for the log conductivity, head and velocity fields. All these functions were given in terms of the parameters which characterize the input log conductivity field and the average head gradient.

Most stochastic analyses of groundwater flow and transport in heterogeneous porous formations assume weak stationary (second–order stationary) of the conductivity or its log transform. When a deterministic trend for conductivity exists, the traditional spectral analysis will not work for deriving the covariances. For a non–stationary conductivity field, where the log conductivity is the superposition of a linear trend and a stationary fluctuation, Li and Mclaughlin derived the analytical covariance solutions. However, they limited their studies to the case where the trend is aligned to the mean head gradient. In the paper, we derive the analytical covariance results and do not limit the trend direction of conductivity. The Greens functions and Monte Carlo simulation were used to solve the perturbation equation. The solutions were extended to a special case and compared with the previous results.

ACKNOWLEDGEMENTS

I would like to express my deepest appreciation to my adviser, Dr. Allan Gutjahr, for his invaluable suggestions, guidance, and fruitful discussion throughout this study. I would especially like to thank Dr. John Wilson for his academic guidance and personal assistance so that I have very good time during my studying in this school. I also thank Dr. Robert Bowman for his willingness and dedication to stand as my committee member.

My thanks are extended to all of my professors at New Mexico Tech for their role in my education.

A special thanks to my friends and colleagues Jinzhong Liu, Xiaohong Du, Jun Lin, Anil Mishra, Bryan Bullard, Sean Hatch, Lance Hughson, John Sigda who helped me at all times.

TONGYING SHUN

Department of Geosciences

New Mexico Institute of Mining and Technology

May, 1995

TABLE OF CONTENTS

ACKNOWLEDGEMENTS i

ABSTRACT ii

TABLE OF CONTENTS iii

LIST OF TABLES v

LIST OF FIGURES vi

CHAPTER I: Stationary Stochastic Analysis for Groundwater Flow through Heterogeneous Porous Media 1

1.1 Introduction 1

1.2 Numerical Spectral Analyses of the Auto–Covariances and Cross–covariances for Groundwater Flow in Heterogeneous Media 6

1.2.1 Relationship between Covariance and Spectral Density Function 6

1.2.2 Spectral Representation Theorem 9

1.2.3 Theory of Numerical Spectral Analysis 12

1.2.4 Numerical Spectral Method to Analyze Statistical Structure of Groundwater Flow through Heterogeneous Media 14

1.3 Application of Monte Carlo Simulation in Analyzing Statistical Structure of Groundwater Flow through Heterogeneous Media 21

1.4 Summary 24

CHAPTER II: Non–stationary Stochastic Analysis for Groundwater Flow through Heterogeneous Trending Porous Media 41

2.1 Introduction 41

2.2 Mathematical Formulation 45

2.3 Mean Head Distribution for Groundwater Flow Through Trending Media.... 48

2.4 Non–stationary Correlation Analysis for Log Hydraulic Conductivity and Hydraulic Head 52

2.4.1 The case where the trend is aligned to the mean gradient 52

2.4.2 The case where the trend is perpendicular to the mean gradient 55

2.4.3 The general case where the angle between the trend B and the mean gradient is arbitrary 56

2.5 Summary 62

REFERENCE 73

LIST OF TABLES

Table 1–1 : List of the properties for autocovariance and spectral density 8

Table 1–2: List of the properties for cross–covariance and cross–spectrum 9

Table 1–3: Inputs for the illustration to solve the auto–solve covariances and cross–covariances of log conductivity, head and velocity by the numerical spectral simulation 18

LIST OF FIGURES

Figure 1–1: Auto–covariance of hydraulic head: a) the contour of the head auto– covariance by the numerical spectral method; b) the contour of the theoretical head auto–covariance; c) the character of the head auto–covariance along different directions. Axes labels of the contour are lag distance.

..... 26

Figure 1–2: Auto–covariance distribution for the velocity v_1 (velocity along x_1 direction): a) the contour of v_1 auto–covariance. b) the character of the v_1 auto–covariance along different directions.

..... 27

Figure 1–3: Auto–covariance distribution for the velocity v_2 (velocity along x_2 direction): a) the contour of v_2 auto–covariance. b) the character of the v_2 auto–covariance along different directions.

..... 28

Figure 1–4: Cross–covariance between log conductivity and head: a) the contour of the cross–covariance between f and h by numerical spectral method; b) the contour of the theoretical cross–covariance between f and h; c) the cross–covariance between f and h along ξ_1; d) the cross–covariance between f and h along ξ_2.

..... 29

Figure 1–5: Cross–covariance between log conductivity and velocity v_1: a) the contour of the cross–covariance between f and v_1 by numerical spectral method; b) the contour of the

theoretical cross–covariance between f and v_1; c) the cross–covariance between f and v_1 along ξ_1; d) the cross–covariance between f and v_1 along ξ_2.

..... 30

Figure 1–6: Cross–covariance between log conductivity and velocity v_2: a) the contour of the cross–covariance between f and v_2 by numerical spectral method; b) the contour of the theoretical cross–covariance between f and v_2; c) the cross–covariance between f and v_2 along ξ_1; d) the cross–covariance between f and v_2 along ξ_2.

..... 31

Figure 1–7: Cross–covariance between head and velocity v_1: a) the contour of the cross–covariance between h and v_1 by numerical spectral method; b) the cross–covariance between h and v_1 along ξ_1; c) the cross–covariance between h and v_1 along ξ_2.

..... 32

Figure 1–8: Cross–covariance between head and velocity v_2: a) the contour of the cross–covariance between h and v_2 by numerical spectral method; b) the cross–covariance between h and v_2 along ξ_1; c) the cross–covariance between h and v_2 along ξ_2.

..... 33

Figure 1–9: Comparison of the cross–covariance between f and h for different domain sizes.

..... 34

Figure 1–10: Comparison of the cross–covariance between f and h for different ratios of the horizontal and vertical log conductivity correlation scales.

..... 35

Figure 1–11: Two–dimensional domain used in Monte Carlo simulation. The left and right boundaries are constant head. The top and bottom boundaries are linear head boundaries. Assume the hydraulic gradient is uniform along x_1 direction. The domain size in the x_1 direction is L and in the x_2 direction is W.

..... 22

Figure 1–12: Cross–covariance between log conductivity and head: a) the contour of the cross–covariance between f and h by Monte Carlo simulation; b) and c) the comparation of the solutions between the Monte Carlo simulation and numerical spectral analysis along ξ_1 and ξ_2.

..... 36

Figure 1–13: Cross–covariance between log conductivity and velocity v_1: a) the contour of the cross–covariance between f and v_1 by Monte Carlo simulation; b) and c) the comparation of the solutions between the Monte Carlo simulation and numerical spectral analysis along ξ_1 and ξ_2.

..... 37

Figure 1–14: Cross–covariance between log conductivity and velocity v_2: a) the contour of the cross–covariance between f and v_2 by Monte Carlo simulation; b) and c) the comparation of the solutions between the Monte Carlo simulation and numerical spectral analysis along ξ_1 and ξ_2.

..... 38

Figure 1–15: Cross–covariance between head and velocity v_1: a) the contour of the cross–covariance between h and v_1 by Monte Carlo simulation; b) and c) the comparation of the solutions between the Monte Carlo simulation and numerical spectral analysis along

ξ_1 and ξ_2.

..... 39

Figure 1–16: Cross–covariance between head and velocity v_2: a) the contour of the cross–covariance between h and v_2 by Monte Carlo simulation; b) and c) the comparation of the solutions between the Monte Carlo simulation and numerical spectral analysis along ξ_1 and ξ_2.

..... 40

Figure 2–1: Schematic of two types boundary conditions where Ω is a bounded domain, $f(\mathbf{x})$ and $g(\mathbf{x})$ are known functions and $\mathbf{n}$ is the unit outward vector normal to the domain boundary: a) Type A: Dirichlet boundary conditions on $\partial\Omega$ b) Type B: Dirichlet boundary conditions on $\partial\Omega_1$ and Neumann boundary conditions on $\partial\Omega_2$.

..... 45

Figure 2–2: Schematic of a specific Type A boundary conditions: the length of bounded domain is L and the width is W.

..... 48

Figure 2–3: The contours of the mean head distributions for type A boundary conditions where θ is the angle between the trend vector $\mathbf{B}$ and the mean head gradient $\mathbf{J}$: a) $\theta = 90^0$; b) $\theta = 60^0$; c) $\theta = 30^0$; d) $\theta = 0^0$.

..... 64

Figure 2–4: Schematic of the specific type B boundary conditions: The length of the domain is L and the width of the domain is W. h_l and h_r are constants, namely the left and right boundaries are constant heads, the bottom and top boundaries are no flow.

..... 50

Figure 2–5: The contours of the mean head distributions for type B boundary conditions where θ is the angle between the trend vector **B** and the mean head gradient **J**: a) $\theta = 90^0$; b) $\theta = 60^0$; c) $\theta = 30^0$; d) $\theta = 0^0$.

..... 65

Figure 2–6: The contours of the log conductivity–head cross–covariance: a) with trend where the trend is aligned to the mean head gradient; b) without trend.

..... 66

Figure 2–7: Comparison of the solution of Monte Carlo Simulation with the analytical solutions of Li–Mclaughlin [1995] and Gelhar [1993] when the trend vector **B** is aligned to the head gradient: a) in longitudinal direction b) in transverse direction.

..... 67

Figure 2–8: The comparison of the head covariance with and without trend: a) the contour of the head covariance with trend where the trend is perpendicular to the mean head gradient; b) the contour of the head covariance without trend; c) the comparison of the head covariance in longitudinal direction; d) the comparison of the head covariance in transverse direction.

..... 68

Figure 2–9: The comparison of the log conductivity– head cross–covariance with and without trend: a) the contour of the cross–covariance with trend where the trend is perpendicular to the mean head gradient; b) the contour of the cross–covariance without trend; c) the comparison of the head covariance in longitudinal direction; d) the comparison of the head covariance in transverse direction.

..... 69

Figure 2–10: Comparison of the solution of Monte Carlo Simulation with the analytical solution of Gelhar [1993] when the trend vector B is perpendicular to the head gradient: a) in longitudinal direction b) in transverse direction.

..... 70

Figure 2–11: Schematic of the flow domain and boundary conditions

..... 56

Figure 2–12: The comparison of the head covariances for different θ where θ is the angle between the trend vector **B** and the head gradient **J**: dot line, $\theta = 30^0$; dash dot line, $\theta = 45^0$; dash line, $\theta = 60^0$.

..... 71

Figure 2–13: The comparison of the log conductivity–head cross–covariances for different θ where θ is the angle between the trend vector **B** and the head gradient **J**: dot line, $\theta = 30^0$; dash dot line, $\theta = 45^0$; dash line, $\theta = 60^0$;

..... 72

CHAPTER I

Stationary Stochastic Analysis for Groundwater Flow through Heterogeneous Porous Media

1.1 Introduction

Aquifers are formed by many geological processes that occur over different time periods. Since aquifers are the end product of complicated processes, hydrogeologists have recognized that the significant variability exists in hydrogeological properties such as hydraulic conductivity. However, it is difficult to predict the data value (e.g., head, hydraulic conductivity) at locations lacking recorded measurements for the heterogeneous media. Simulation models to generate predictions have generally been based upon simplifying assumptions that neglect aquifer variability. Even those numerical simulations that consider the heterogeneity of the aquifer neglect the continuous nature of aquifer variability. Nevertheless stochastic simulation methods, based on geostatistical models of spatial variability, still can be effective for describing aquifer variability. [cf. Gelhar, 1974; Gutajahr et. al., 1978; Gelhar and Axness, 1983].

Commonly, the stochastic approaches [cf. Gelhar, 1986; Dagan, 1986; Neuman and Zhang, 1990] view the hydraulic conductivity $K(\mathbf{x})$ (or the transmissivity $T(\mathbf{x})$) as a random function (RF) (with $\mathbf{x}$ denoting the space coordinate and boldface letters denoting vectors). Then through the physical flow equations, both the head $H(\mathbf{x})$ and velocity $V(\mathbf{x})$ are also random functions and the ultimate goal is to predict their statistical properties rather than deriving single–valued estimates. This goal has been achieved by analytical methods [Gelhar and Axness, 1983; Dagan,1987; Sposito and Barry, 1987 and other studies] under the assumption that K is a stationary RF. Most significant is the additional assumption that σ_Y^2,

the variance of log conductivity Y (Y = Ln K), is smaller than unity. The assumption of small σ_Y^2 is required so that a perturbation expansion of the flow equation can be used.

Recently, the use of conditional simulation has been developed in the prediction of transport [Graham et. al, 1989; Rubin,1990], ground water flow path, velocity and groundwater travel time [Gutjahr, 1994]. In the stochastic models, conditioning can be viewed as a Bayesian updating process, serving to limit the ensemble of possible hydraulic conductivity, head and velocity field realizations to only those which are in agreement with the measured data. The conditional simulations preserve the proper covariance and cross–covariance structures of the transmissivity and head. Simultaneously, one would like the generated transmissivity and head fields satisfy the flow equation and agree with the field measurements.

For example, one may have measurements of the transmissivity, head and velocity at a few locations, e.g. based upon some geologic logs. Based upon this information, we want to predict the movement of a contaminant plume and give a cost–effective recommendation for the remediation scheme. In fact this is an inverse problem. One method proposed to attack it by Marsily et. at. (1983) introduces Pilot Points for transmissivity values by examining the sensitivity of the heads to transmissivity values. These added quasi–data points are then adjusted to bring the generated heads into closer agreement with the observations. This method is very expensive in CPU time. Another method is a joint conditional simulation approach which was developed by Gutjahr et. al.(1994). Incorporating the measurements of the transmissivity and head, the groundwater flow path lines are considerably narrower and the variance of travel time is reduced. Furthermore, the transport of the contaminant will be predicted more effectively and CPU time may be saved. Other researchers [Graham et. al. ,1989; Rubin, 1990] used conditional simulation to predict transport migration in heterogeneous media. Their research works showed that conditioning improves predictions of the spatial moments of the transport by employing velocity covariances for modeling transport.

Since the covariances take on very important roles in conditional simulation for groundwater flow and transport, it's very important to derive the covariance and cross–covariance function of the head, log conductivity (transmissivity) and velocity.

The physical relationship between conductivity, head and velocity can be described by a stochastic partial differential equation; that is to say a partial differential equation with statistically specified coefficients. Because this mathematical relation cannot be expressed in a closed form, many approximate methods have been proposed. Freeze [1975] used a Monte Carlo technique to estimate the covariance between the log conductivity and the head, as did others [Smith and Freeze, 1979a,b; Schwartz, 1977; Smith and Schwartz, 1980, 1981a, b]. Monte Carlo methods directly derive the covariance, but their usefulness is somewhat limited because of their computational costs. Dagan [1979, 1981] developed the self–consistent embedding matrix approximation, and Chirlin and Dagan [1980] applied the method to a two–dimensional field to find the head variogram.

When approximations are made to solve the stochastic equation describing groundwater flow, the computational cost can be significantly reduced if the variance of log conductivity is small. In this case, the "small perturbation" assumption allows us to avoid the rigorous simulations. Under these conditions, analytical solutions of covariance and cross–covariance between log conductivity, head and velocity can be developed. One of more important analytical techniques is the spectral method, which makes use of Fourier–Stieltjes transform along with the small pertubation assumptionto produce closed–form covariances. Since this method was introduced into field of hydrogeology by Gelhar et. al. [1974], it has been applied to investigate a great variety of hydrogeology problems [Bakr et al., 1978; Gutjahr and Gelhar, 1978; Gelhar and Axness, 1983]. Among the other assumptions made in this approach is that the random field must be statistically homogeneous and that the domain is infinite [Bakr et al., 1978; Gutjahr and Gelhar, 1981; Mizell et al., 1982, Graham et al., 1989] or semi–infinite [Naff and Vecchia, 1986] and also the hydraulic gradient is constant. Dagan [1989] has developed the another analytical method by defining "generating" functions.

From these previous researchers' works, derivation of analytical covariances is a difficult task. Analytical solutions are possible only in special case where covariances are mathematically convenient analytical expressions. Rubin [1990, 1992] introduced the covariance and cross–covariance of velocity, head and log conductivity in the case where log conductivity has a exponential correlation. However, when the input covariance (e.g. log hydraulic conductivity) is anisotropic (i.e. the integral scales for the covariance of LnK(**x**) are different in diffefrent directions), the form of the covariance and cross–covariance for the analytical solution is very complicated [Rubin, 1992]. To date, the analytical solutions are not yet available for most covariances of the conductivity, head and velocity.

Numerical methods for approximately solving the stochastic equation for groundwater flow have been developed. Sagar [1979] proposed a Galerkin finite element method to find the head variance from conductivity information, while Hoeksema and Kitanidis [1985] used a finite difference scheme. Dikow [1988] used spectral methods to compute fluxes at outflow boundaries.

One purpose of this study is to propose a very efficient numerical spectral method to obtain a series of spatial autocovariances as well as the velocity–head, velocity–log conductivity and head–log conductivity cross covariances. All these functions are given in terms of the parameters which characterize the input log conductivity field and the average head gradient. The results of this method will be compared with those from previous methods. In this paper a Monte Carlo method to estimate the covariances is developed by using the inverse Fast Fourier Transform to calculate the sampling covariances. Although the Monte Carlo method usually takes a large amount of CPU time, it can be used to analyze the stationary and non–stationary random fields. The solution of the Monte Carlo method will be useful to check the analytical or numerical spectral solutions. In next Chapter, the solution for the non–stationary situation will be discussed.

The remainder of this chapter proceeds as follows. In section 2 the numerical spectral methods to obtain the covariance and cross–covariance of random fields in groundwater

flow are developed. The relation between the log conductivity, head and the velocity proposed for the groundwater flow equation is based on the work by Gelhar et al. [1983]. The discussion of the algorithm for finding the covariance and cross–covariance from the spectral density function by an inverse Fast Fourier Transform is part of this section. The results of numerical spectral analysis are compared with the theoretical results. In section 3 the Monte Carlo simulation procedure is discussed along with its advantages and limitations.

1.2 Numerical Spectral Analyses of the Auto–Covariances and Cross–covariances for Groundwater Flow in Heterogeneous Media

Based the implicit relationship between covariance and spectral density function, the Fourier Transform can be used to find the covariance when the spectral density function is known. In order to analyze the statistical structure of groundwater flow models represented by partial differential equations, the spectral representation theoreom is introduced.

1.2.1 Relationship between Covariance and Spectral Density Function

Assume V(**x**) is a random process given at locations **x** which represents the coordinate space. A simple description of V(**x**) is based on first moment and second moment. The first moment is defined by the mean, μ(**x**), where:

$$\mu(\boldsymbol{x}) = E[V(\boldsymbol{x})] \qquad (1\text{–}1\text{–}1)$$

and the second moment is defined by the covariance, Cov[V(**x**),V(**y**)], where:

$$Cov[V(\boldsymbol{x}), V(\boldsymbol{y})] = E[(V(\boldsymbol{x}) - \mu(\boldsymbol{x}))(V(\boldsymbol{y}) - \mu(\boldsymbol{y}))] \qquad (1\text{–}1\text{–}2)$$

Here E[ ] is the expectation operator and Cov[ ] is the covariance operator.

Usually, it's not possible to describe a random field entirely by these two moments. However, if a random field is normal (a gaussian process), it is then completely determined by its mean and covariance function.

We are interested in stationary (statistically homogeneous) random fields because of the resulting simplifications, and because it is often possible to regard real situations as approximately stationary. If the random field V(x) is stationary, the two properties 1–1–1 and 1–1–2 become:

$$i) : E[V(\boldsymbol{x})] = \mu;$$

$$ii) : Cov[V(\boldsymbol{x} + \boldsymbol{s}), V(\boldsymbol{x})] = C(\boldsymbol{s})$$

where μ is a constant, i.e. the mean of $V(\mathbf{x})$ is the constant and the covariance of $V(\mathbf{x})$ which is the function of the lag or separation **s** does not depend on location **x** and only depends on **s**.

Usually $C(\mathbf{s})$ is called autocovariance of $V(\mathbf{x})$. The Fourier transform of $C(\mathbf{s})$ is called spectral density function $S(\mathbf{u})$ (i.e. spectrum), where:

$$S(\boldsymbol{u}) = \int_{-\infty}^{-\infty} e^{-i2\pi \boldsymbol{u}\cdot\boldsymbol{s}} C(\boldsymbol{s}) d\boldsymbol{s} \qquad (1\text{–}1\text{–}3)$$

and the inverse Fourier Transform of $S(\mathbf{u})$ is the covariance $C(\mathbf{s})$, where:

$$C(\boldsymbol{s}) = \int_{-\infty}^{-\infty} e^{i2\pi \boldsymbol{u}\cdot\boldsymbol{s}} S(\boldsymbol{u}) d\boldsymbol{u} \qquad (1\text{–}1\text{–}4)$$

In (2–1–3) and (2–1–4) the dot product is defined such that:

$$\boldsymbol{u} \cdot \boldsymbol{s} = u_1 s_1 + u_2 s_2, \ldots, u_p s_p \qquad (1\text{–}1\text{–}5)$$

and the integral sign represents a p–fold integral of the form

$$\int_{-\infty}^{\infty} G(\boldsymbol{k}) = \int_{-\infty}^{\infty} \int_{-\infty}^{\infty}, \ldots, \int_{-\infty}^{\infty} G(k_1, k_2, \ldots, k_p dk_1 dk_2, \ldots, dk_p \qquad (1\text{–}1\text{–}6)$$

where p represents the number of dimensions.

Consequently $C(\mathbf{s})$ and $S(\mathbf{u})$ are a Fourier–Stieltjes transform pair. This relationship between $C(\mathbf{s})$ and $S(\mathbf{u})$ is very important because it is the theoretical basis of the numerical spectral method used in this chapter. $C(\mathbf{s})$ and $S(\mathbf{u})$ have several useful properties (see table 1–1).

Considering two correlated random fields, for example, hydraulic conductivity and

head or velocity which are related by groundwater flow equations and Darcy's law, we can use the cross–covariance to describe certain relationship between two fields.

Table 1–1: List of the properties for autocovariance and spectral density

Autocovariance C(u)	Spectral Density S(u)
i) The autocovariance is symmetric. $C(s) = C(-s)$	*i) The spectral density is symmetric.* $S(u) = S(-u)$
ii) The variance is equal to the autocovariance at zero lag. $Var(V(x)) = C(0)$	*ii) The variance is the integral of the spectral density.* $Var(V(x)) = \int_{-\infty}^{\infty} S(u)du$
iii) The absolute value of the autocovariance is not greater than the variance. $\lvert C(s)\rvert \leq C(0)$	*iii) The spectral density is non–negative for all* u. $S(u) \geq 0$

The relation between the two jointly distributed random fields can be measured using cross–covariance function:

$$Cov\left[V_j(x), V_k(y)\right] = E\left[\left(V_j(x) - E\left(V_j(x)\right)\right)\left(V_k(y) - E(V_k(y))\right)\right] \qquad (1\text{–}1\text{–}7)$$

where $V_j(\mathbf{x})$ and $V_k(\mathbf{y})$ are distinct random fields for $j \neq k$. The joint relations between $V_j(\mathbf{x+s})$ and $V_k(\mathbf{y})$ may also be studied as a function of lag **s**. The stronger the relation is between $V_j(\mathbf{x+s})$ and $V_k(\mathbf{y})$ at lag **s**, the larger the cross–covariance is. The condition that two random fields are jointly stationary, requires that both means $E(V_j(\mathbf{x})) = \mu_x$ and $E(V_k(\mathbf{y})) = \mu_y$ be constant and both autocovariance and cross–covariance only a function of the lag **s**.

$$Cov\left[V_j(s + s), V_k(x)\right] = C_{jk}(s) \qquad (1\text{–}1\text{–}8)$$

If $E(V_j(\mathbf{x})) = 0$ and $E(V_k(\mathbf{y})) = 0$, then

$$C_{jk}(s = E\left[V_j(x + s), V_k(x)\right] \qquad (1\text{–}1\text{–}9)$$

We again define the Fourier Transform of a cross–covariance to be a cross–spectral density (simply, called cross–spectrum),$S_{jk}(\mathbf{u})$, where:

$$S_{jk}(\boldsymbol{u}) = \int_{-\infty}^{\infty} e^{-i2\pi \boldsymbol{u}\cdot s} C_{jk}(\boldsymbol{s})d\boldsymbol{s} \qquad (1\text{–}1\text{–}10)$$

Once again the inverse Fourier Transform of the cross–spectrum is the cross–covariance, where:

$$C_{jk}(\boldsymbol{s}) = \int_{-\infty}^{\infty} e^{i2\pi \boldsymbol{u}\cdot s} S_{jk}(\boldsymbol{u})d\boldsymbol{u} \qquad (1\text{–}1\text{–}11)$$

And hence $S_{jk}(\mathbf{u})$ and $C_{jk}(\mathbf{s})$ are a Fourier–Stieltjes transform pair. Some important properties of these functions are listed in table 1–2.

Table 1–2: List of the properties for cross–covariance and cross–spectrum

Cross–covariance $C_{jk}(\mathbf{s})$	Cross–spectrum $S_{jk}(\mathbf{u})$
i) $C_{jk}(\boldsymbol{s}) = C_{kj}(-\boldsymbol{s})$	*i)* $S_{jk}(\boldsymbol{u}) = S_{kj}(-\boldsymbol{u})$
ii) $C_{jk}(\boldsymbol{s}) \leq \left[Var\left(V_j(\boldsymbol{x})\right)Var(V_k(\boldsymbol{x}))\right]^{\frac{1}{2}}$	*ii)* $S_{jk}(\boldsymbol{u}) = S_{kj}^{*}(\boldsymbol{u})$
iii) Cross–covariance must be real function.	*iii) Usually, cross–spectrum is a complex function.*

Note: $S_{kj}^{*}(\mathbf{u})$ is the complex conjugate of $S_{kj}(\mathbf{u})$

1.2.2 Spectral Representation Theorem

Let $V(\mathbf{x})$ be a statistically stationary (or statistically homogeneous) random field where $E[V(\mathbf{x})] = 0$, then $V(\mathbf{x})$ has spectral representation:

$$V(\boldsymbol{x}) = \int_{-\infty}^{\infty} e^{i2\pi \boldsymbol{u}\cdot\boldsymbol{x}} dZ(\boldsymbol{u}) \qquad (1\text{–}2\text{–}1)$$

where $i=(-1)^{1/2}$, $\mathbf{u}$ is the wave number or angular frequency vector, and $dZ(\mathbf{u})$ is a complex random variable of the form [Robin et al., 1993]:

$$dZ(\boldsymbol{u}) = dZ_R(\boldsymbol{u}) + i dZ_I(\boldsymbol{u}) \qquad (1\text{–}2\text{–}2)$$

where the subscripts R and I represent the real and imaginary components. The representation (1–2–1) is called spectral representation theorem.

Like the Laplace Transform and Fourier Transform, the spectral representation is also a transform which transforms the random variable defined in spatial space into a random variable in the frequency domain. The spectral representation of a single random field realization can be understood intuitively as a field of amplitudes, where the coordinates are the frequencies of wave numbers. Statistically speaking, the probability space of the spatial random field $V(\mathbf{x})$ is transformed into the probability space of the spectral random field $dZ(\mathbf{u})$. The new probability space of the random variables $dZ(\mathbf{u})$ in (1–2–1) has several very important properties:

i) $$E[dZ(\boldsymbol{u})] = \int_{-\infty}^{\infty} e^{-i2\pi \boldsymbol{u}\cdot\boldsymbol{x}} E[V(\boldsymbol{x})] d\boldsymbol{x} = 0$$

ii) $$E\left[|dZ(\boldsymbol{u})|^2\right] = S(\boldsymbol{u}) d\boldsymbol{u}$$

iii) $$E\left[dZ(\boldsymbol{u}_1) dZ^*(\boldsymbol{u}_2)\right] = 0 \quad \text{for all} \quad \boldsymbol{u}_1 \neq \boldsymbol{u}_2$$

The first property states the mean $E[dZ(\mathbf{u})]$ of the random variables $dZ(\mathbf{u})$ is equal to the Fourier Transform of the mean of the random variable $V(\mathbf{x})$. From $E[V(\mathbf{x})]=0$, the mean of $dZ(\mathbf{u})$ must be zero. The second property defines the variance of the complex random variables $dZ(\mathbf{u})$. The term $S(\mathbf{u})d\mathbf{u}$ is a measure of the average "energy per–unit area" or "power" contribution of the amplitude of a frequency $\mathbf{u}$ to the random field $V(\mathbf{x})$. $S(\mathbf{u})$ is the spectrum of the random field $V(\mathbf{x})$ that we have defined previously. $S(\mathbf{u})$ depends purely on

the probabilitistic properties of the random field $V(\mathbf{x})$ since it is simply the Fourier Transform of the covariance $C(\mathbf{s})$ of $V(\mathbf{x})$. The third property states that the increments $dZ(\mathbf{u_1})$ and $dZ(\mathbf{u_2})$ at different frequencies $\mathbf{u_1}$ and $\mathbf{u_2}$ are uncorrelated. Such a random field is also called an "orthogonal" random field [Robin et al., 1993].

Considering two jointly stationary $V_j(\mathbf{x})$ and $V_k(\mathbf{y})$ where $E[V_j(\mathbf{x})]=0$, $E[V_k(\mathbf{y})]=0$, from the Spectral Representation Theorem it can be inferred that

$$V_j(\boldsymbol{x}) = \int_{-\infty}^{\infty} e^{i2\pi \boldsymbol{u}\cdot\boldsymbol{x}} dZ_j(\boldsymbol{u}) \qquad (1\text{–}2\text{–}3)$$

$$V_k(\boldsymbol{x}) = \int_{-\infty}^{\infty} e^{i2\pi \boldsymbol{u}\cdot\boldsymbol{x}} dZ_k(\boldsymbol{u}) \qquad (1\text{–}2\text{–}4)$$

and $dZ_j(\mathbf{u})$ and $dZ_k(\mathbf{u})$ have the following properties:

i) $E\left[dZ_j(\boldsymbol{u})\right] = 0;\ E[dZ_k(\boldsymbol{u})] = 0$

ii) $E\left[dZ_j(\boldsymbol{u})dZ_k^*(\boldsymbol{u})\right] = S_{jk}(\boldsymbol{u})d\boldsymbol{u}$

iii) $E\left[dZ_j(\boldsymbol{u}_1)dZ_k^*(\boldsymbol{u}_2)\right] = 0 \quad for\ all \quad \boldsymbol{u}_1 \neq \boldsymbol{u}_2$

The importance of Spectral Representation Theorem is that it replaces a spatially correlated structure in the **x** domain with an uncorrelated structure in the frequency domain. In dealing with the stochastic groundwater flow and transport equations, the spectral transformation of the equations usually is a linear polynomial. Solving the linear polynomial equation in the frequency domain is much easier than solving the partial differential equation in the spatial domain [Gelhar and Axness, 1983]. On the other hand, the spectral representation of a spatially correlated random field will yield a random field an uncorrelated random field in the complex domain. This uncorrelated property makes the analysis in the new domain much easier

1.2.3 Theory of Numerical Spectral Analysis

Previously a transform was introduced that related the covariance $C_{jk}(\mathbf{s})$ between $V_j(\mathbf{x+s})$ and $V_k(\mathbf{x})$ and the spectrum $S_{jk}(\mathbf{u})$

$$C_{jk}(\boldsymbol{s}) = \int_{-\infty}^{\infty} e^{i2\pi \boldsymbol{u}\cdot\boldsymbol{s}} S_{jk}(\boldsymbol{u}) d\boldsymbol{u} \qquad (1\text{–}3\text{–}1)$$

In order to simplify the exposition for derivation of the covariance, $V_j(\mathbf{x+s})$ and $V_k(\mathbf{x})$ are defined over a two dimensional domain (though we could also consider three dimensional domains). Equations (1–3–1) and (1–3–2) have the form of a continuous Fourier Transform, which can be evaluated numerically by introducing two approximations. Firstly, the frequency domain must be discretized into a finite number of frequency intervals in each dimension:

$$\Delta \boldsymbol{u} = (\Delta u_1, \Delta u_2) \qquad (1\text{–}3\text{–}2)$$

Secondly, the frequency domain must be truncated at finite frequency, known as the Nyquist frequency, at each end of the domain, namely, at $\pm u_{Nj}$ for j=1,2. The number of frequency intervals in dimension j is $2N_j$ such that

$$N_j \Delta u_j = u_{N_j} \qquad (1\text{–}3\text{–}3)$$

Then we can approximate $C_{jk}(\mathbf{s})$ by:

$$C_{jk}(\boldsymbol{s}) \cong \hat{C}_{jk}(\boldsymbol{s}) = \sum_{m} e^{i2\pi \boldsymbol{u}\cdot\boldsymbol{s}} \hat{S}_{jk}(\boldsymbol{u}) \Delta \boldsymbol{u} \qquad (1\text{–}3\text{–}4)$$

where the summation uses the convention that is analogous to the one for the integration in (1–3–1), and **u** is discretized as

Therefore $\hat{C}_{jk}(\boldsymbol{s})$ and $\hat{S}_{jk}(\boldsymbol{u})$ form a discrete Fourier Transform pair and have same properties as $C_{jk}(\mathbf{s})$ and $S_{jk}(\mathbf{s})$.

$$\boldsymbol{u} = (u_1,\ u_2) = (m_1\Delta u_1,\ m_2\Delta u_2) \qquad (1\text{–}3\text{–}5)$$

$$m_{j=} - N_j, - N_j + 1,\ldots, - 1, 0, 1,\ldots, N_j - 1 \qquad (1\text{–}3\text{–}6)$$

$$j = 1,2$$

L is defined the length of the domain of random variable in spatial space, where **L**=(L_1, L_2). The space discretization of the lag is Δ**s**=(Δs_1, Δs_2) and the number of gridpoints in the random field is $2N_1$ by $2N_2$. Therefore:

$$\boldsymbol{L} = (2N_1\Delta s_1,\ 2N_2\Delta s_2) \qquad (1\text{–}3\text{–}7)$$

The covariance function is descretized into a regular two dimensional grid with an equal number and size of gridpoints in each direction:

$$\boldsymbol{s} = (m_1\Delta s_1,\ m_2\Delta s_2) \qquad (1\text{–}3\text{–}8)$$

$$m_1 = - N_1,\ldots, N_1 - 1$$
$$m_2 = - N_2,\ldots, N_2 - 1$$

The relationship between Δs_j and u_{Nj} must be

$$(2u_{N_j})^{-1} = \Delta s_j \qquad j=1,2 \qquad (1\text{–}3\text{–}9)$$

in each dimension j. The overall length of the domain in each dimension is

$$T_j = (\Delta u_j)^{-1} \qquad j=1,2 \qquad (1\text{–}3\text{–}10)$$

It is apparent from (1–3–9) that the real field spacing will dictate the magnitude of the spectral truncation error. Similarly, (1–3–10) shows that the size of the spatial domain (real field) will dictate the frequency domain spacing which, in turn, will affect the magnitude of the spectral discretation error.

The discrete Fourier transform pair compatible with the transform (1–3–1) is in two dimensions.

We change the intervals ($-N_j$, N_j-1) of the summations (1–3–11) and (1–3–13) into the intervals (0, $2N_j-1$) of the summations (1–3–12) and (1–3–14) comparing with (1–3–1) be-

$$\hat{C}_{jk}(j_1,j_2) = \sum_{m_1=-N_1}^{m_1=N_1-1} \sum_{m_2=-N_2}^{m_2=N_2-1} e^{\frac{i2\pi m_1 j_1}{2N_1}} e^{\frac{i2\pi m_2 j_2}{2N_2}} S_{jk}\left(\frac{m_1}{2N_1\Delta s_1}, \frac{m_2}{2N_2\Delta s_2}\right) \cdot \frac{1}{2N_1\Delta s_1} \cdot \frac{1}{2N_2\Delta s_2} \qquad (1\text{–}3\text{–}11)$$

$$\hat{C}'_{jk}(j_1,j_2) = \sum_{m_1=0}^{m_1=2N_1-1} \sum_{m_2=0}^{m_2=2N_2-1} e^{\frac{i2\pi m_1 j_1}{2N_1}} e^{\frac{i2\pi m_2 j_2}{2N_2}} S_{jk}\left(\frac{m_1}{2N_1\Delta s_1}, \frac{m_2}{2N_2\Delta s_2}\right) \cdot \frac{1}{2N_1\Delta s_1} \cdot \frac{1}{2N_2\Delta s_2} \qquad (1\text{–}3\text{–}12)$$

where

$$\hat{C}_{jk}(-j_1,-j_2) = \hat{C}'_{jk}(2N_1 - j_1, 2N_2 - j_2)$$

$$\hat{C}_{jk}(j_1,-j_2) = \hat{C}'_{jk}(j_1, 2N_2 - j_2)$$

$$\hat{C}_{jk}(-j_1,j_2) = \hat{C}'_{jk}(2N_1 - j_1, j_2)$$

$$\hat{C}_{jk}(j_1,j_2) = \hat{C}'_{jk}(j_1,j_2)$$

$$1 \le j_1 \le N_1;\ 1 \le j_2 \le N_2;$$

cause the Fast Fourier Transform requires that the dimensional array be packed from frequency zero through increasing positive frequencies to the Nyquist frequency.

The described algorithm is very fast and flexible. It can handle any spectral density function (even though the spectrum contains discrete component at distinct frequencies) and deal with the anisotropic random processes with no modification. Next I will use this algorithm to analyze the statistical structure of groundwater flow and do comparision with analytical results.

1.2.4 Numerical Spectral Method to Analyze Statistical Structure of Groundwater Flow through Heterogeneous Media

For the sake of illustration we concentrate on steady flow in a heterogeneous two–dimensional porous media. We assume that the log hydaulic conductivity is a stationary random field with a known spatially variable ensemble mean and spectral density function.

Two–dimensional, steady state groundwater flow in a saturated aquifer, with heterogeneous conductivity, has the following flow equation:

$$\frac{\partial}{\partial x_i}\left(K\frac{\partial \phi}{\partial x_i}\right) = 0 \qquad (1\text{–}4\text{–}1)$$

where K is hydraulic conductivity and ϕ is hydraulic head.

Equation (2–4–1) can be rewritten in terms of lnK:

$$\frac{\partial^2 \phi}{\partial x_i^2} + \frac{\partial \ln K}{\partial x_i}\frac{\partial \phi}{\partial x_i} = 0 \qquad (1\text{–}4\text{–}2)$$

Representing h and lnK in terms of their means plus a zero–mean pertubation,

$$\phi = H + h \; ; \; E(\phi) = H \; ; \; E(h) = 0$$

$$lnK = F + f \; ; \; E(lnK) = F \; ; \; E(f) = 0$$

leads to

$$\frac{\partial^2 H}{\partial x_i^2} + \frac{\partial^2 h}{\partial x_i^2} + \frac{\partial H}{\partial x_i}\frac{\partial f}{\partial x_i} + \frac{\partial F}{\partial x_i}\frac{\partial h}{\partial x_i} + \frac{\partial f}{\partial x_i}\frac{\partial h}{\partial x_i} = 0 \qquad (1\text{–}4\text{–}3)$$

The equation for mean flow is found by taking the expectation of Equation (2–4–3):

$$\frac{\partial^2 H}{\partial x_i^2} + E\left(\frac{\partial f}{\partial x_i}\frac{\partial h}{\partial x_i}\right) = 0 \qquad (1\text{–}4\text{–}4)$$

We assume no trend exists in the hydraulic conductivity field, i.e. F is a constant. Subtracting (1–4–4) from (1–4–3) results in the equation governing perturbation in groundwater flow,

$$\frac{\partial^2 h}{\partial x_i^2} - J_i\frac{\partial f}{\partial x_i} = 0 \qquad (1\text{–}4\text{–}5)$$

where $J_i = -\partial H/\partial x_i$ is the mean gradient in i direction. In general, the perturbation of the input log conductivity is assumed small and second–order perturbation products are negnected.

From the equation (1–4–5), the head process is stationary. According to the Spectral Representation Thoreom (SRT) [Lumley and Panofsky, 1964], f and h can be expressed as:

$$h(\boldsymbol{x}) = \int_{-\infty}^{\infty} e^{i2\pi \boldsymbol{u}\cdot\boldsymbol{x}} dZ_h(\boldsymbol{u})$$

$$f(\boldsymbol{x}) = \int_{-\infty}^{\infty} e^{i2\pi \boldsymbol{u}\cdot\boldsymbol{x}} dZ_f(\boldsymbol{u}) \qquad (1\text{–}4\text{–}6)$$

where dZ_h and dZ_f are complex Fourier amplitudes of the fluctuations.

Substituting (1–4–6) to equation (1–4–5) and using uniqueness of the SRT leads to

$$dZ_h = -\frac{i(J_1u_1 + J_2u_2)}{2\pi(u_1^2 + u_2^2)}dZ_f \qquad (1\text{–}4\text{–}7)$$

Finally from (1–2–4) and (1–2–5), the spectrum of head is:

$$S_{hh} = \frac{u_1^2J_1^2 + u_2^2J_2^2}{4\pi^2(u_1^2 + u_2^2)^2}S_{ff} \qquad (1\text{–}4\text{–}8)$$

where S_{hh} is the head spectrum and S_{ff} is the spectrum of lnK.

From (1–2–9) and (1–2–10), the cross–spectrum between log conductivity and head is:

$$S_{fh} = -\frac{i(J_1u_1 + J_2u_2)}{2\pi(u_1^2 + u_2^2)}S_{ff} \qquad (1\text{–}4\text{–}9)$$

where S_{fh} is the cross–spectrum of hydraulic conductivity and head.

According to Darcy's Law, the velocity of groundwater flow has the following equation:

$$V_i = -\frac{K}{n}\frac{\partial\phi}{\partial x_i} \qquad (1\text{–}4\text{–}10)$$

$$i = 1,2$$

where V_i is the velocity along i direction and n is the spatially uniform poriosity.

Since we have assumed the perturbation of conductivity is very small, the higher order terms of f can be neglected. Then the velocity is approximately expressed by the following form

$$V_i = -\frac{k_G}{n}\frac{\partial\phi}{\partial x_i}e^f \simeq \frac{K_G}{n}\left[J_i - \frac{\partial h}{\partial x_i}\right][1 + f + f^2] \qquad (1\text{–}4\text{–}11)$$

where $K_G = \exp[E(\ln K)]$.

If the products of pertubations are neglected, the equations for the mean velocity and

velocity pertubation can be derived from (1–4–11)

$$V_i = \bar{v}_i + v_i \; ; \; E(V_i) = \bar{v}_i \; ; \; E(v_i) = 0$$

$$\bar{v}_i = \frac{K_G}{n} J_i \qquad (1\text{–}4\text{–}12)$$

$$v_i = \frac{K_G}{n}\left[fJ_i - \frac{\partial h}{\partial x_i} \right] \qquad (1\text{–}4\text{–}13)$$

where $\bar{v}_1$ is mean velocity along x_1 direction;

$\bar{v}_2$ is mean velocity along x_2 direction;

v_1 is velocity perturbation along x_1 direction;

v_2 is velocity perturbation along x_2 direction;

Following the analysis of Galhar and Axness [1983], the relationship between the complex Fourier amplitudes of pore velocity and log conductivity is

$$dZ_{v_i} = \frac{K_g}{n}\left[J_i - u_i \frac{(u_1 J_1 + u_2 J_2)}{(u_1^2 + u_2^2)} \right] dZ_f \qquad (1\text{–}4\text{–}14)$$

Based on the SRT, (2–4–7) to (2–4–14) combine to give the following spectra and cross–spectra

$$S_{v_i v_i} = \frac{K_g^2}{n^2}\left[J_i - u_i \frac{(u_1 J_1 + u_2 J_2)}{(u_1^2 + u_2^2)} \right]^2 S_{ff} \qquad (1\text{–}4\text{–}15)$$

$$S_{v_i f} = \frac{K_g}{n}\left[J_i - u_i \frac{(u_1 J_1 + u_2 J_2)}{(u_1^2 + u_2^2)} \right] S_{ff} \qquad (1\text{–}4\text{–}16)$$

$$S_{v_i h} = \frac{K_g}{n}\left[J_i - u_i \frac{(u_1 J_1 + u_2 J_2)}{(u_1^2 + u_2^2)} \right]\left[\frac{i J_i u_i}{2\pi(u_1^2 + u_2^2)} \right] S_{ff} \qquad (1\text{–}4\text{–}17)$$

$$S_{v_i v_j} = \frac{K_g^2}{n^2}\left[J_i - u_i \frac{(u_1 J_1 + u_2 J_2)}{(u_1^2 + u_2^2)} \right]\left[J_j - u_j \frac{(u_1 J_1 + u_2 J_2)}{(u_1^2 + u_2^2)} \right] S_{ff} \qquad (1\text{–}4\text{–}18)$$

where S_{uv} is the cross–spectrum between random fields u and v.

The autocovariances or cross–covariances for log–conductivity, head and velocity are derived by applying the previous numerical spectral theorem (1–3–11) and (1–3–12).

In order to demonstrate the numerical spectral method, we select the isotropic log hydraulic conductivity covariance function from Mizell et al [1982] (called the Mizell–A spectrum). This function satisfies the integral conditions needed to obtain a stationary two–dimensional hydraulic head field [Mizell et al, 1982] and the closed forms of covariances and cross–covariance for head, velocity and log conductivity have been derived [Graham and Mclaughlin, 1989, P2341). The Mizell–A spectrum of log conductivity is

$$S_{ff}(u_1, u_2) = \frac{8\pi\sigma^2\alpha^2(u_1^2 + u_2^2)}{[(2\pi u_1)^2 + (2\pi u_2)^2 + \alpha^2]^3} \qquad (1\text{–}4\text{–}18)$$

$$\alpha = \frac{\pi}{4\lambda}$$

where λ is the integer scale and σ^2 the variance of the log conductivity process.

Table 1–3 lists the input parameters used for the two–dimensional experimental analyses. In order to compare the derived analytical results, the same assumption was made that the mean flow direction of the groundwater is aligned with the x_1 coordinate.

Table 1–3: Inputs for the illustration to solve the auto–solve covariances and cross–covariances of log conductivity, head and velocity by the numerical spectral simulation

parameters	Value
Ln K variance	$\sigma^2 = 1.0$
Ln K correlation scale	$\lambda = 1.0$
Ln K geometric mean	$LnK_G = -3.0$
Mean hydraulic head gradient	$J_0 = -\frac{\partial H}{\partial x_1} = 0.1$
Poriosity	$n = 0.30$
Domain grid size	*128 by 128*

Figure 1–1 compares the head auto–covariance of the numerical spectral method and

theoretical analysis. The results from the two methods coincide very well. From the lower graph c, we see that the head covariance is anisotropic despite the input of the isotropic correlation function for the LnK process. In the perpendicular direction, the correlation function reaches a maximum value. Furthermore as the lag distance increases, the correlation function approach zero for all directions, implying that head observations separated by some sufficiently large distance are uncorrelated.

The autocovariances of v_1 and v_2 are depicted in Figure 1–2 and 1–3, respectively. Both display a symmetric and anisotropic behavior.

The cross–covariances between f and h, f and v_1, f and v_2, h and v_1, h and v_2 from the numerical spectral method are shown in Figure 1–4, 1–5 , 1–6, 1–7, and 1–8. Compared with the previous auto–covariances of h, v_1 and v_2, all cross–covariances are antisymmetric. This phenomena can be explained by the properties of cross–covariance in table 1–2. In Figure 1–4, 1–5, 1–6, the solutions of two methods are depicted. We see that the numerical spectral method results closely match the theoretical solutions.

In the previous subsection, I have indicated that the domain size and spacing will influence the magnitude of the spectral truncation error. Figure 1–9 demonstrates that when the domain grid size increases, the results from numerical spectral method will approach the theoretical solution.

While the numerical spectral method asymptotically do reach the theoritical covariance function, these methods are very useful where the analytical solution are not readily available, especially for the three–dimensional case. The three–dimensional case is illustrate by an example using the common log conductivity exponential covariance–spectral pair [Gutjahr, 1989; Gelhar and Axness, 1983]:

where λ_i is the correlation scale vector, u is the wave vector and ξ is the lag vector.

Assume $\lambda_1=\lambda_2=\lambda_H$, $\lambda_3=\lambda_P$, and let the ratio $r=\lambda_P/\lambda_H$. Figure 1–10 shows the log conductivity–head crosscovariance for $\xi_2=\xi_3=0$. The magnitude of cross–correlation increases with the ratio r. When r=0, the correlation between f and h vanishes. When the ratio becomes

Spectrum:
$$S(\boldsymbol{u}) = S(u_1, u_2, u_3) = \frac{(2\pi)^3\sigma^2\lambda_1\lambda_2\lambda_3}{\pi^2[1 + (2\pi u_1\lambda_1)^2 + (2\pi u_2\lambda_2)^2 + (2\pi u_3\lambda_3)^2]^2} \quad (1\text{–}4\text{–}19)$$

Covariance:
$$C(\xi) = C(\xi_1, \xi_2, \xi_3) = \sigma^2 \exp\left\{ - \left(\frac{\xi_1^2}{\lambda_1^2} + \frac{\xi_2^2}{\lambda_2^2} + \frac{\xi_3^2}{\lambda_3^2} \right)^{\frac{1}{2}} \right\} \quad (1\text{–}4\text{–}20)$$

larger, the correlation of the three dimensional case is closer to the correlation of the two dimensional case, which implies that the flow tends to be two–dimensional for large r.

Therefore we can conclude that the numerical spectral method can be applied to asymptotically evaluate the covariance and cross–covariance functions of groundwater flow if the log conductivity stochastic process is stationary.

1.3 Application of Monte Carlo Simulation in Analyzing Statistical Structure of Groundwater Flow through Heterogeneous Media

Monte Carlo Simulation has been widely used to treat the problems of groundwater flow in heterogeneous media [Warren and Price, 1961; Freeze,1975; etc.]. This method deals with the problem as a stochastic differential equation, computes a set of repetitive simulations with a mathematical model and then analyzes the collection of the generating realiztions statistically.

The computation procedure of Monte Carlo Simulation can be summarized by the following steps:

i). First step: Generate a realization of log hydraulic conductivity with mean zero. For example one could use two dimensional Fast Fourier Transform generation method [Gutjahr et al, 1994] to carry out this stage. Then add in the mean of log conductivity to the realization and change back to the conductivity field.

ii). Second step: Input the generated hydraulic field to the flow equation 4–2–1. After adding the boundary conditions to the flow field, any numerical simulation can be used to solve the head distribution. If we substitute the solved head solution into equation 4–2–10, we can get the distribution of the velocity along two directions.

iii) Third step: Analyze the mean head and velocity distributions and obtain the head and velocity perturbations by removing the mean from the solved fields.

iv) Fourth step: Use the Fast Fourier Transform to analyze the auto–covariance and cross –covariance of the log conductivity, head and velocity.

These four steps will be repeated many times. Theoretically, the number of repetitions

should be large enough so that the simulated results will be close to the theoretical solution. To illustrate this, consider a two–dimensional steady state flow in a saturated aquifer. In order to compare with the previous theoretical solution, assume the input covariance of log hydraulic conductivity again is a Mizell–A. The flow domain , flow direction and boundary conditions are shown in Figure 1–11

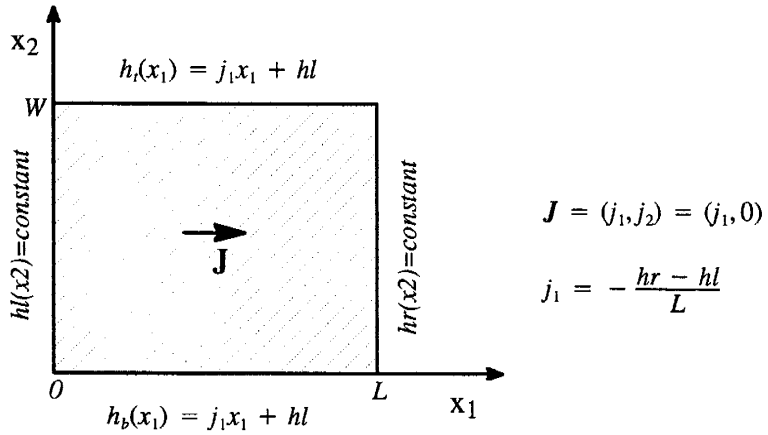

Figure 1–11: Two–dimensional domain used in Monte Carlo simulation. The left and right boundaries are constant head. The top and bottom boundaries are linear head boundaries.Assume the hydraulic gradient is uniform along x_1 direction. The domain size in the x_1 direction is L and in the x_2 direction is W.

Figure 1–12 shows the results for the cross–covariance between log conductivity and head fields. This simulation involved 100 Monte Carlo solutions of steady state flow along a 12.8 by 12.8 domain. The mean of log conductivity is –3.0 and the other parameters are same as the previous analysis. The lower graphs b and c show the comparison of Monte Carlo simulation and the theoretical solution. We see that the two solutions coincide very well at a small separation lag. While the lag length is close to the length of the domain, the solution from Monte Carlo simulation is not near the theoretical result. The difference is most likely due to the boundary effect. In order to decrease the boundary effect on the covariance, usually we select the domain size ten times longer than the correlation scale.

Figure 1–13, 1–14, 1–15 and 1–16 depict the comparisons for the cross–covariances

of log conductivity and velocity, head and velocity between the solutions of Monte Carlo simulation and numerical spectral simulation. The solutions of Monte Carlo simulation closely match the results of numerical spectral simulation.

In the previous discussion, we didn't make any assumptions about the log conductivity when we use Monte Carlo simulation to analyze the covariances and cros–covariances of log conductivity, head and velocity. Even though the log conductivity is not stationary, Monte Carlo simulation still can be used to analyze the stochastic structure of groundwater flow. Monte Carlo simulation directly solves the flow equation by propagating the generated input conductivity field. It does not depend on the linearized perturbation equation. And hence the Monte Carlo silmulation can be used to verify if the theoretical solution is reasonable. Nevertheless, Monte Carlo simulation usually takes more extensive CPU time than the numerical spectral method.

1.4 Summary

In this chapter, the auto–covariances and cross–covariances of the random fields in groundwater flow were derived by the numerical spectral method and Monte Carlo simulation. We presented the characteristics of the auto–covariance and cross–covariance functions for the log conductivity, head and velocity fields. All these functions are given in terms of the parameters which characterize the input log conductivity field and the average head gradient. They will be very useful in the conditioning simulation for predicting the risk of the waste contaminant and solute transport.

In order to illustrate the flexibility of the methods, we compared the solutions of both methods with the theoretical results for a simple case where good agreement is obtained. Because the Fast Fourier Transform algorithm was introduced to approximate the infinite integral of (2–3–1), the computation of the covariance for the numerical spectral method only needs $N\log_2 N$ operations. If the domain grid size is reasonably selected, the solution of the numerical spectral method is close to the theoretical solution, and the numerical spectral method is much faster than the Monte Carlo simulation.

In general, one would like to find a closed analytical solutions for the covariances or cross–covariances. Unfortunately, the analytical solution can be obtained for only a few cases under rather simplified assumptions. For the three dimensional problem, even though the analytical solutions for some special cases are available, the final result needs to be solved by numerical method [Rubin, 1992]. The numerical spectral method provides a very powerful technique for finding the covariance function instead of analytically evaluating the integral of a spectrum or cross spectrum.

The numerical spectral method is based on the relationship between the spectrum (or

cross–spectrum) and the input spectrum. If the stochastic processes are not stationary (For example, a trend is existing in log conductivity), the spectral representation theorem will not work for deriving the correlations of those random fields in groundwater flow. In this situation, the numerical spectral method can not be used to derive the stochastic structure of the groundwater flow.

Although the Monte Carlo simulation is limited due to the computational effort, it has the important advantage that it does not introduce any assumption about small variations of the random fields. For nonstationary stochastic problem, Monte Carlo simulation can be used to get an approximate solution.

CHAPTER II

Non–stationary Stochastic Analysis for Groundwater Flow through Heterogeneous Trending Porous Media

2.1 Introduction

In the previous chapter, we discussed the stochastic analysis of groundwater flow in heterogeneous porous media where the log conductivity was assumed to be statistically homogeneous or stationary. The stationarity assumption for log conductivity enabled us to use the spectral representation theorem to solve the stochastic flow problem. In practice, this simplified hypothesis for log conductivity may not always reflect the actual field findings. Woodbury and Sudicky [1991], Rehfeldt et al. [1992] and Loaiciga et al. [1993] have done some field investigations which imply that a deterministic trend for the log hydraulic conductivity could exist over a wide range of an area so that the assumption of stationarity for the log conductivity may be questionable.

Gelhar [1993], Rubin [1994] and Li and Mclaughlin [1995] have attempted to analyze the effect of log hydraulic conductivity with a trend on the stochastic structure of groundwater flow. Their studies were limited to the cases where the trend of the log conductivity is parallel or orthogonal to the mean gradient of the flow. Regarding the trend as varying slowly and the product of the trend and correlation scale is small relative to 1, Gelhar assumed that local stationarity will exist. Then he used the Spectral Representation Theorem to analyze the stochastic character of groundwater flow.

By introducing a non–stationary spectral theory, Li and Mclaughlin [1995] developed

the stochastic analysis for groundwater flow when lnK has a linear trend only along the mean gradient direction. They assumed that the head perturbation could be expressed as the extension of the Fourier–Stieljes integral representation:

$$h(\boldsymbol{x}) = \int_{-\infty}^{\infty} \phi_{hf}(\boldsymbol{x},\boldsymbol{k}) dZ_f(\boldsymbol{k}) \qquad (2\text{–}1\text{–}1)$$

where $\phi_{fh}(\mathbf{x},\mathbf{k})$ is an unknown complex–valued transfer function.

After substituting this transformation into the perturbation equation, $\phi_{fh}(\mathbf{x},\mathbf{k})$ was solved as

$$\phi_{fh}(\boldsymbol{x},\boldsymbol{k}) = \frac{ik_1 J(x)}{k^2 + iB_1 k_1} e^{i\boldsymbol{k}\cdot\boldsymbol{x}} \qquad (2\text{–}1\text{–}3)$$

where B_1 is the slope of the log conductivity trend along the mean gradient direction. and $J(x_1)$ is the mean gradient.

In the stationary spectral approach we can be sure of an unique spectral representation. However, for the non–stationary problem, the uniqueness can not be assured. Alternately, one can find an "exact" solution for the head perturbation h(**x**) by using Greens function. The free–space Greens function for h(**x**) is [Gutjahr, 1994]

$$h(\boldsymbol{x}) = -\frac{1}{2\pi} \int_{-\infty}^{\infty} K_0\left[\beta|\boldsymbol{x} - \boldsymbol{y}|e^{\beta y_1} J(y_1) \frac{\partial f(y)}{\partial y_1} dy\right] \qquad (2\text{–}1\text{–}2)$$

$$\beta = \frac{B_1}{2}$$

where the integral is a double integral over y_1, y_2 space and K_0 is a modified Bessel function of zero order.

The analytical result we solved for the log conductivity–head cross–covariance is exactly the same as the solution which Li and Mclaughlin deduced by the non–stationary spectral representation.

The Greens function analysis directly solves the perturbation equation and does not

make any assumptions about the head perturbation. Since both the Greens function and non–stationary solutions agree, at least in this case the non–stationary spectral approach is unique.

For the non–stationary spectral method, only if $\phi_{fh}(\mathbf{x},\mathbf{k})$ can be expressed as

$$\phi_{fh}(x,k) = f(x)g(k) \qquad (2\text{–}1\text{–}3)$$

is this method meaningful. Li and Mclaughlin assumed that the trend is along the mean gradient direction so that the mean head partial differential equation becomes an ordinary differential equation which is easily solved. For that special case, $\phi_{fh}(\mathbf{x},\mathbf{k})$ can be solved to be the form of (2–1–3). However, if the trend does not coincide with the mean gradient, the non–stationary spectral method of Li and Mclaughlin may not be as useful.

Finally, although Li and Mclaughlin stated their problem formulation with the simple Dirichlet and Neuman boundaries, their solution is free from the boundary condition. By comparison with our free–space Green function analysis, the solution of the non–stationary spectral method consequently is suitable for the infinite domain.

Note that the Greens function analysis is generally more meaningful because it does not require any special assumption for the trend. On the other hand, the non–stationary spectral method is a simple method to apply. Rubin and Seong [1994] used the Greens function to analyze the moments of the velocity and the hydraulic head for the cases where the trend of log conductivity is aligned or perpendicular to the head gradient.

The variability of hydrogeological properties such as hydraulic conductivity is generally attributed to the cumulative effects of different geological processes. It reflects the character of the sedimentary formations. However, the groundwater flow direction is influenced by the regional discharge and recharge of an aquifer. Thus in the most general cases, the gradient vector **J** and the trend vector **B** form some arbitrary angle in space.

The purpose of this study is to derive the cross–covariance between the log conductivity and hydraulic head and not limit the trend direction of the log conductivity; namely, the angle between the trend of the log conductivity and the flow gradient is arbitrary. Both Greens functions and Monte Carlo simulation will be used to approach this problem. The solutions will be extended to a special case and compared with the previous analytical forms.

The remainder of this chapter proceeds as follows. Section 2 presents the problem formulation for groundwater flow in trending, heterogeneous media. In this part, we separate the original equation into two subequations which are the mean equation and the perturbation equation. In section 3, the mean equations for two typical boundaries are solved. The results are presented for trends of different magnitudes and the influence of the trend on the mean head distribution is discussed. Section 4 is main part of this chapter where both Monte Carlo simulation and Greens functions analysis will be used to analyze the correlation structure between the head and the log conductivity with trend in any direction. The solutions are extended to a special case and compared with the previous analytical forms [Li and Mclaughlin, 1994, Gelhar, 1993].

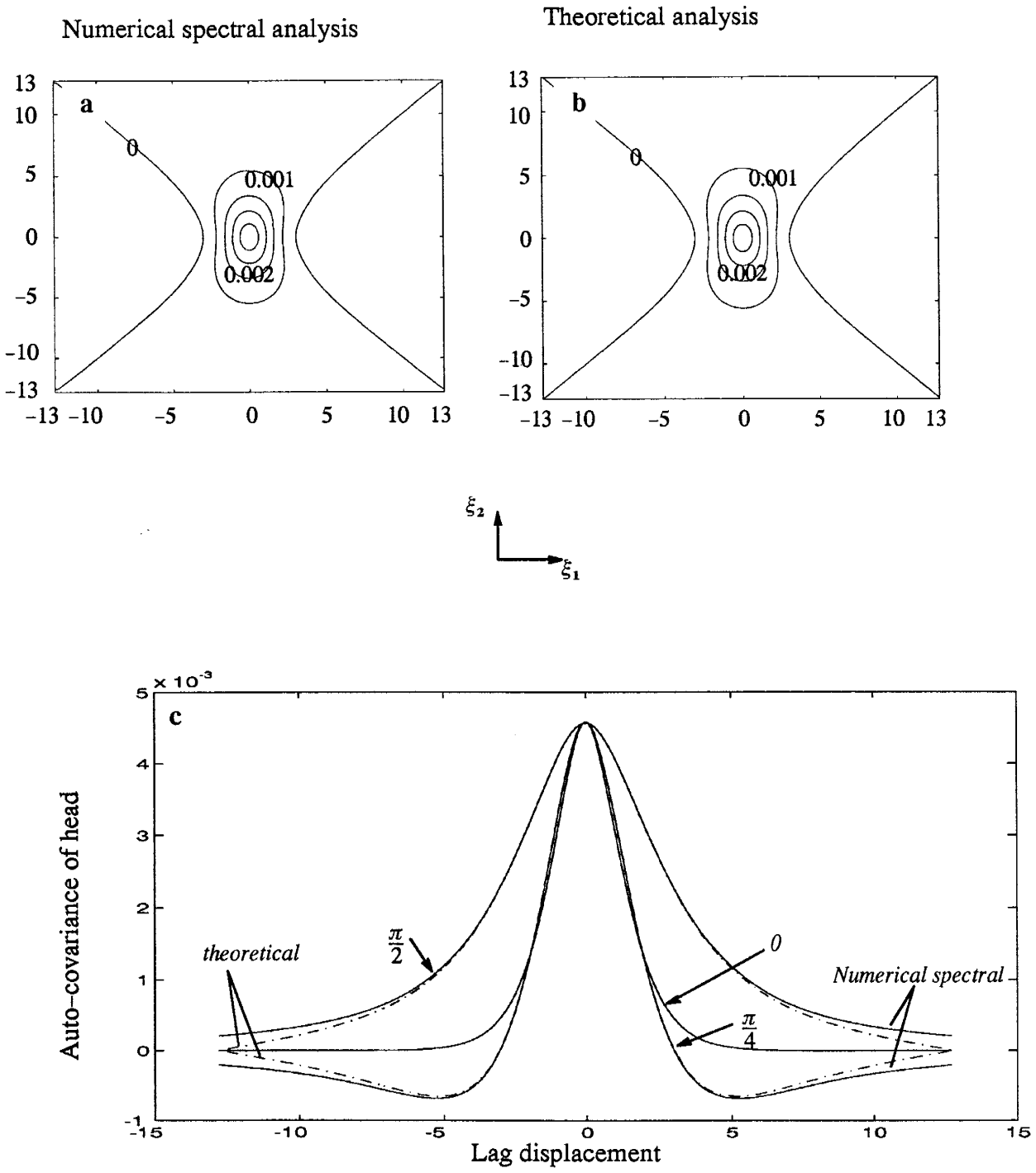

Figure 1-1: Auto-covariance of hydraulic head: a) the contour of the head auto-covariance by the numerical spectral method; b) the contour of the theoretical head auto-covariance; c) the character of the head auto-covariance along different directions. Axes labels of the contour are lag distance.

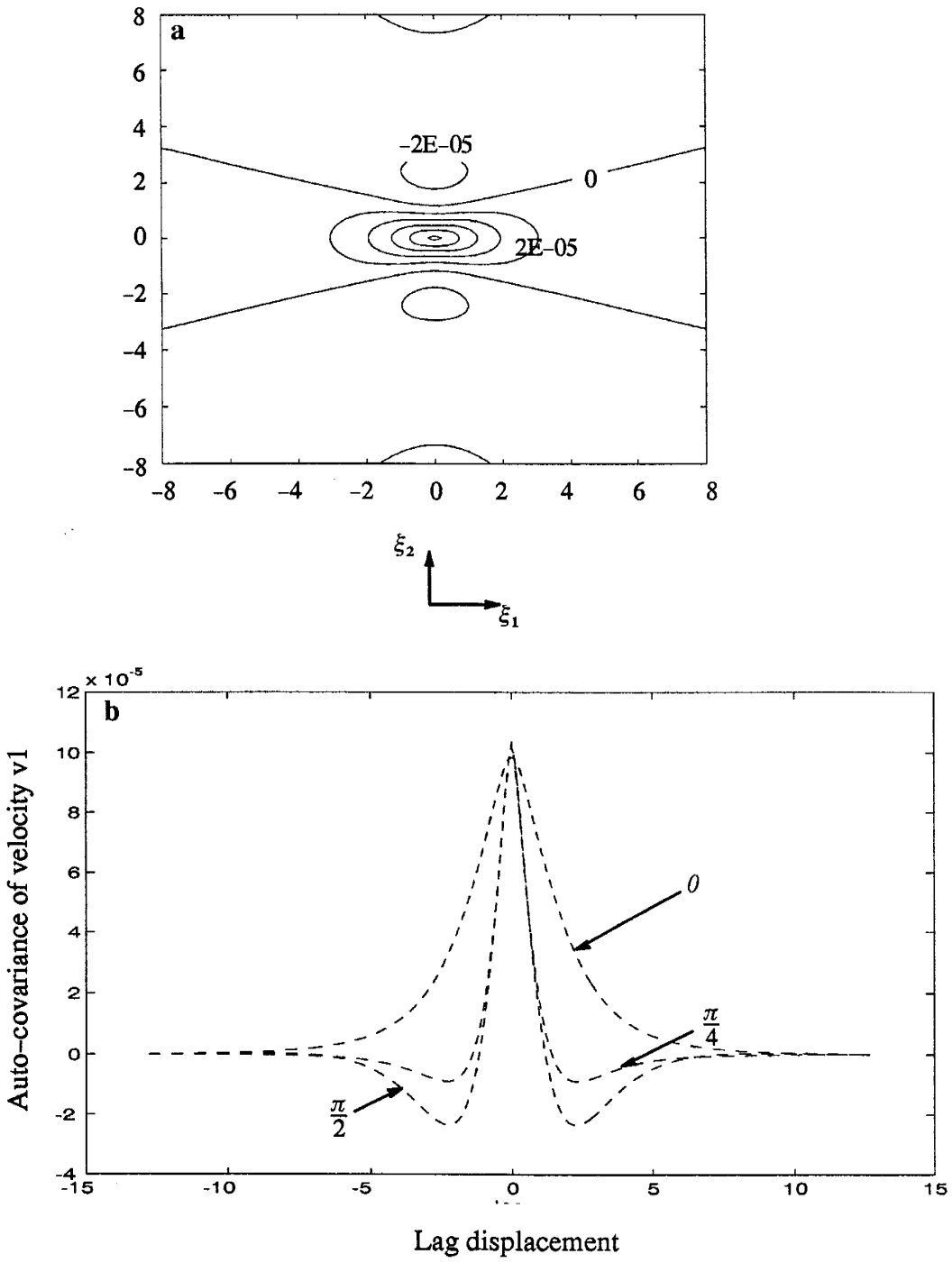

Figure 1-2: Auto-covariance distribution for the velocity v_1 (velocity along x_1 direction): a) the contour of v_1 auto-covariance. b) the character of the v_1 auto-covariance along different directions.

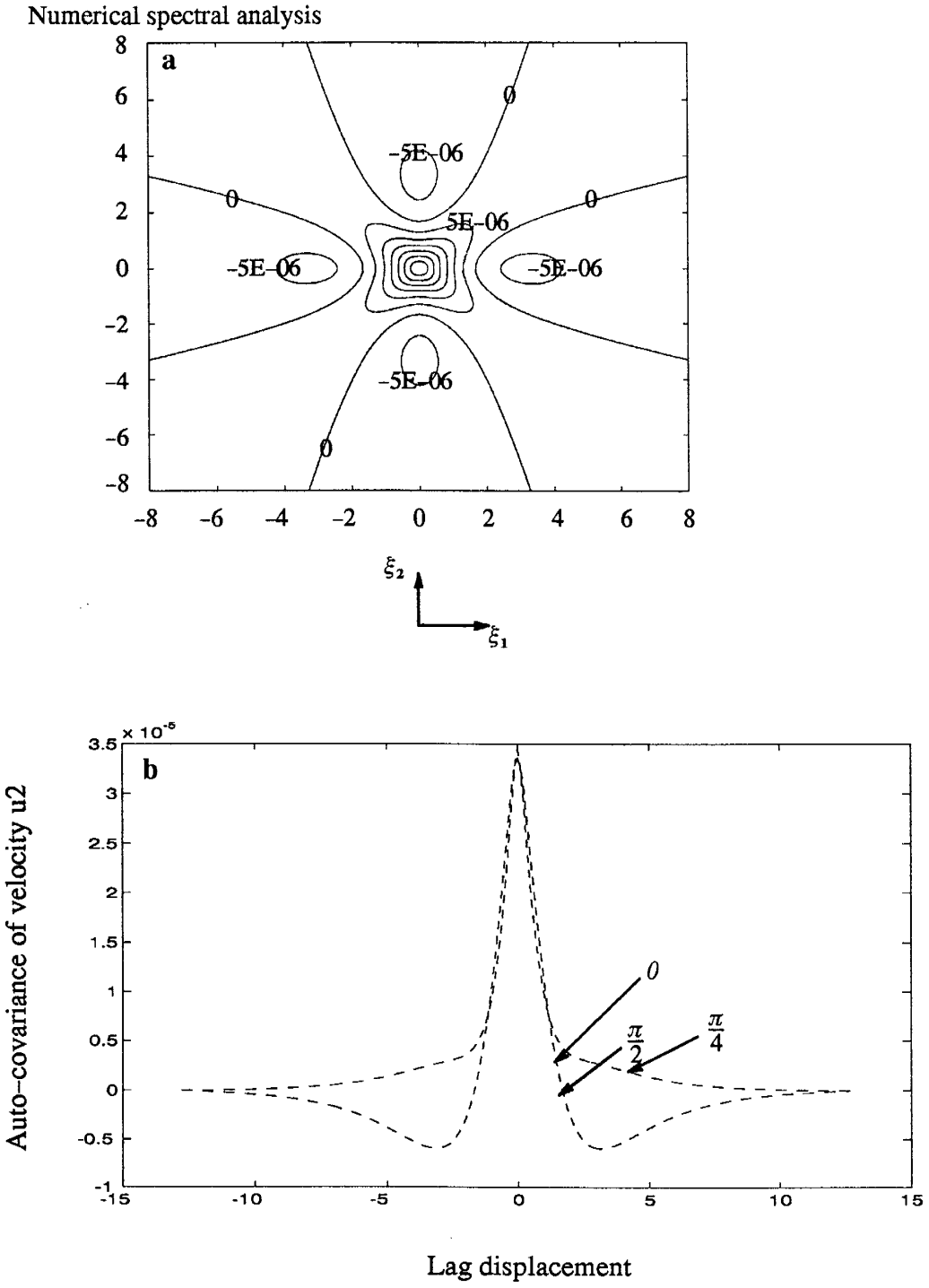

Figure 1-3: Auto-covariance distribution for the velocity v_2 (velocity along x_2 direction): a) the contour of v_2 auto-covariance. b) the character of the v_2 auto-covariance along different directions.

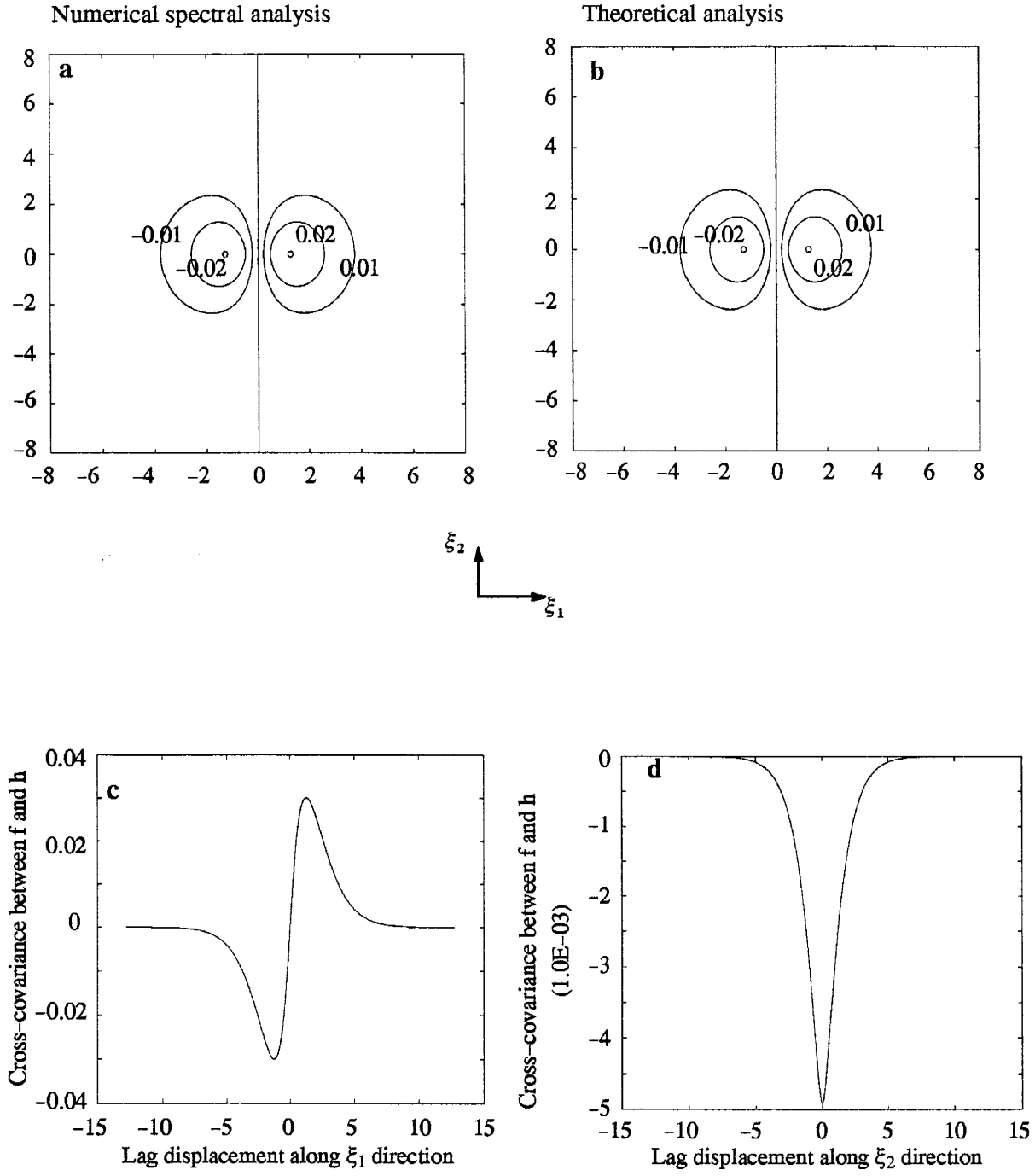

Figure 1-4: Cross-covariance between log conductivity and head: a) the contour of the cross-covariance between f and h by numerical spectral method; b) the contour of the theoretical cross-covariance between f and h; c) the cross-covariance between f and h along ξ_1; d) the cross-covariance between f and h along ξ_2.

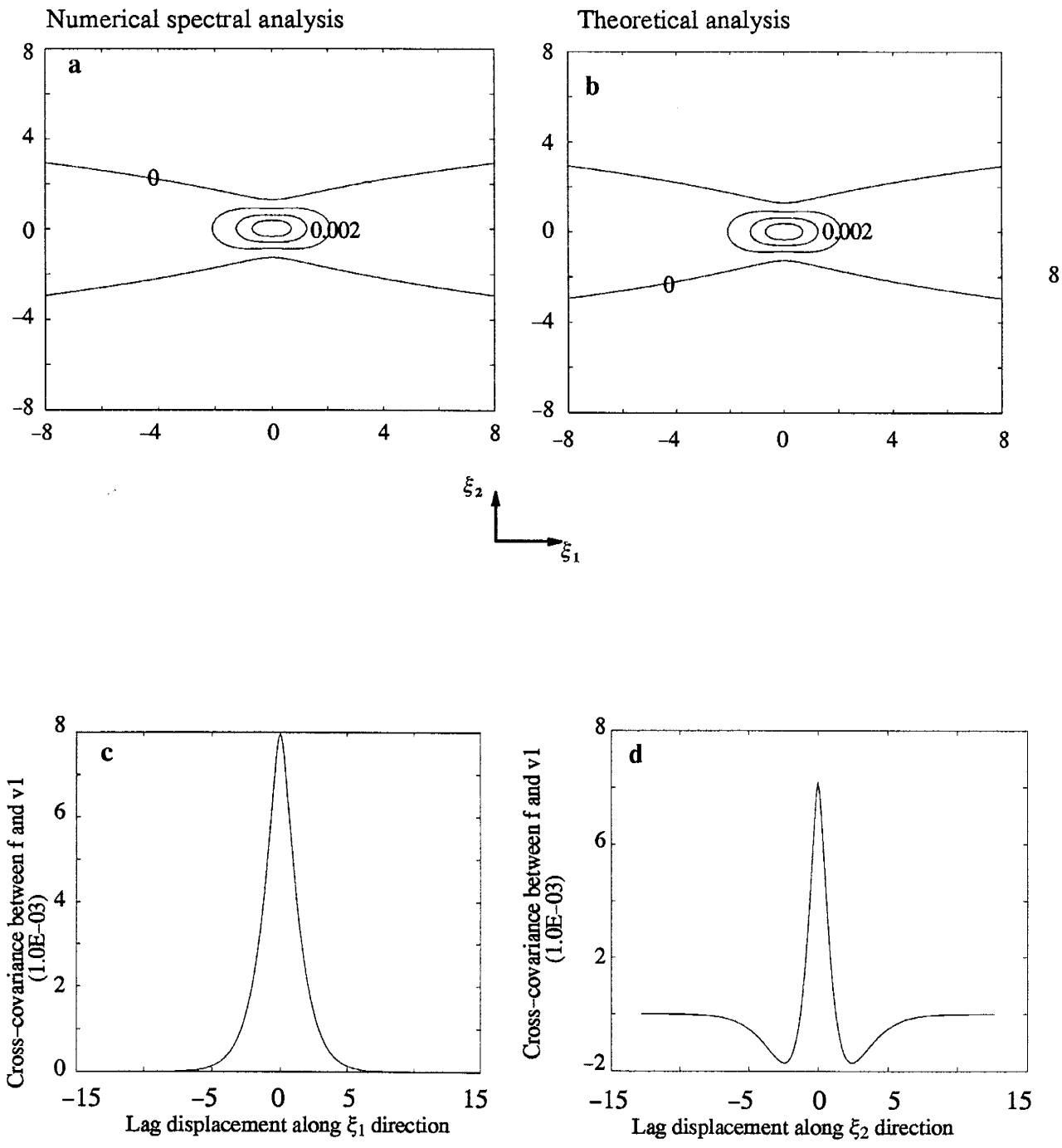

Figure 1-5: Cross-covariance between log conductivity and velocity v_1: a) the contour of the cross-covariance between f and v_1 by numerical spectral method; b) the contour of the theoretical cross-covariance between f and v_1; c) the cross-covariance between f and v_1 along ξ_1; d) the cross-covariance between f and v_1 along ξ_2.

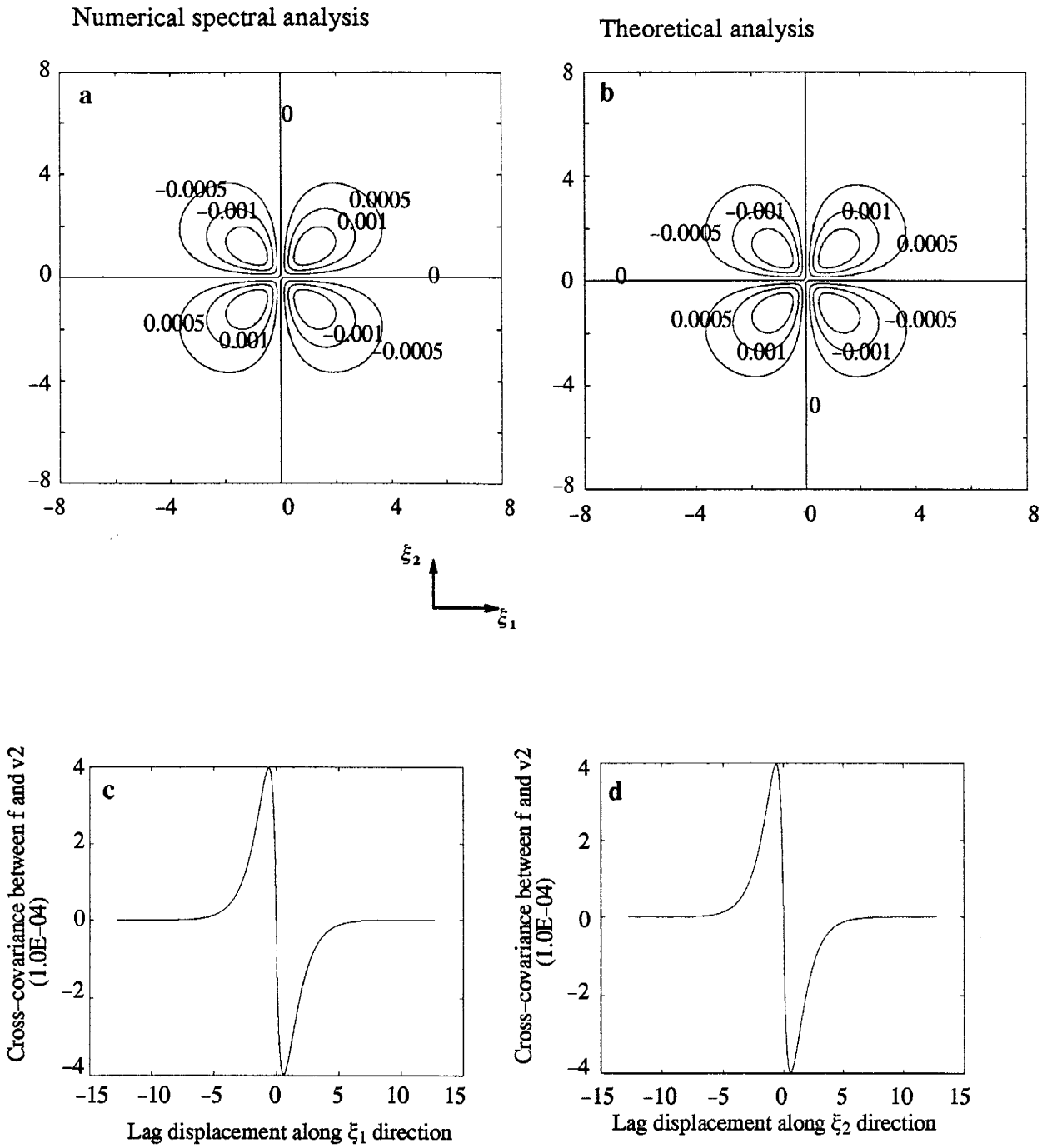

Figure 1-6: Cross-covariance between log conductivity and velocity v_2: a) the contour of the cross-covariance between f and v_2 by numerical spectral method; b) the contour of the theoretical cross-covariance between f and v_2; c) the cross-covariance between f and v_2 along ξ_1; d) the cross-covariance between f and v_2 along ξ_2.

Numerical spectral analysis

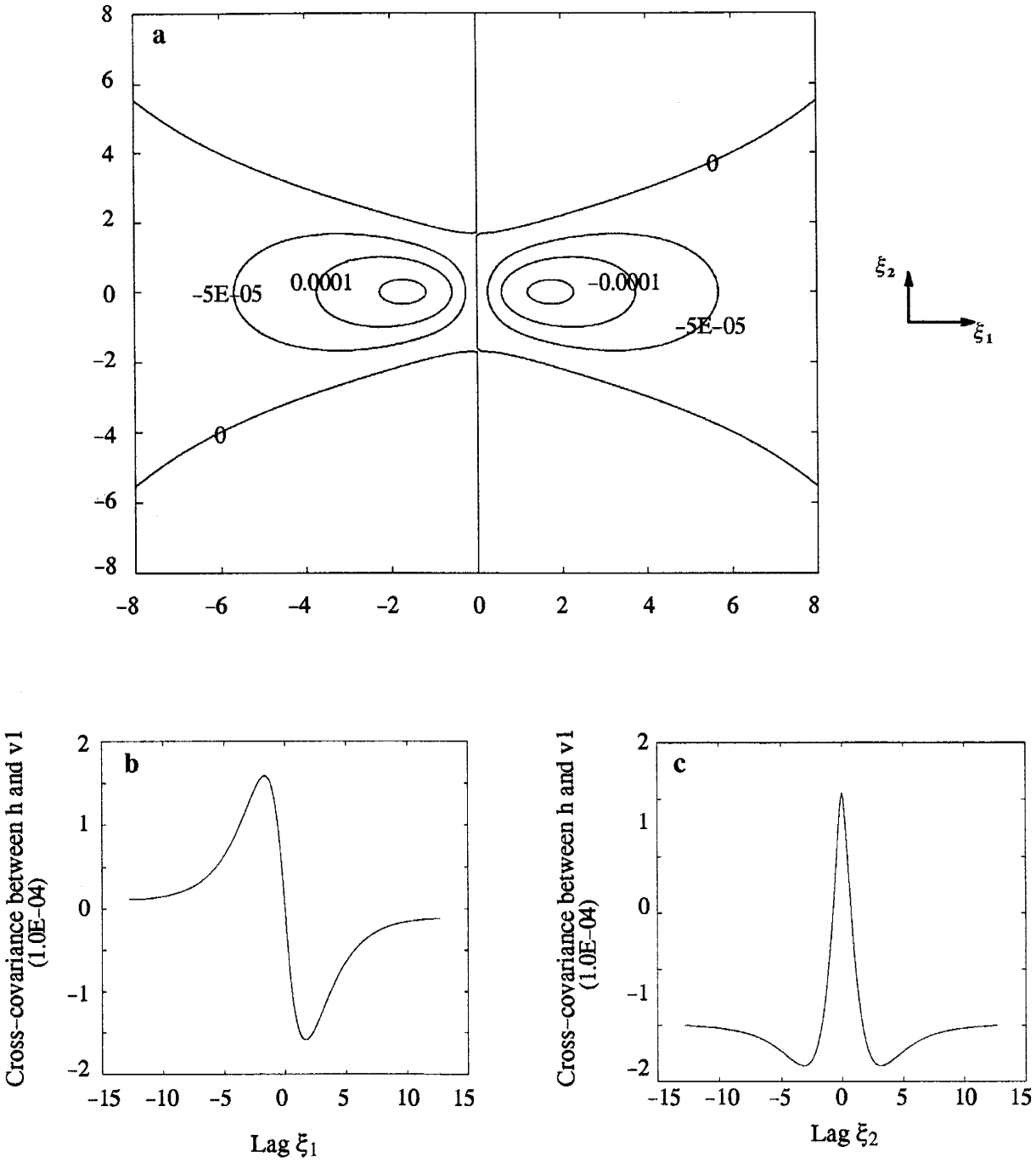

Figure 1-7: Cross-covariance between head and velocity v_1: a) the contour of the cross-covariance between h and v_1 by numerical spectral method; b) the cross-covariance between h and v_1 along ξ_1; c) the cross-covariance between h and v_1 along ξ_2.

Numerical spectral analysis

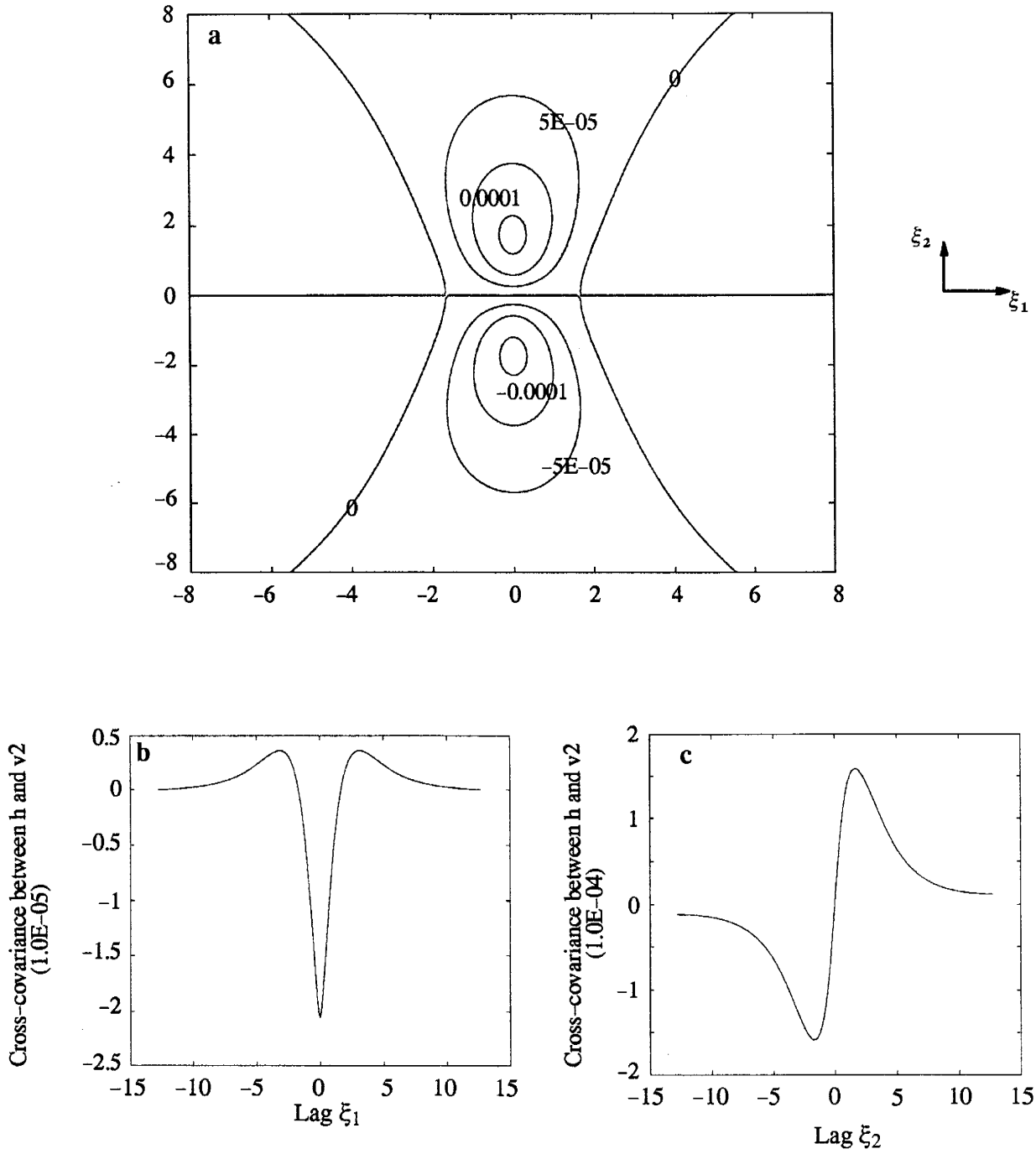

Figure 1-8: Cross-covariance between head and velocity v_2: a) the contour of the cross-covariance between h and v_2 by numerical spectral method; b) the cross-covariance between h and v_2 along ξ_1; c) the cross-covariance between h and v_2 along ξ_2.

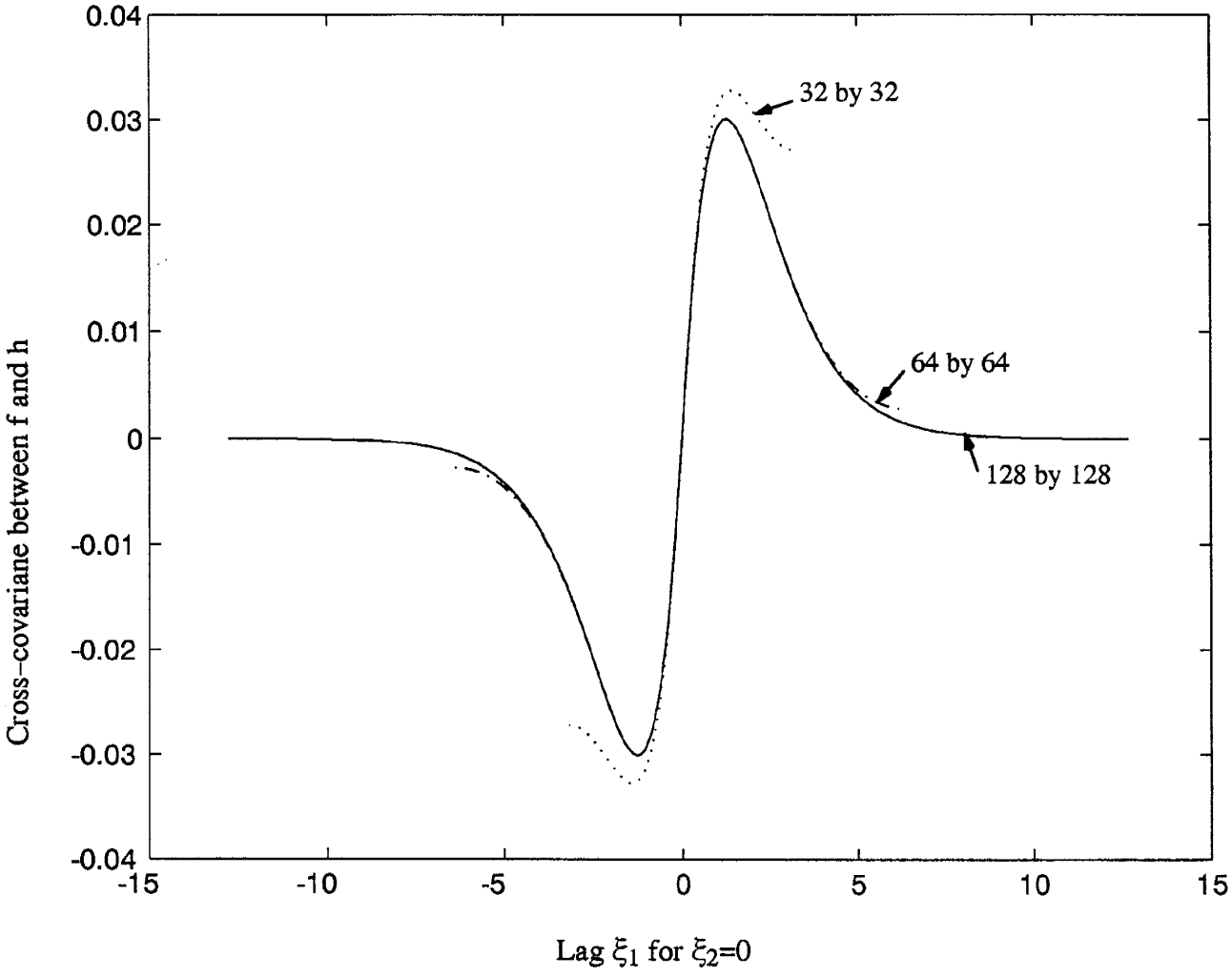

Figure 1-9: Comparison of the cross-covariance between f and h for different domain sizes.

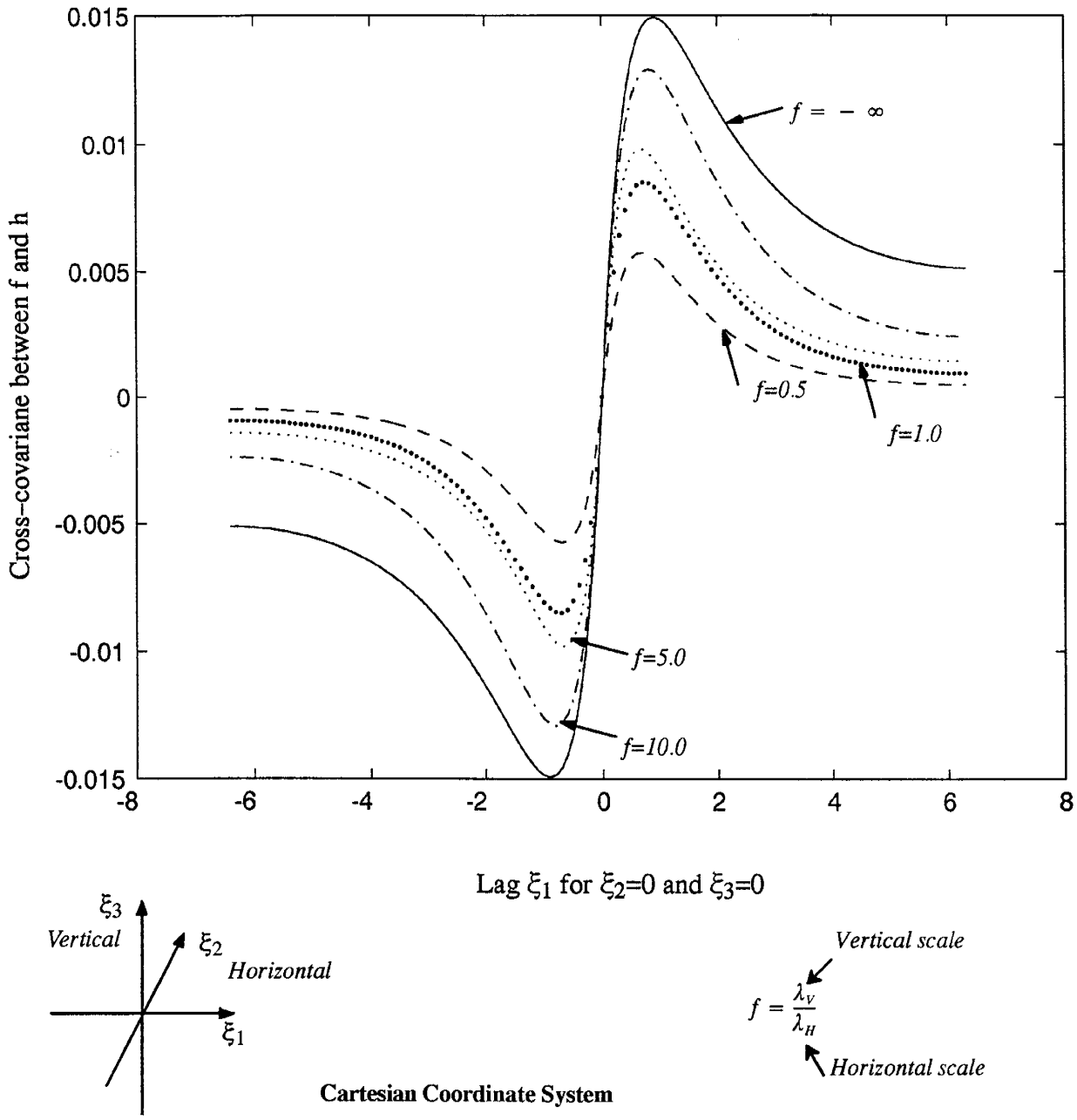

Figure 1-10: Comparison of the cross-covariance between f and h for different ratios of the horizontal and vertical log conductivity correlation scales.

Monte Carlo simulation

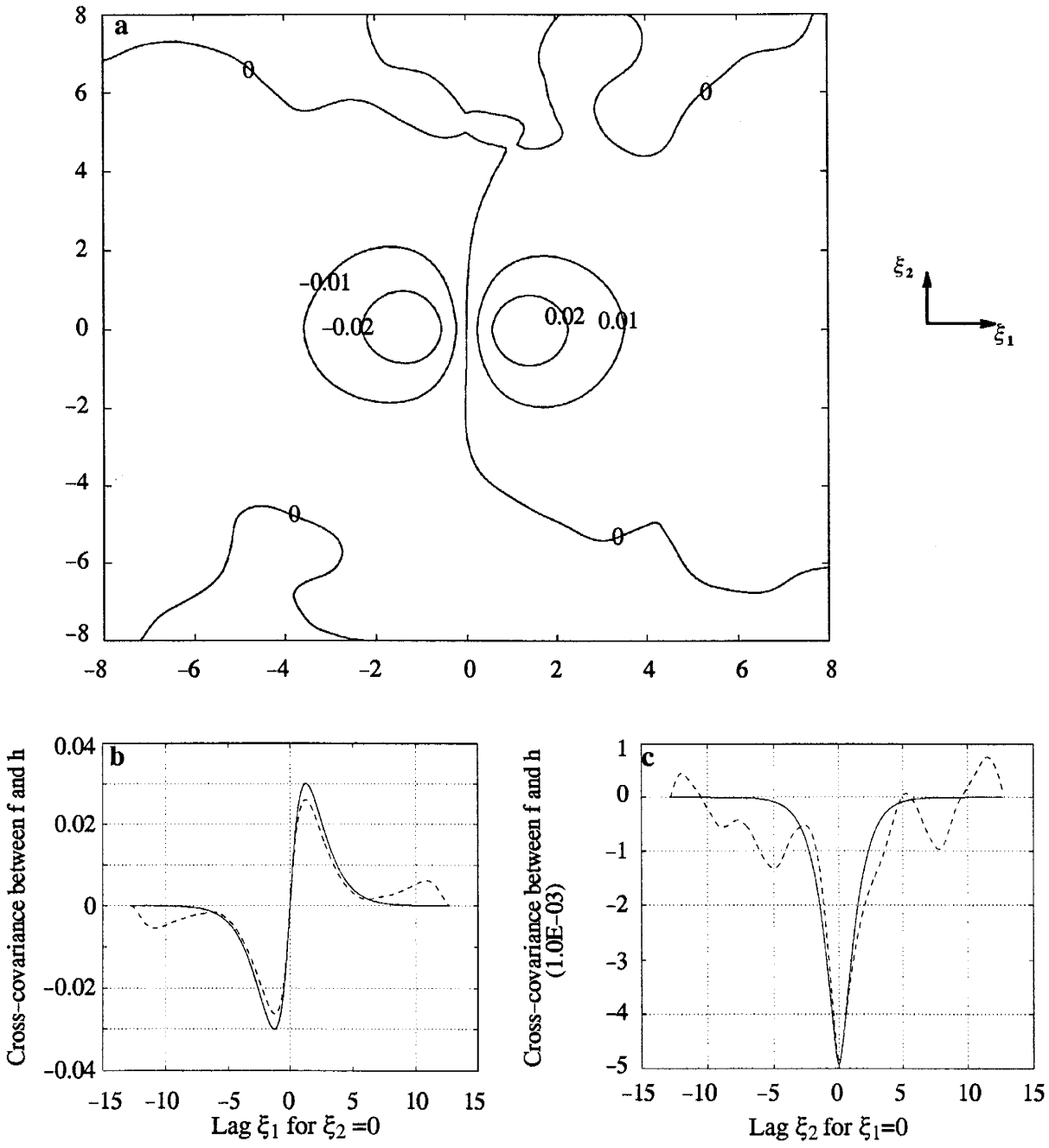

Figure 1-12: Cross-covariance between log conductivity and head: a) the contour of the cross-covariance between f and h by Monte Carlo simulation; b) and c) the comparation of the solutions between the Monte Carlo simulation and numerical spectral analysis along ξ_1 and ξ_2.

Monte Carlo simulation

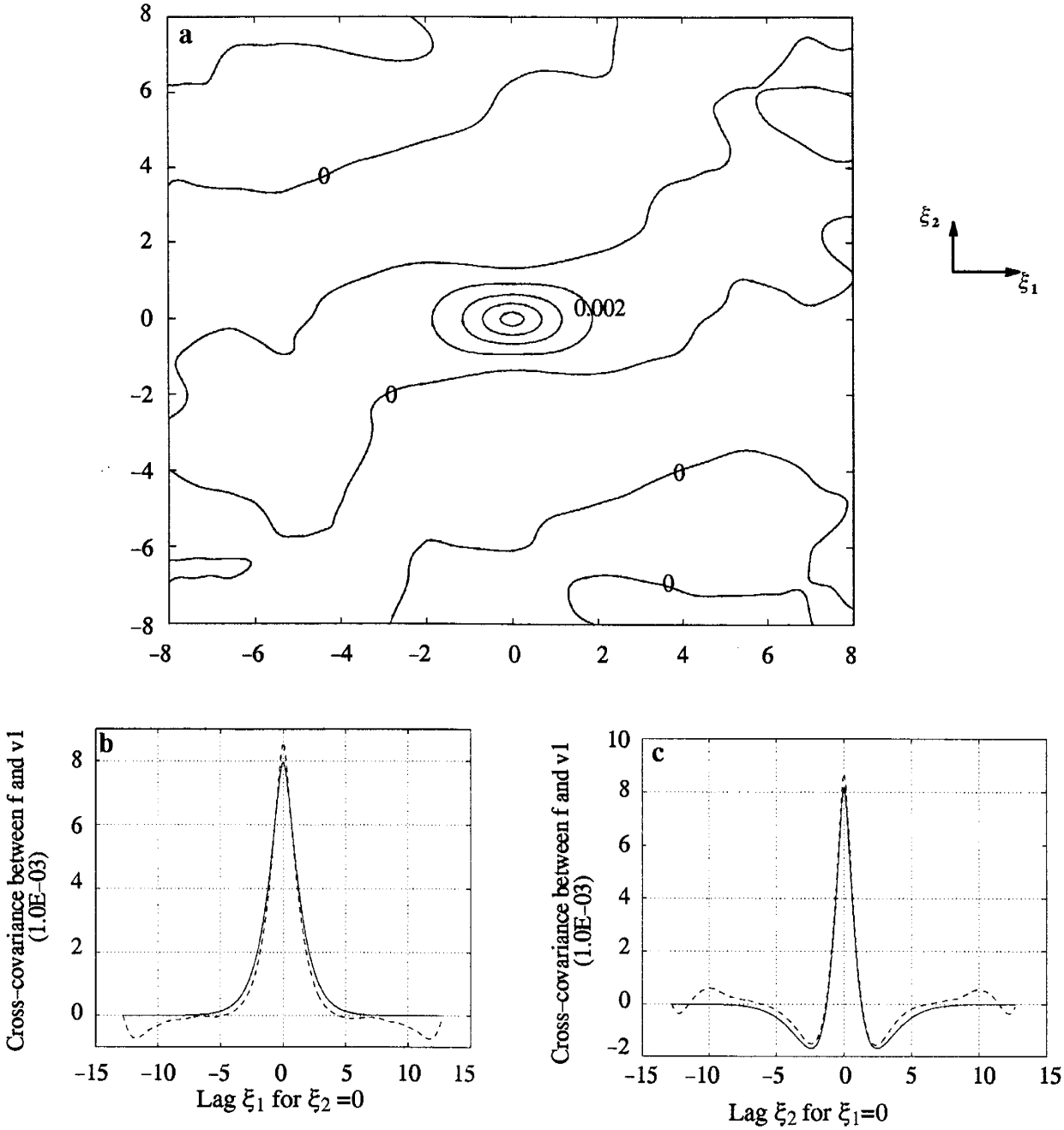

Figure 1-13: Cross-covariance between log conductivity and velocity v_1: a) the contour of the cross-covariance between f and v_1 by Monte Carlo simulation; b) and c) the comparation of the solutions between the Monte Carlo simulation and numerical spectral analysis along ξ_1 and ξ_2.

Monte Carlo simulation

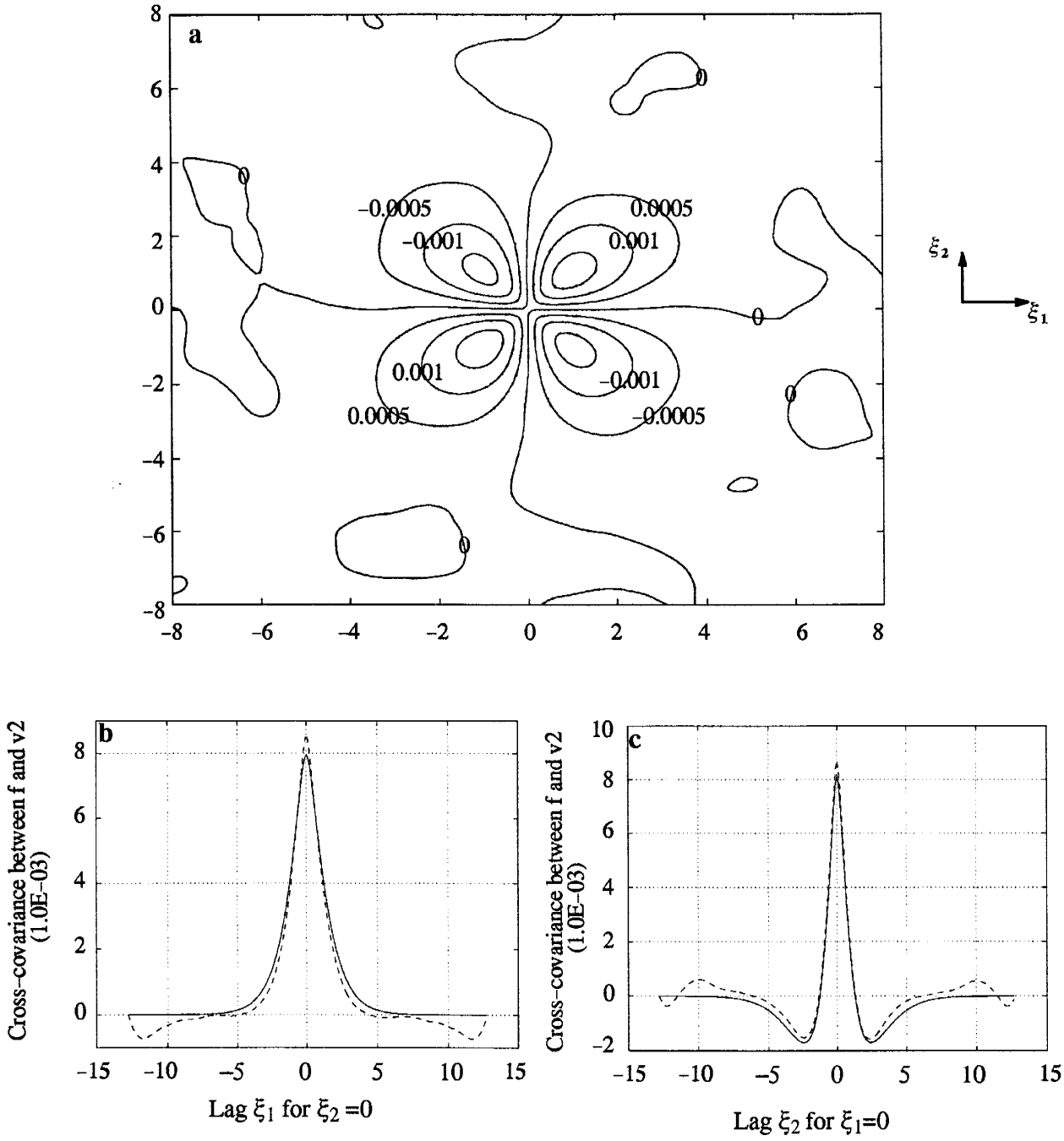

Figure 1-14: Cross-covariance between log conductivity and velocity v_2: a) the contour of the cross-covariance between f and v_2 by Monte Carlo simulation; b) and c) the comparation of the solutions between the Monte Carlo simulation and numerical spectral analysis along ξ_1 and ξ_2.

Monte Carlo simulation

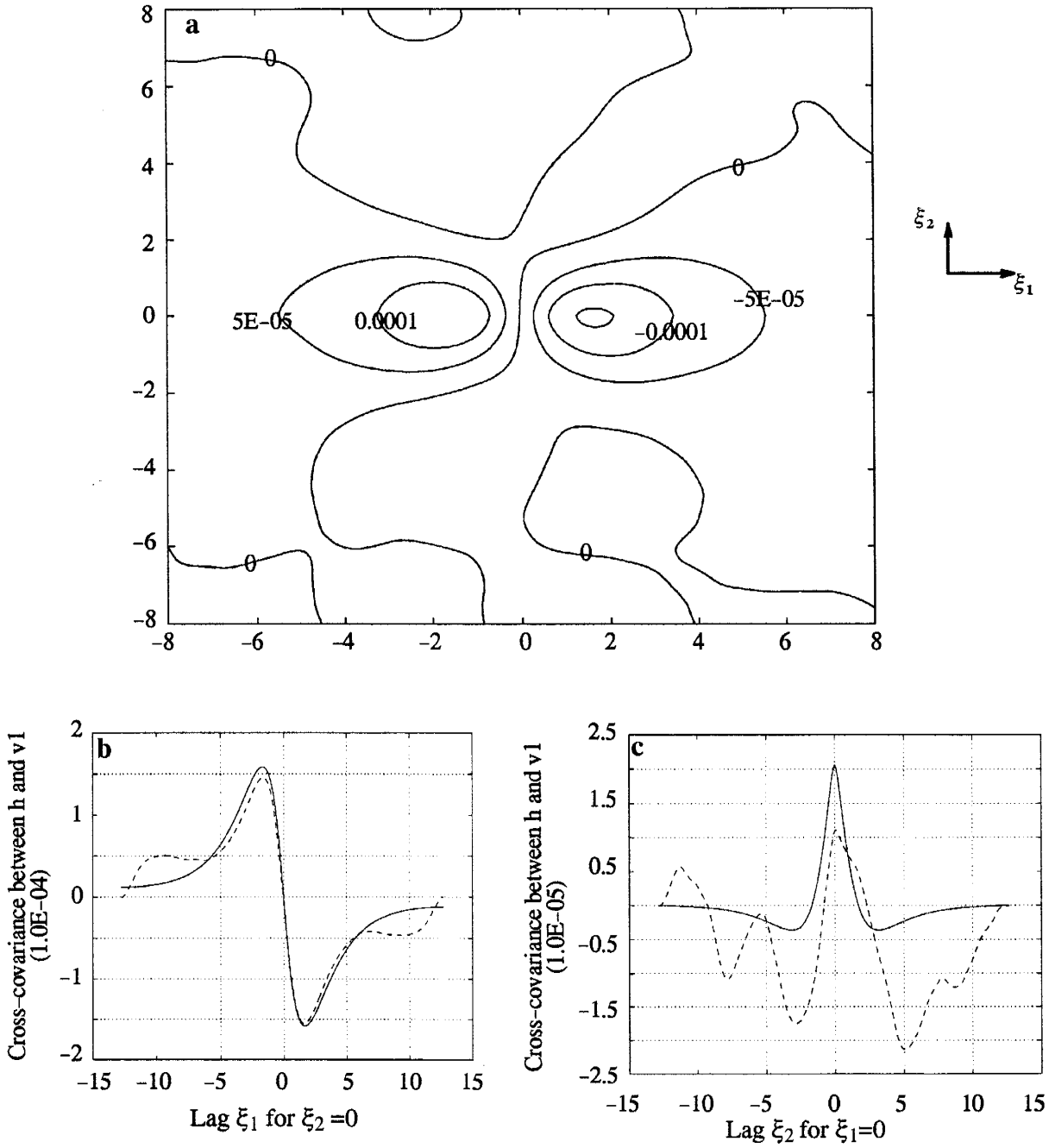

Figure 1-15: Cross-covariance between head and velocity v_1: a) the contour of the cross-covariance between h and v_1 by Monte Carlo simulation; b) and c) the comparation of the solutions between the Monte Carlo simulation and numerical spectral analysis along ξ_1 and ξ_2.

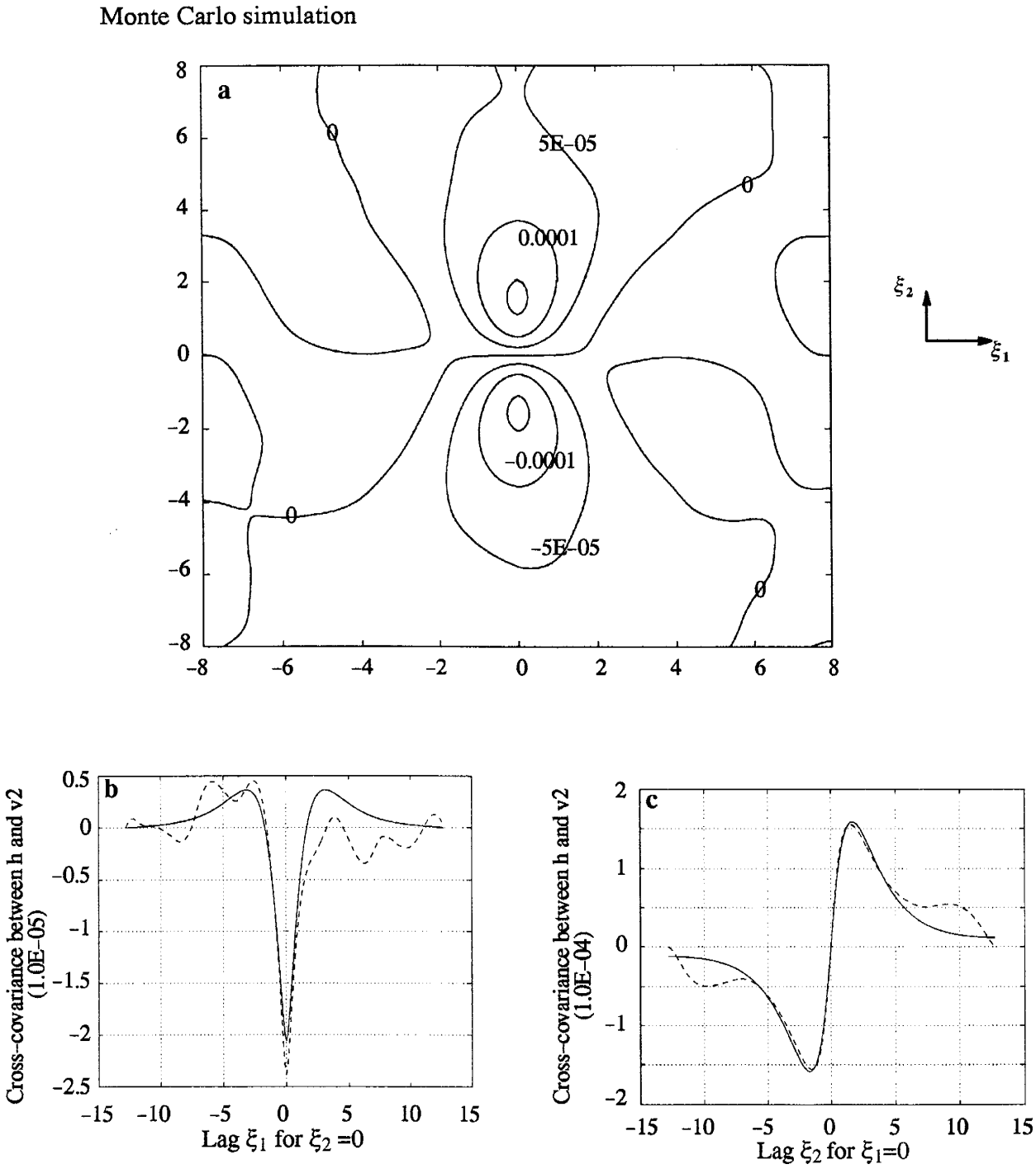

Figure 1-16: Cross-covariance between head and velocity v_2: a) the contour of the cross-covariance between h and v_2 by Monte Carlo simulation; b) and c) the comparation of the solutions between the Monte Carlo simulation and numerical spectral analysis along ξ_1 and ξ_2.

2.2 Mathematical Formulation

In this section we develop the mean flow equation whose solution describes the dominant behavior of the hydraulic heads and the governing perturbation equation whose solution represents the spatial variability in head induced by aquifer heterogeneity. The log conductivity is assumed to have a linear trend. The partitioning of the log conductivity with a linear trend is:

$$LnK = \mu + \boldsymbol{B} \cdot x + f(x) \qquad (2\text{–}2\text{–}1)$$

$$E[LnK] = \mu + \boldsymbol{B} \cdot x$$

where μ and $\mathbf{B}= (B_1, B_2, ..., B_m)$, i=1, ..., m, are constants. The random fluctuation, f(x), is assumed to be weakly stationary, of zero mean. This model has been considered by Gelhar [1986, 1993] and Loaiciga et al. [1993].

We consider the case of steady state, two–dimensional flow with heterogeneous conductivity governed by the following flow equation:

$$\nabla^2\phi(x) + \nabla(LnK(x)) \cdot \nabla\phi(x) = 0 \qquad x \in \Omega \qquad (2\text{–}2\text{–}2)$$

where $K(\mathbf{x})$ is hydraulic conductivity and $\phi(\mathbf{x})$ is hydraulic head, and Ω is a bounded domain.

Two types of the common boundary conditions are used with the equation (2–2–2). They are shown as following:

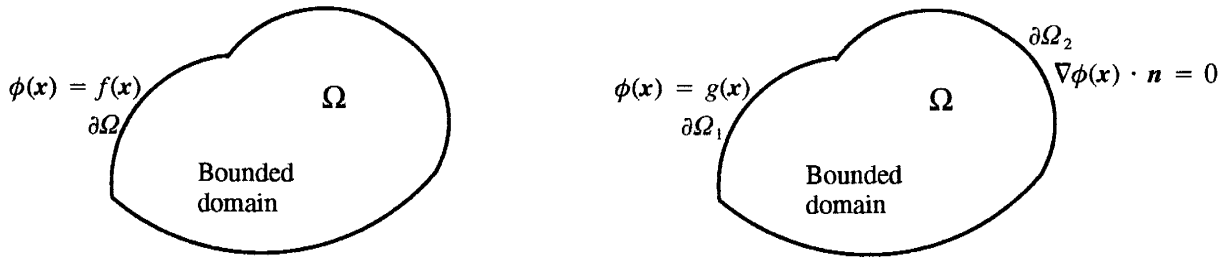

Type A (a) Type B (b)

Figure 2–1: Schematic of two types boundary conditions where Ω is a bounded domain, $f(\mathbf{x})$ and $g(\mathbf{x})$ are known functions and $\mathbf{n}$ is the unit outward vector normal to the domain boundary: a) Type A: Dirichlet boundary conditions on $\partial\Omega$. b) Type B: Dirichlet boundary conditions on $\partial\Omega_1$ and Neumann boundary conditions on $\partial\Omega_2$.

As in the previous analysis, LnK and $\phi(\mathbf{x})$ are expressed as the sum of deterministic (ensemble average) and perturbation components; namely

$$\begin{aligned} LnK(\boldsymbol{x}) &= F(\boldsymbol{x}) + f(\boldsymbol{x}); \qquad E[f(\boldsymbol{x})] = 0 \\ \phi(\boldsymbol{x}) &= H(\boldsymbol{x}) + h(\boldsymbol{x}) \quad ; \qquad E[h(\boldsymbol{x})] = 0 \end{aligned} \qquad (2\text{–}2\text{–}3)$$

where $F(x)=E[lnk]=\mu+\mathbf{B}\cdot\mathbf{x}$, $\mathbf{B}$ is a linear trend for LnK and $H(\mathbf{x})$ is the ensemble mean of the hydraulic head; both $f(\mathbf{x})$ and $h(\mathbf{x})$ are zero mean perturbations.

Substituting (2–2–3) into equation (2–2–2) leads to

$$\nabla^2 H(\boldsymbol{x}) + \nabla^2 h(\boldsymbol{x}) + \boldsymbol{B}\cdot\nabla H(\boldsymbol{x}) + \boldsymbol{B}\cdot\nabla h(\boldsymbol{x}) + \nabla f(\boldsymbol{x})\cdot\nabla H(\boldsymbol{x}) + \nabla f(\boldsymbol{x})\cdot\nabla h(\boldsymbol{x}) = 0 \qquad (2\text{–}2\text{–}4)$$

The equation for mean flow is found by taking the expectation of (2–2–4)

$$\nabla^2 H(\boldsymbol{x}) + \boldsymbol{B}\cdot\nabla H(\boldsymbol{x}) = 0 \qquad (2\text{–}2\text{–}5)$$

where $E[\nabla f(\mathbf{x})\cdot\nabla h(\mathbf{x})]$ is dropped. Corresponding to the mean equation (2–2–7), the boundary conditions are:

Type A: $$H(\boldsymbol{x}) = f(\boldsymbol{x}) \qquad \boldsymbol{x}\in\partial\Omega \qquad (2\text{–}2\text{–}6)$$

Type B: $$\begin{aligned} H(\boldsymbol{x}) &= g(\boldsymbol{x}) \qquad \boldsymbol{x}\in\partial\Omega_1 \\ \nabla H(\boldsymbol{x})\cdot\boldsymbol{n} &= 0 \quad \boldsymbol{x}\in\partial\Omega_2 \end{aligned} \qquad (2\text{–}2\text{–}7)$$

Subtracting (2–2–5) from (2–2–4) yields the governing perturbation equation by neglecting the second order perturbation products:

$$\nabla^2 h(\boldsymbol{x}) + \boldsymbol{B}\cdot\nabla h(\boldsymbol{x}) + \nabla H(\boldsymbol{x})\cdot\nabla f(\boldsymbol{x}) = 0 \qquad (2\text{–}2\text{–}8)$$

The boundary conditions of the perturbation equation will be

Type A: $$h(\boldsymbol{x}) = 0 \qquad \boldsymbol{x}\in\partial\Omega \qquad (2\text{–}2\text{–}9)$$

Type B $$\begin{aligned} h(\boldsymbol{x}) &= 0 \qquad \boldsymbol{x}\in\partial\Omega_1 \\ \nabla h(\boldsymbol{x})\cdot\boldsymbol{n} &= 0 \quad \boldsymbol{x}\in\partial\Omega_2 \end{aligned} \qquad (2\text{–}2\text{–}10)$$

We are interested in finding the correlation between log conductivity and head from the perturbation equation. If the log conductivity is a stationary process with no trend, the Fourier–Stieltjes representation theorem can be used to obtain the cross–covariance of log conductivity and head. Extensive discussions for the stationary case have been presented in the previous chapter. Here we consider the case where log conductivity has a linear trend. In this case, an unique non–stationary spectral representation is not ensured. Instead the log conductivity–head cross–covariance will be derived by directly solving the perturbation equation (2–2–8).

From equation (2–2–8), a head fluctuation h(**x**) can not be solved unless a mean head H(**x**) is known. Consequently, our stochastic analysis for the non–stationary problem will begin by solving the mean flow equation (2–2–5).

2.3 Mean Head Distribution for Groundwater Flow Through Trending Media

As an illustration, consider the rectangular domain below with type A boundary conditions:

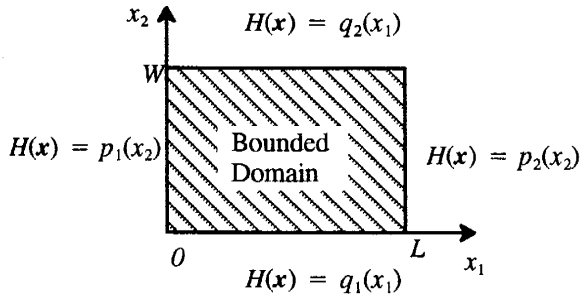

Figure 2–2: Schematic of a specific Type A boundary conditions: the length of bounded domain is L and the width is W.

Then the mean head partial differential flow equation for this problem domain and type A boundary can be expressed as:

$$\begin{aligned} &\nabla^2 H(x) + \boldsymbol{B} \cdot \nabla H(x) = 0 \\ &H(0, x_2) = p_1(x_2) \\ &H(L, x_2) = p_2(x_2) \\ &H(x_1, 0) = q_1(x_1) \\ &H(x_1, W) = q_2(x_1) \end{aligned} \qquad (2\text{–}3\text{–}1)$$

Equation (2–3–1) is solved by the Separation of Variables method. After some manipulation, the solution of H(**x**) obtained is :

$$H(x) = H_A(x) + H_B(x) + H_C(x) + H_D(x) \qquad (2\text{–}3\text{–}2)$$

where

$$H_A(x) = \sum_{n=1}^{\infty} C_n^A e^{(-\frac{B\cdot x}{2})} \sin(\frac{n\pi x_1}{L}) \sinh[\gamma_n(W - x_2)]$$

$$C_n^A = \frac{2}{L\sinh(\gamma_n W)} \int_0^L q_1(x_1) e^{\frac{B_1}{2}} \sin(\frac{n\pi x_1}{L}) dx_1$$

$$H_B(x) = \sum_{n=1} C_n^B e^{(-\frac{B\cdot x}{2})} \sin(\frac{n\pi x_1}{L}) sinh(\gamma_n x_2)$$

$$C_n^B = \frac{2}{L\sinh(\gamma_n W)} e^{(\frac{B_2 W}{2})} \int_0^L q_2(x_1) e^{\frac{B_1 x_1}{2}} \sin(\frac{n\pi x_1}{L}) dx_1$$

$$H_C(x) = \sum_{n=1} C_n^C e^{(-\frac{B\cdot x}{2})} \sin(\frac{n\pi x_2}{W}) sinh[\delta_n(L - x_1)]$$

$$C_n^C = \frac{2}{W\sinh(\delta_n L)} \int_0^W p_1(x_2) e^{\frac{B_2 x_2}{2}} \sin(\frac{n\pi x_2}{W}) dx_2$$

$$H_D(x) = \sum_{n=1} C_n^D e^{(-\frac{B\cdot x}{2})} \sin(\frac{n\pi x_2}{W}) \sinh(\delta_n x_1)$$

$$C_n^D = \frac{2}{W\sinh(\delta_n L)} e^{(\frac{B_1 L}{2})} \int_0^W p_2(x_2) e^{\frac{B_2 x_2}{2}} \sin(\frac{n\pi x_2}{W}) dx_2$$

$$\gamma_n = \left(\frac{B_1^2 + B_2^2}{4} + \frac{n^2\pi^2}{L^2}\right)^{\frac{1}{2}}$$

$$\delta_n = \left(\frac{B_1^2 + B_2^2}{4} + \frac{n^2\pi^2}{W^2}\right)^{\frac{1}{2}}$$

We can use the closed form (2–3–2) to analyze the mean head distribution for the type A boundary condition.

Figure 2–3 shows the different mean head distributions with the change of the direction for the trend vector **B**. Here, we consider $p_1(x_2)=h_0$, $p_2(x_2)=0$, $q_1(x_1)=q_2(x_1)=h_0-h_0*x_1/L$, and a moderate trend $\|\mathbf{B}\|=0.30$. Figure 2–3 reveals that the influence of the trend vector **B** on the mean head distribution increases with the magnitude of the trend component in the mean head gradient (along x_1 axis). The graph shows that the mean head distribution is not influenced by the trend when the trend vector **B** is

orthogonal to the mean head gradient, whereas the mean head distribution largely depends on the magnitude of the trend vector **B** when the trend is aligned with the mean head gradient.

Next we consider the mean flow equation for a type B boundary:

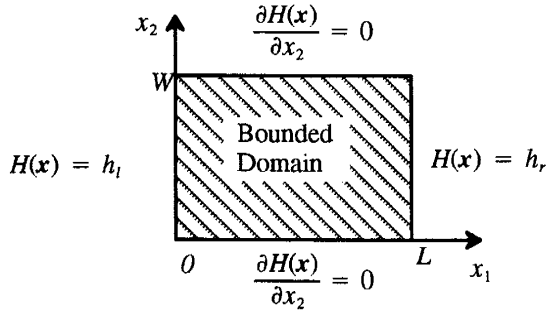

Figure 2–4: Schematic of the specific type B boundary conditions: The length of the domain is L and the width of the domain is W. h_l and h_r are constants, namely the left and right boundaries are constant heads, the bottom and top boundaries are no flow.

Then the mean head partial differential flow equation for this type B boundary can be obtained from (2–2–5) and (2–2–6):

$$\begin{aligned} &\nabla^2 H(\boldsymbol{x}) + \boldsymbol{B} \cdot \nabla H(\boldsymbol{x}) = 0 \\ &H(0, x_2) = h_l \\ &H(L, x_2) = h_r \\ &\frac{\partial H}{\partial x_2}(x_1, 0) = 0 \\ &\frac{\partial H}{\partial x_2}(x_1, W) = 0 \end{aligned} \qquad (2\text{–}3\text{–}3)$$

The partial differential equation (2–3–3) is homogeneous with the heterogeneous boundary conditions. let

$$g(\boldsymbol{x}) = H(\boldsymbol{x}) - h_l - \frac{(h_r - h_l)x_1}{L} \qquad (2\text{–}3\text{–}4)$$

Substituting (2–3–4) into equation (2–3–3) leads to

The equation (2–3–5) is non–homogeneous together with the homogeneous boundary conditions and can be solved by a Greens function method. The solution of g(**x**) obtained is: Substituting (2–3–6) into (2–3–4), we can solve for H(**x**):

$$\nabla^2 g(x) + \boldsymbol{B} \cdot \nabla g(x) = \frac{(h_l - h_r)}{L} \qquad (2\text{–}3\text{–}5)$$

$$g(0, x_2) = 0$$

$$g(L, x_2) = 0$$

$$\frac{\partial g}{\partial x_2}(x_1, 0) = 0$$

$$\frac{\partial g}{\partial x_2}(x_1, W) = 0$$

$$g(x) = Ae^{-\frac{B \cdot x}{2}} \sum_{m=0}^{\infty} \sum_{n=0}^{\infty} R(m,n) \sin\left(\frac{m\pi x_1}{L}\right)\left[\sin\left(\frac{n\pi x_2}{W}\right) + \frac{n\pi}{wB_2}\cos\left(\frac{n\pi x_2}{W}\right)\right] \qquad (2\text{–}3\text{–}6)$$

$$A = \frac{32 B_1 B_2{}^3 l^2 W^5 (h_r - h_l)}{\pi^2 (1 - e^{-B_1 L})(1 - e^{-B_2 W})}$$

$$R(m,n) = \frac{\left(1 - e^{-\frac{B_1 L}{2}}\cos(m\pi)\right)\left(1 - e^{-\frac{B_2 W}{2}}\cos(n\pi)\right)}{mn(5B_2{}^2 W^2 + 4n^2\pi^2)(B_1{}^2 L^2 W^2 + B_2{}^2 L^2 W^2 + 4m^2\pi^2 W^2 + 4n^2\pi^2 L^2)}$$

$$B_1 \neq 0$$
$$B_2 \neq 0$$

$$H(x) = g(x) + h_l + \frac{h_r - h_l}{L} x_1 \qquad \textit{when} \quad B_1 \neq 0 \;\; \& \;\; B_2 \neq 0$$

$$H(x) = h_l + \frac{(h_r - h_l)(1 - e^{-B_1 x_1})}{(1 - e^{-B_1 L})} \qquad \textit{when} \quad B_2 = 0 \qquad (2\text{–}3\text{–}7)$$

$$H(x) = h_l + \frac{h_r - h_l}{L} x_1 \qquad \textit{when} \quad B_1 = 0$$

Figure 2–5 shows the mean head distribution for different directions of the trend vector **B** when type B boundary conditions exist. Note that the mean head distribution is not influenced by the trend **B** when the direction of the vector **B** is perpendicular to the mean head gradient, whereas the hydraulic gradient J(**x**) depends on the trend **B** when the trend **B** is not perpendicular to the mean head gradient.

2.4 Non–stationary Correlation Analysis for Log Conductivity and Hydraulic Head

The head covariance $C_{hh}(\mathbf{x}, \mathbf{x}')$ and the log conductivity–head cross–covariance $C_{fh}(x, x')$ are defined as:

$$C_{fh}(\boldsymbol{x},\boldsymbol{x}') = E[f(\boldsymbol{x})h(\boldsymbol{x}')] \qquad (2\text{–}4\text{–}1)$$

$$C_{hh}(\boldsymbol{x},\boldsymbol{x}') = E[h(\boldsymbol{x})h(\boldsymbol{x}')] \qquad (2\text{–}4\text{–}2)$$

where both $f(\mathbf{x})$ and $h(\mathbf{x})$ are zero mean perturbations.

By directly solving the perturbation equation (2–2–8), the relationship between $f(\mathbf{x})$ and $h(\mathbf{x})$ can be found. Then with (2–4–1) and (2–4–2), we can derive the head covariance and log conductivity–head cross–covariance.

When a trend is aligned or vertical to the mean gradient, the mean head and perturbation equations will be simplified. The simple closed solutions can be solved and compared with the results of Li–Mclaughlin [1995] and Gelhar [1993]. Then the general case that the angle between a trend vector **B** and mean gradient **J** is arbitrary will be considered.

2.4.1 The case where the trend is aligned to the mean gradient

Assume that the mean gradient is along the direction of x_1 and no gradient is in x_2 direction. For this case $B_2(x_2) = 0$, then we obtain the mean head equation:

$$\frac{\partial^2 H(\boldsymbol{x})}{\partial x_1} + B_1 \frac{\partial H(\boldsymbol{x})}{\partial x_1} = 0 \qquad (2\text{–}4\text{–}3)$$

Let $\quad J(x_1) = -\dfrac{\partial H(\boldsymbol{x})}{\partial x_1}$

Then $J(x_1)$ can be solved from (2–4–3) as follows

$$J(x_1) = J_0 e^{-B_1 x_1} \qquad (2\text{–}4\text{–}4)$$

where J_0 is the value of $J(x_1)$ at the reference location $\mathbf{x} = 0$.

Substituting (2–4–4) into (2–2–8), the perturbation equation is simplified as:

$$\nabla^2 h(\boldsymbol{x}) + B_1 \frac{\partial h(\boldsymbol{x})}{\partial x_1} = J(x_1) \frac{\partial f(\boldsymbol{x})}{\partial x_1} \qquad (2\text{–}4\text{–}5)$$

Let $g = e^{\frac{B_1 x_1}{2}} h(\boldsymbol{x})$

then equation (2–4–5) is transformed into:

$$\nabla^2 g(\boldsymbol{x}) - \beta^2 g(\boldsymbol{x}) = e^{\beta x_1} J(x_1) \frac{\partial f(\boldsymbol{x})}{\partial x_1} \qquad (2\text{–}4\text{–}6)$$

$$-\infty < x_1, x_2 < \infty$$

Where $\beta = B_1/2$.

The equation (2–4–6) is nothing but the modified Helmholtz equation. It's solution is [Zauderer, 1989]:

$$g(\boldsymbol{x}) = \frac{1}{2\pi} \int_{-\infty}^{\infty} \int_{-\infty}^{\infty} K_0(\beta r) e^{\beta y_1} J(y_1) \frac{\partial f(\mathbf{y})}{\partial y_1} dy_1 dy_2 \qquad (2\text{–}4\text{–}7)$$

$$K_0(\beta r) = \int_0^{\infty} \frac{\varrho J_0(\varrho r)}{\varrho^2 + \beta^2} d\varrho$$

$$r = \sqrt{(x_1 - y_1)^2 + (x_2 - y_2)^2}$$

where K_0 is the modified Bessel function of the second kind.

Finally, the solution for the head perturbation h(**x**) is:

$$h(\boldsymbol{x}) = \frac{e^{-\beta x_1}}{2\pi} \int_{-\infty}^{\infty} \int_{-\infty}^{\infty} K_0(\beta r) e^{\beta y_1} J(y_1) \frac{\partial f(\mathbf{y})}{\partial y_1} dy_1 dy_2 \qquad (2\text{–}4\text{–}8)$$

Substituting the spectral representation of the log conductivity perturbation f(**x**) into (2–4–8), h(**x**) is solved as follows, by some manipulation,

$$h(\boldsymbol{x}) = -\int_{-\infty}^{\infty} \frac{i k_1 J(x_1) e^{i\boldsymbol{k}\cdot\boldsymbol{x}}}{k^2 + i B_1 k_1} dZ_f \qquad (2\text{–}4\text{–}9)$$

This solution is exactly the same as the non–stationary spectral representation of Li–Mclaughlin [1995]. Substituting (2–4–9) into (2–4–1) and (2–4–2), the closed forms of the head covariance $C_{hh}(\mathbf{x}, \mathbf{x}')$ and the log conductivity–head cross–covariance $C_{fh}(\mathbf{x}, \mathbf{x}')$ are:

$$C_{fh}(x,x') = C_{fh}(x,x+s) = \int_{-\infty}^{\infty}\int_{-\infty}^{\infty} \frac{ik_1 J(x'_1)e^{-ik\cdot s}}{k^2 - iB_1k_1} S_{ff}\, dk_1 dk_2 \qquad (2\text{–}4\text{–}10)$$

$$C_{hh}(x,x') = C_{hh}(x,x+s) = \int_{-\infty}^{\infty}\int_{-\infty}^{\infty} \frac{k_1^2 J(x_1)J(x'_1)e^{-ik\cdot s}}{k^4 + B_1^2 k_1^2} S_{ff}\, dk_1 dk_2 \qquad (2\text{–}4\text{–}11)$$

where S_{ff} is the spectral density function of the perturbation f.

Given S_{ff}, the head covariance $C_{hh}(\mathbf{x}, \mathbf{x}')$ and the log conductivity–head cross–covariance $C_{fh}(\mathbf{x}, \mathbf{x}')$ can be solved from (2–4–10) and (2–4–11). The Fast Fourier transform can be used to solve $C_{hh}(\mathbf{x}, \mathbf{x}')$ and $C_{fh}(\mathbf{x}, \mathbf{x}')$. Compared with the numerical integration method used by Li– Mclaughlin [1995], this method is simple and faster.

In order to illustrate the effect of a log conductivity trend, the covariance–spectrum pair of the log conductivity is assumed to be Mizell–A [Mizell et al., 1982] with the spectral density:

$$S_{ff}(k) = \frac{2\sigma_f^2 a^2 k^2}{\pi(k^2 + a^2)^3} \qquad (2\text{–}4\text{–}12)$$

where $a = \pi/4\lambda$ and λ is the integral scale.

Figure 2–6 shows the contours of the log conductivity–head cross–covariance $C_{fh}(\mathbf{x}, \mathbf{x}')$ with and without trend.

In the previous chapter, we indicated that Monte Carlo method can be used to simulate the non–stationary processes. Figure 2–7 shows that the comparison of the log conductivity–head cross–covariance of Monte Carlo simulation with the results of Li–Mclaughlin [1995] and Gelhar [1993]. We see that the solution of Monte Carlo simulation coincides with the result of Li–Mclaughlin; namely, the non–stationary spectral method of Li–Mclaughlin can be used to predict the correlations when the log conductivity trend is aligned to the mean gradient.

2.4.2 The case where the trend is perpendicular to the mean gradient

Assume that the mean gradient is along the direction of x_1 and there is no gradient in

the x_2 direction. For this case $B_1(x_1) = 0$. Then we obtain the mean head equation:

$$\frac{\partial^2 H(x)}{\partial x_1^2} = 0 \qquad (2\text{–}4\text{–}13)$$

Let $J(x_1) = -\frac{\partial H(x)}{\partial x_1}$

Then $J(x_1)$ can be solved from (2–4–13) as follows:

$$J(x_1) = J_0 \qquad (2\text{–}4\text{–}14)$$

where J_0 is the value of $J(x_1)$ at the reference location $\mathbf{x} = 0$.

In this case, the log conductivity trend does not effect on the hydraulic gradient. Substituting (2–4–14) into (2–2–8), we obtain the perturbation equation:

$$\nabla^2 h(x) + B_2 \frac{\partial h(x)}{\partial x_2} = J_0 \frac{\partial f(x)}{x_2} \qquad (2\text{–}4\text{–}15)$$

$$-\infty < x_1, x_2 < \infty$$

Similarly, the equation (2–4–15) can be solved by the same method as the previous case. The solution of $h(\mathbf{x})$ is:

$$h(x) = -\int_{-\infty}^{\infty} \frac{ik_1 J_0 e^{ik\cdot x}}{k^2 - iB_2 k_1} dZ_f \qquad (2\text{–}4\text{–}16)$$

By assuming local stationarity, Gelhar [1993] derived the same form as (2–4–16) by the stationary spectral representations (1–4–6). This coincidence is because the mean head distribution is not be influenced by the perpendicular trend.

The closed forms of the head covariance $C_{hh}(\mathbf{x}, \mathbf{x}')$ and the log conductivity–head cross–covariance $C_{fh}(\mathbf{x}, \mathbf{x}')$ for this case are:

$$C_{fh}(x,x') = C_{fh}(x,x+s) = \int_{-\infty}^{\infty}\int_{-\infty}^{\infty} \frac{ik_1 J_0 e^{-ik\cdot s}}{k^2 - iB_2 k_1} S_{ff}\, dk_1 dk_2 \qquad (2\text{–}4\text{–}17)$$

$$C_{hh}(x,x') = C_{hh}(x,x+s) = \int_{-\infty}^{\infty}\int_{-\infty}^{\infty} \frac{k_1^2 J_0^2 e^{-ix\cdot s}}{k^4 + B_2^2 k_1^2} S_{ff}\, dk_1 dk_2 \qquad (2\text{–}4\text{–}18)$$

Figure 2–8 shows the comparison of the head covariance with and without trend. The head covariance decreases in the both transverse and longitudinal directions and drops more

rapidly when the trend is perpendicular to the mean head gradient.

Figure 2–9 shows the comparison of the log conductivity–head cross–covariances with and without trend. When the trend exists, the cross–covariance is asymmetric in the transverse direction. In the longitudinal direction, the trend cross–covariance decreases when the lag displacement s_1 is positive and increases when the lag displacement s_1 is negative.

In order to confirm the analytical solution for this case, the cross–covariance is estimated by Monte Carlo simulation. Figure 2–10 shows the comparison of the simulated results with the analytical solution. We see that the two solutions are close and consequently in this case the analytical solutions of Gelhar are reasonable.

2.4.3 The general case where the angle between the trend B and the mean gradient is arbitrary

In the most general case, the mean gradient and trend **B** form some arbitrary angle. Practically, it will be more important to develop our correlation analysis for the general case.

As an illustration, we consider the two–dimensional steady flow in the rectangular region with the type A boundary.

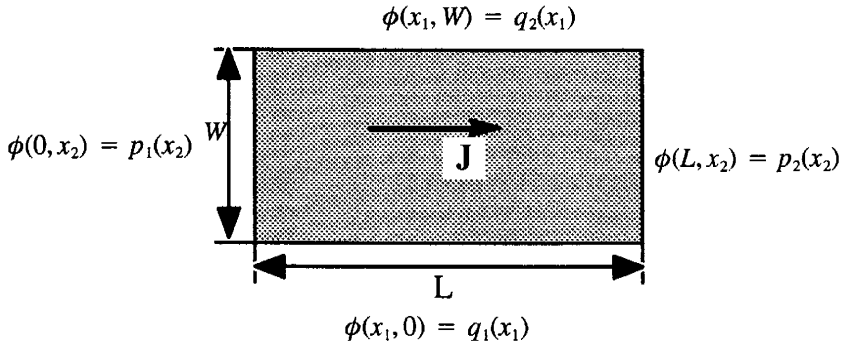

Figure 2–11: Schematic of the flow domain and boundary conditions

The mean head distribution has been solved by the previous section. The Greens function is applied to solve the perturbation equation with the finite boundary conditions:

$$\nabla^2 h(\boldsymbol{x}) + \boldsymbol{B} \cdot \nabla h(\boldsymbol{x})(\boldsymbol{x}) + \nabla H(\boldsymbol{x}) \cdot \nabla f(\boldsymbol{x}) = 0$$
$$h(0,x_2)=0 \qquad (2\text{–}4\text{–}19)$$
$$h(L,x_2)=0$$
$$h(x_1,0)=0$$
$$h(x_1,w)=0$$

Let $u = h \cdot e^{(\boldsymbol{B}\cdot\boldsymbol{x})}$, Then (2–4–19) becomes:

$$\nabla^2 u - \left[\left(\frac{B1}{2}\right)^2 + \left(\frac{B2}{2}\right)^2\right] u = -e^{(\frac{\boldsymbol{B}}{2}\cdot x)}(\nabla H \cdot \nabla f)$$

Let $\phi(x_1, x_2) = -e^{\left(\frac{B_1 x_1 + B_2 x_2}{2}\right)}(\nabla H \cdot \nabla f)$

$$k^2 = \left(\frac{B_1}{2}\right)^2 + \left(\frac{B_2}{2}\right)^2$$

Thus we get the modified Holmholtz Equation:

$$\nabla^2 u(\boldsymbol{x}) - k^2 u(\boldsymbol{x}) = \phi(\boldsymbol{x})$$
$$u(0,x_2)=0 \qquad (2\text{–}4\text{–}20)$$
$$u(L,x_2)=0$$
$$u(x_1,0)=0$$
$$u(x_1,w)=0$$

The corresponding value problem of the equation (2–4–20) on the Greens function contains homogeneous boundary conditions. The adjoint equation is obtained from (2–4–20): [Greenberg, 1971]

$$L^*G = G_{\xi_1\xi_1} + G_{\xi_2\xi_2} - k^2 G = \delta(\xi_1 - x_1,\ \xi_2 - x_2)$$
$$G(\xi_1, 0) = 0$$
$$G(\xi_1, w) = 0 \qquad (2\text{–}4\text{–}21)$$
$$G(0,\ \xi_2) = 0$$
$$G(L,\ \xi_2) = 0$$

According to the principle solution method, we seek the Greens function G in the form:

$$G(\xi_1,\xi_2;x_1,x_2) = U(\xi_1,\xi_2;x_1,x_2) + g(\xi_1,\xi_2;x_1,x_2) \qquad (2\text{–}4\text{–}22)$$

where U is a particular solution of (2–4–21), which need not satisfy the required boundary conditions, and g is a solution of the homogeneous equation L*G = 0, such that the combination U + g does satisfy the boundary conditions.

The solution for U is [Greenberg, 1971]:

$$U = -\frac{1}{2\pi}K_0(kr) \qquad (2\text{–}4\text{–}23)$$

$$r = \sqrt{(\xi_1 - x_1)^2 + (\xi_2 - x_2)^2}$$

From (2–4–22) and (2–4–23), the equation and boundary conditions of g are set up:

$$L^*g = \nabla^2 g(\boldsymbol{x},\xi_1,\xi_2) - k^2 g(\boldsymbol{x},\xi_1,\xi_2) = 0$$

$$g(\xi_1,0) = \frac{1}{2\pi}K_0(kr_1) \qquad (2\text{–}4\text{–}24)$$

$$g(\xi_1,w) = \frac{1}{2\pi}K_0(kr_2)$$

$$g(0,\xi_2) = \frac{1}{2\pi}K_0(kr_3)$$

$$g(L,\xi_2) = \frac{1}{2\pi}K_0(kr_4)$$

$$r_1 = \sqrt{(\xi_1 - x_1)^2 + x_2^2}$$

$$r_2 = \sqrt{(\xi_1 - x_1)^2 + (w - x_2)^2}$$

$$r_3 = \sqrt{x_1^2 + (\xi_2 - x_2)^2}$$

$$r_4 = \sqrt{(L - x_1)^2 + (\xi_2 - x_2)^2}$$

The solution for g is obtained as follows

$$g(\boldsymbol{x},\xi_1,\xi_2) =$$

$$\sum_{n=1}^{\infty}\Big[C_n^{A}Sinh[\lambda_n(w-\xi_2)] + C_n{}^{B}Sinh[\lambda_n\xi_2]\Big]Sin(\frac{n\pi\xi_1}{L}) + \Big[C_n^{C}Sinh[\gamma_n(L-\xi_1)] + C_n{}^{D}Sinh[\gamma_n\xi_1]\Big]Sin(\frac{n\pi\xi_2}{W}) \qquad (2\text{–}4\text{–}25)$$

where

$$\lambda_n = \sqrt{\left(\frac{n\pi}{L}\right)^2 + k^2}$$

$$\gamma_n{}^2 = \sqrt{\left(\frac{n\pi}{W}\right)^2 + k^2}$$

$$C_n^A = \frac{\int_0^L K_0(kr_1)Sin(\frac{n\pi\xi_1}{L})d\xi_1}{L\pi\ Sinh(\lambda_n w)}$$

$$C_n^B = \frac{\int_0^L K_0(kr_2)Sin(\frac{n\pi\xi_1}{L})d\xi_1}{L\pi\ Sinh(\lambda_n w)}$$

$$C_n^C = \frac{\int_0^w K_0(kr_3)Sin(\frac{n\pi\xi_2}{w})d\xi_2}{L\pi\ Sinh(\gamma_n L)}$$

$$C_n^D = \frac{\int_0^w K_0(kr_4)Sin(\frac{n\pi\xi_2}{w})d\xi_2}{L\pi\ Sinh(\gamma_n L)}$$

Then u(**x**) is obtained:

$$u(\boldsymbol{x}) = \int_0^w\int_0^L [U(\xi_1,\xi_2;x_1,x_2) + g(\xi_1,\xi_2;x_1,x_2)]\phi(\xi_1,\xi_2)d\xi_1 d\xi_2 \qquad (2\text{–}4\text{–}26)$$

Thus the solution of the head perturbation h is:

$$h(\boldsymbol{x}) = e^{-\frac{B_1 x_1 + B_2 x_2}{2}} \int_0^w \int_0^L (U + g)\phi d\xi_1 d\xi_2 \qquad (2\text{–}4\text{–}27)$$

We consider the correlation of log conductivity is characterized by Mizell–A [Mizell et al., 1982]. Substituting (2–4–27) into (2–4–1), the analytical solution of the cross–covariance between log conductivity–head is obtained after some manipulation:

$$C_{fh}(\boldsymbol{x}, \boldsymbol{x}') =$$

$$\sigma^2 e^{-\frac{\boldsymbol{B}\cdot\boldsymbol{x}'}{2}} \int_0^w \int_0^L [U(\boldsymbol{x}', \xi_1, \xi_2) + g(\boldsymbol{x}', \xi_1, \xi_2)] \left[-2\alpha^2 K_0(\alpha\xi) + \frac{1}{2}\alpha^2 \xi K_1(\alpha\xi) \right] \left(\frac{\partial H}{\partial \xi_1} \cdot \xi_1 + \frac{\partial H}{\partial \xi_2} \cdot \xi_2 \right) d\xi_1 d\xi_2 \qquad (2\text{–}4\text{–}28)$$

$$\xi^2 = \xi_1^2 + \xi_2^2, \quad \alpha = \frac{\pi}{4\lambda}$$

where λ is the integral scale; K_0 is the zero order modified Bessel function; K_1 is the first order modified Bessel function.

The closed form for the coefficients C_0^A, C_0^B, C_0^C, C_0^D of the equation (2–4–25) is being developed. Up to date, the numerical solution of the cross–covariance from (2–4–8) has not been obtained due to limitation of CPU time. The further work will overcome this obstacle.

In the first chapter, I mentioned that Monte Carlo simulation can be used to approximately estimate the covariances and cross–covariances. Here, we still consider two–dimensional steady state flow. Assume the magnitude of the trend **B** is moderate ($\|\mathbf{B}\|$ =0.3). Monte Carlo simulation is used to analyze the log conductivity–head cross–covariance and head covariance for the different directions of the trend **B**.

Figure 2–12 compares the head covariances for different directions of the trend **B**. The magnitude of **B** (i.e., $\|\mathbf{B}\|$) is 0.30 and θ represents the angle between the trend **B** and mean gradient. The smaller the angle θ, the larger the head covariance. Note that the variation of the trend direction does not change the region of the head correlation. This result indicates that a log conductivity trend **B** produces a increase in head covariance when the component of the trend **B** in the mean gradient direction increases.

Figure 2–13 shows the comparison of the log conductivity– head cross–covariance for different directions of the trend **B**. Conversely, a log conductivity trend results in a decrease in the cross–covariance when the angle θ decreases, namely, the greater the trend component in the mean direction, the smaller the cross–covariance between log conductivity and head.

Both Figure 2–12 and 2–13 indicate that the trend direction is an important factor for head covariance and log conductivity–head cross–covariance. In the presence of a trend, although Gelhar and Li–Mclaughlin derived the simple analytical solutions, their results only can be used in the special cases where the trend is aligned or perpendicular to the mean head gradient. If a log conductivity trend direction is arbitrary, the head covariance and log conductivity–head cross–covariance can be estimated by Monte Carlo simulation and our developing analytical solution.

2.5 Summary

This chapter investigates the stochastic structure of groundwater flow in a heterogeneous porous medium with a trend in log hydraulic conductivity. The analysis of the head covariance and log conductivity–head cross–covariance for the two–dimensional steady state flow with a linear trend is illustrated. In the general case a linear trend is represented by a vector **B**, and in the two–dimensional case the trend parameter $\mathbf{B} = (B_1, B_2)$. By partitioning a flow equation into a mean head flow equation and a perturbation equation, we can use the Greens function or Monte Carlo simulation to estimate the non–stationary head covariance and log conductivity–head cross–covariance for an arbitrary trend vector **B**. For the special cases where a trend is parallel or perpendicular to the mean head gradient (i.e., $B_1=0$ or $B_2=0$), the simplified solutions are derived.

When a linear trend is present, the mean head distribution becomes skewed unless the trend is perpendicular to the mean gradient. The mean head distributions for the two types boundary conditions are analyzed. The results reveal that the trend direction takes an important role to influence the mean head distribution. A decrease in the component of the trend **B** in the direction of the mean gradient **J** leads the mean head distribution more skewed. For the case where the trend is aligned to the mean head gradient, the head perturbation obtained by the Greens function method is exactly the same as the non–stationary spectral representation of Li– Mclaughlin [1995]. The Fast Fourier Transform is used to solve the head covariance and log conductivity–head cross–covariance. This analytical solution of Li–Mclaughlin for the log conductivity–head cross–covariance are tested by Monte Carlo simulation, the two solutions coincide well.

For another special case where the trend is perpendicular to the mean head gradient, our analytical solution for the head perturbation is the same as the form that Gelhar [1993] derived by the stationary spectral method (namely, classical spectral method). This coincidence is because the mean head distribution is not influenced by the perpendicular trend. Our comparison of the analytical solutions for the log conductivity–head cross–covariance with

the results of Monte Carlo simulation indicates that the stationary spectral method can be used to estimate the covariance and cross–covariance when the trend is perpendicular to the mean head gradient.

In the most general case, the mean head gradient and the trend vector form some arbitrary angle. We investigated the consequence for the different trend directions on the head covariance and log conductivity–head cross–covariance by the Greens function method and Monte Carlo simulation. Our results showed that when the component of the trend in the mean head gradient direction increases, the head covariance increases and conversely, the log conductivity–head cross–covariance decreases. Hence in field application, ignoring the influence of the trend direction leads to the erroneous covariance and cross–covariance structures, and this in turn leads to an error on the conditional simulation of groundwater travel time and flow path which is based on the estimation of the correlation structure.

Further work needs to be done in complementing the Greens function method to estimate the non–stationary correlation structures and applying the analytical results to the conditional simulation of a site (e.g., WIPP site). The flow paths and travel time of the contaminant obtained by non–stationary covariance analysis will be compared with the results of the previous conditional simulation which did not consider the influence of the trend in log conductivity.

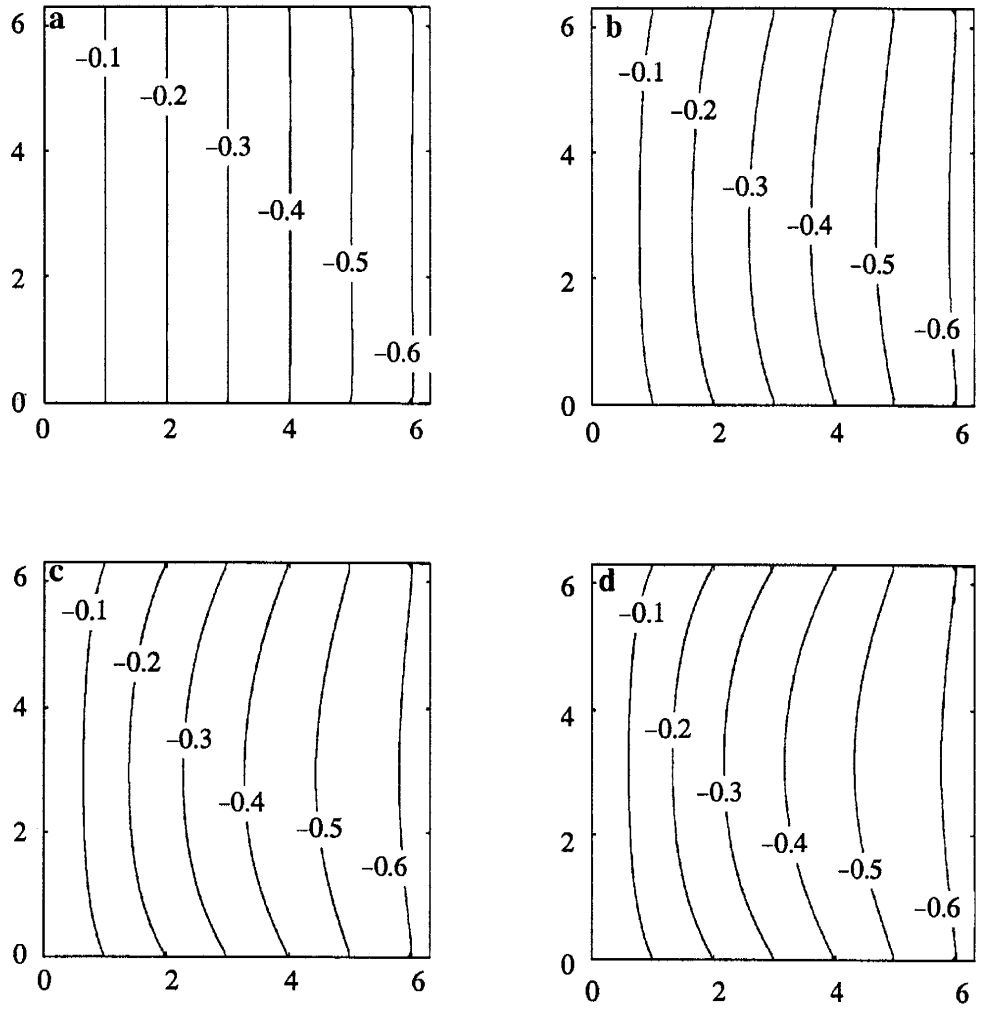

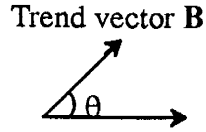

Figure 2-3: The contours of the mean head distributions for type A boundary conditions where θ is the angle between the trend vector **B** and the mean head gradient **J**: a) $\theta = 90^0$; b) $\theta = 60^0$; c) $\theta = 30^0$; d) $\theta = 0^0$.

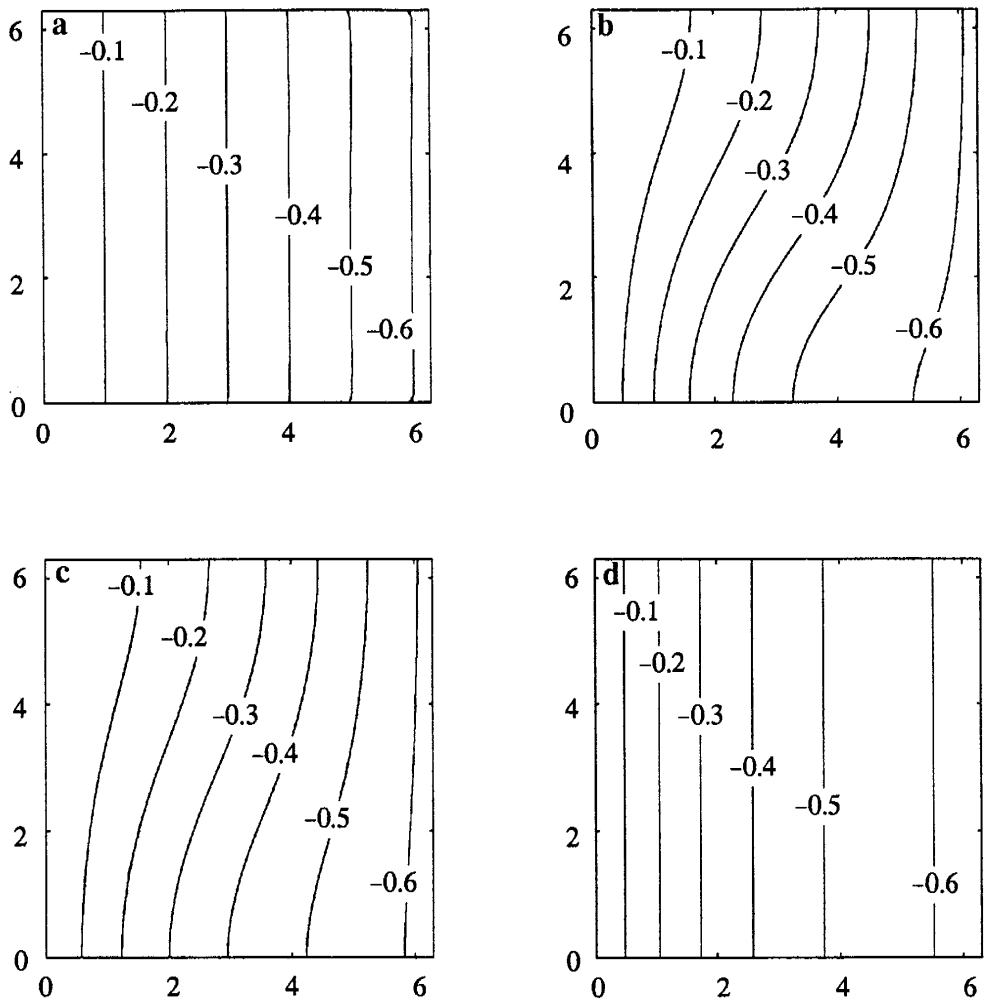

Figure 2-5: The contours of the mean head distributions for type B boundary conditions where θ is the angle between the trend vector **B** and the mean head gradient **J**: a) $\theta = 90^0$; b) $\theta = 60^0$; c) $\theta = 30^0$; d) $\theta = 0^0$.

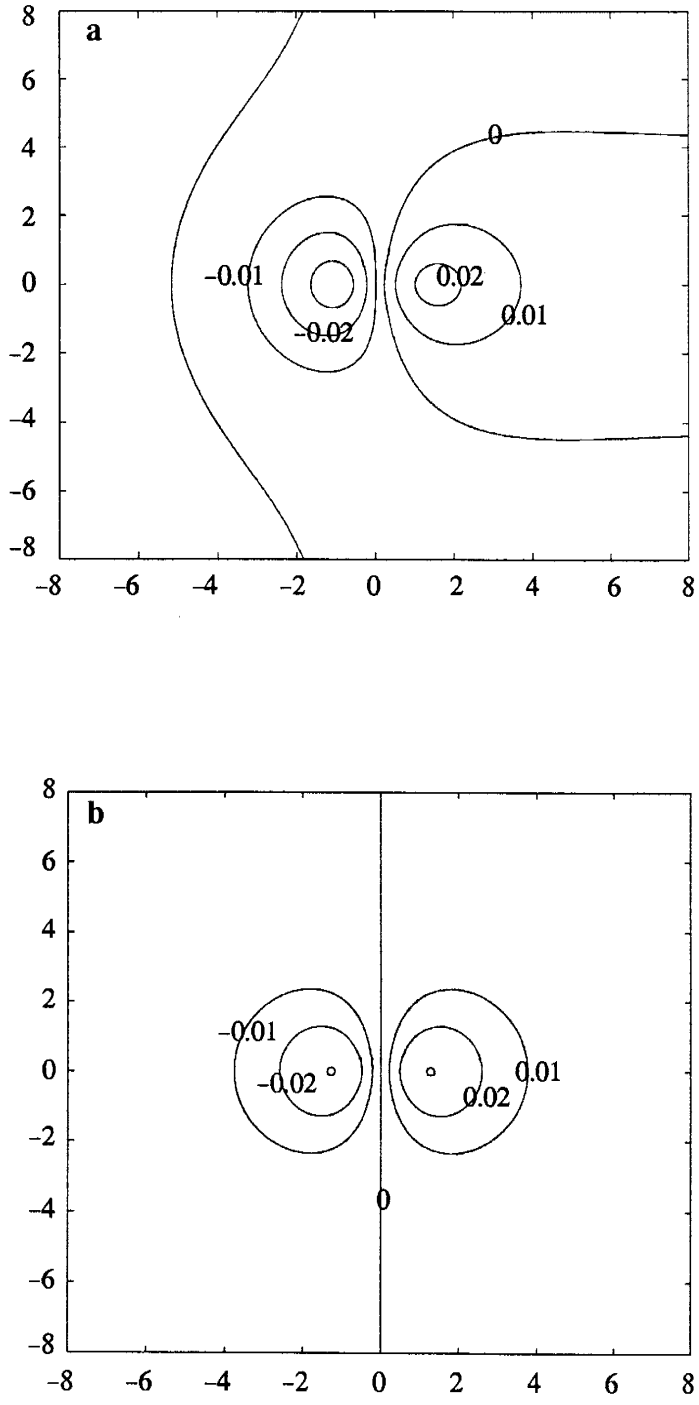

Figure 2-6: The contours of the log conductivity-head cross-covariance: a) with trend where the trend is aligned to the mean head gradient; b) without trend.

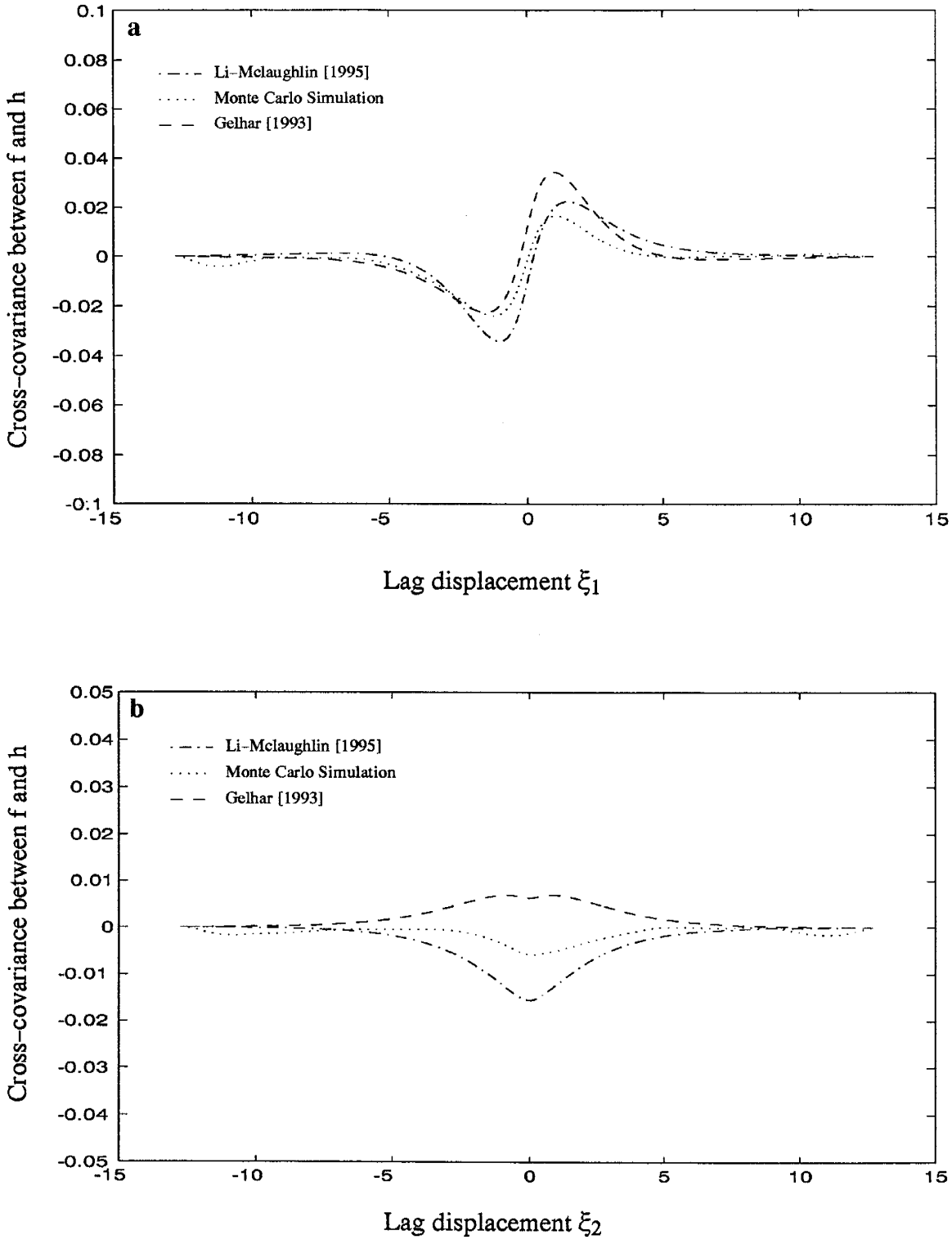

Figure 2-7: Comparison of the solution of Monte Carlo Simulation with the analytical solutions of Li-Mclaughlin [1995] and Gelhar [1993] when the trend vector **B** is aligned to the head gradient: a) in longitudinal direction b) in transverse direction.

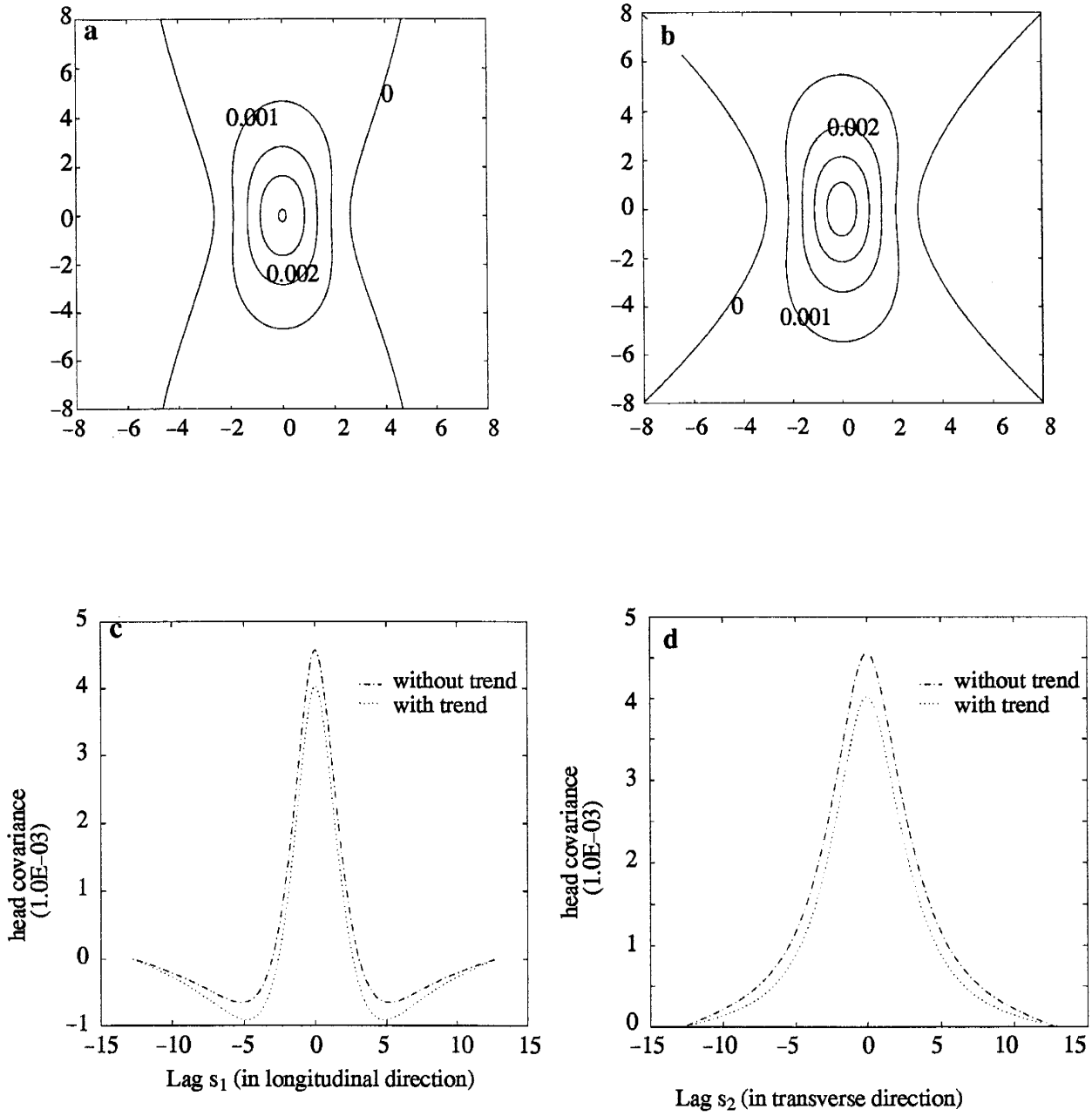

Figure 2-8: The comparison of the head covariance with and without trend: a) the contour of the head covariance with trend where the trend is perpendicular to the mean head gradient; b) the contour of the head covariance without trend; c) the comparison of the head covariance in longitudinal direction; d) the comparison of the head covariance in transverse direction.

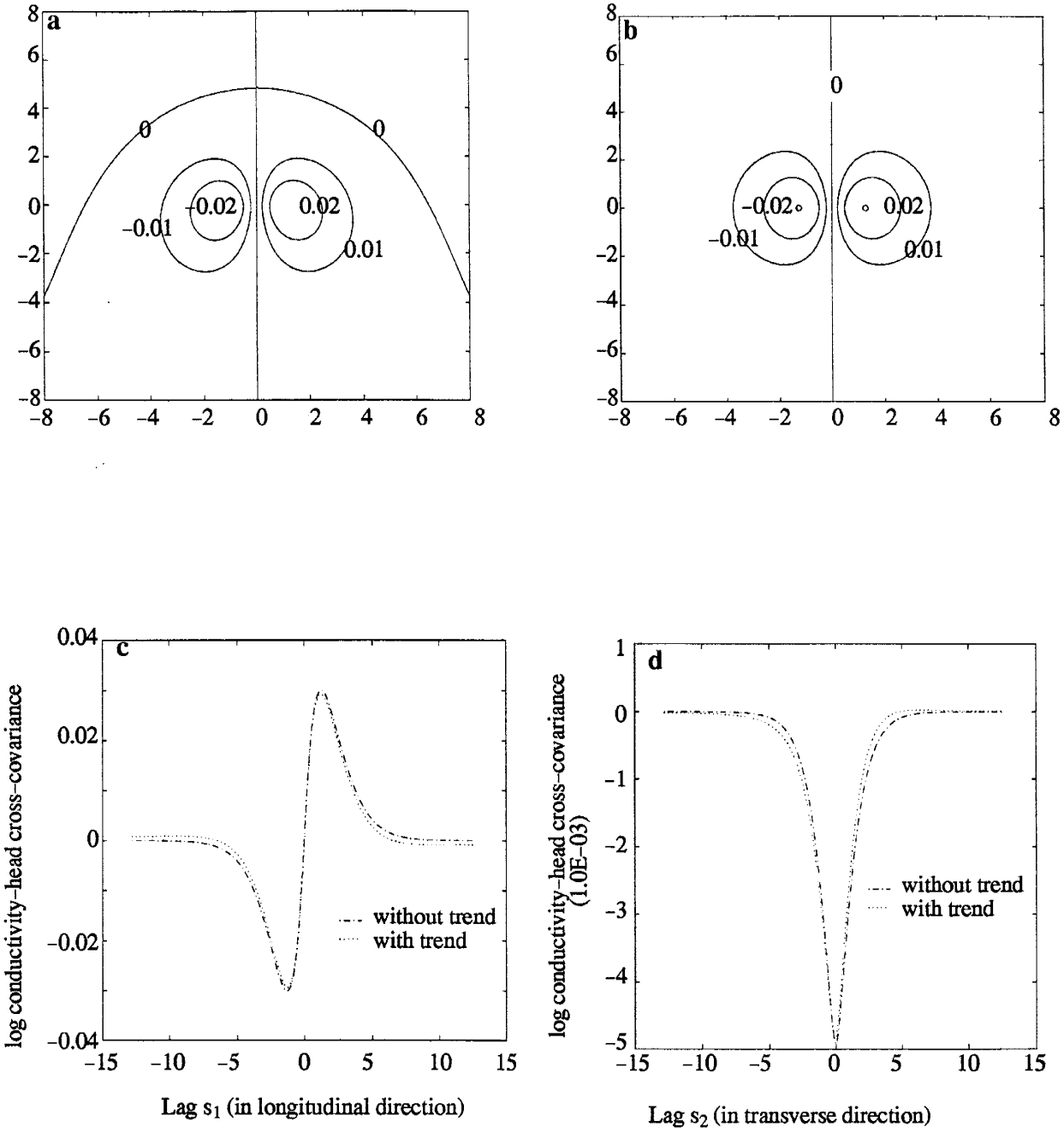

Figure 2-9: The comparison of the log conductivity- head cross-covariance with and without trend: a) the contour of the cross-covariance with trend where the trend is perpendicular to the mean head gradient; b) the contour of the cross-covariance without trend; c) the comparison of the head covariance in longitudinal direction; d) the comparison of the head covariance in transverse direction.

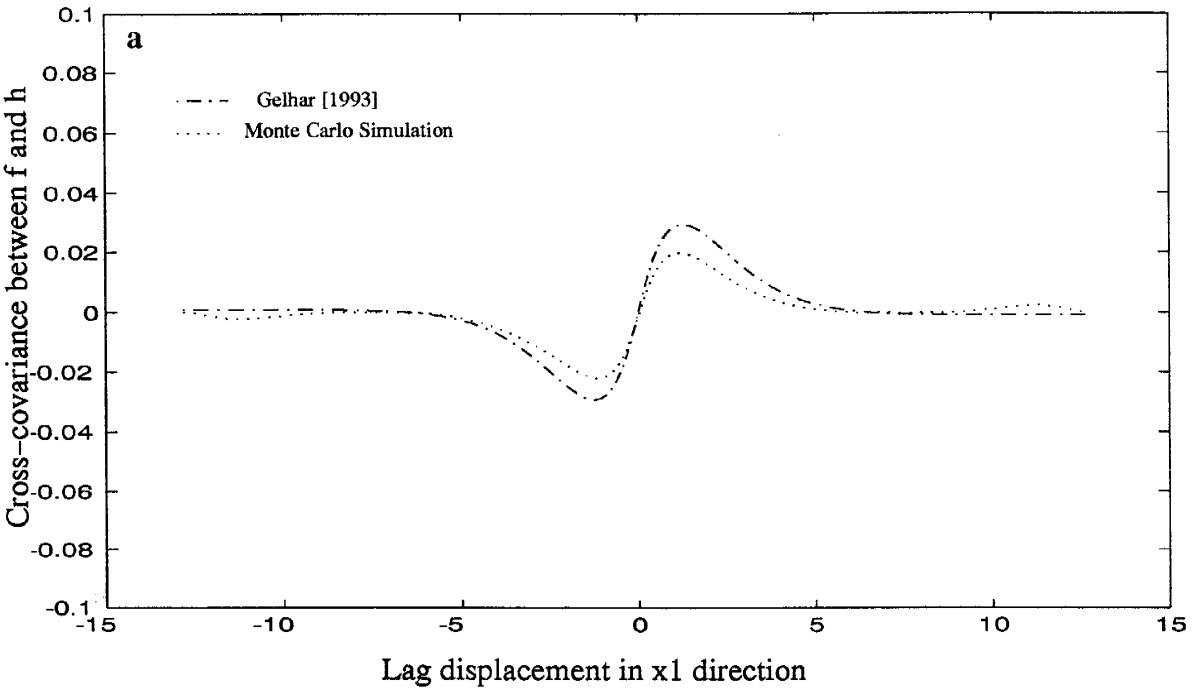

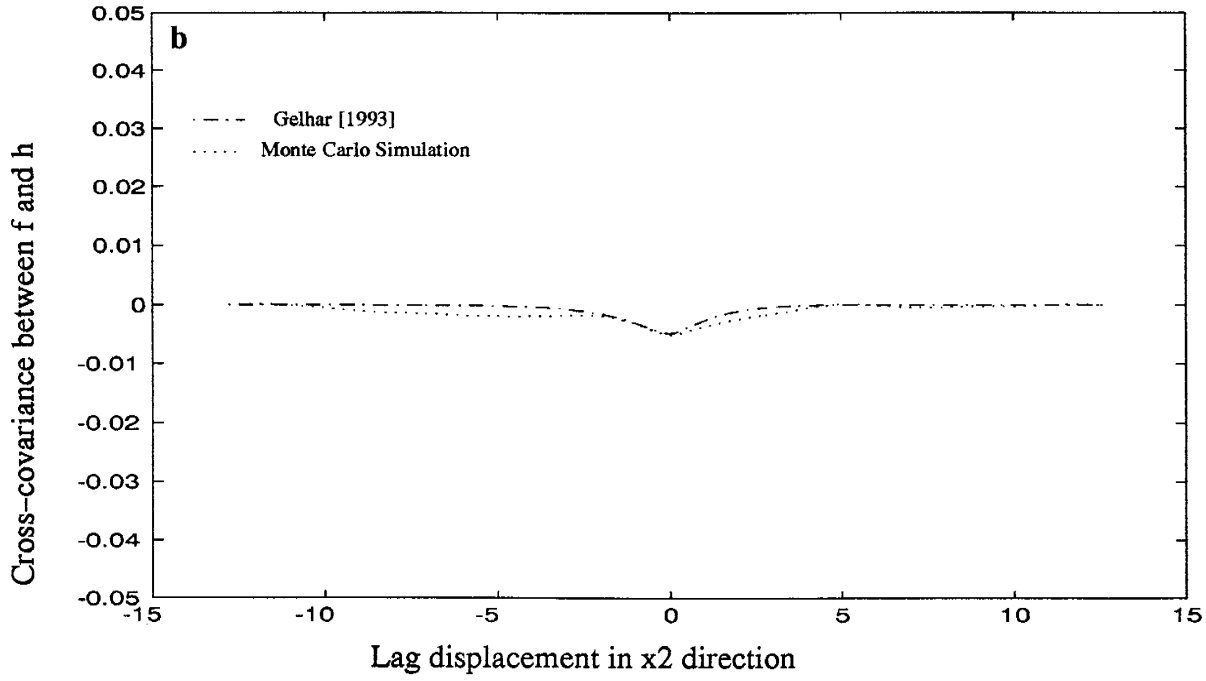

Figure 2-10: Comparison of the solution of Monte Carlo Simulation with the analytical solution of Gelhar [1993] when the trend vector B is perpendicular to the head gradient: a) in longitudinal direction b) in transverse direction.

Monte Carlo Simulation:

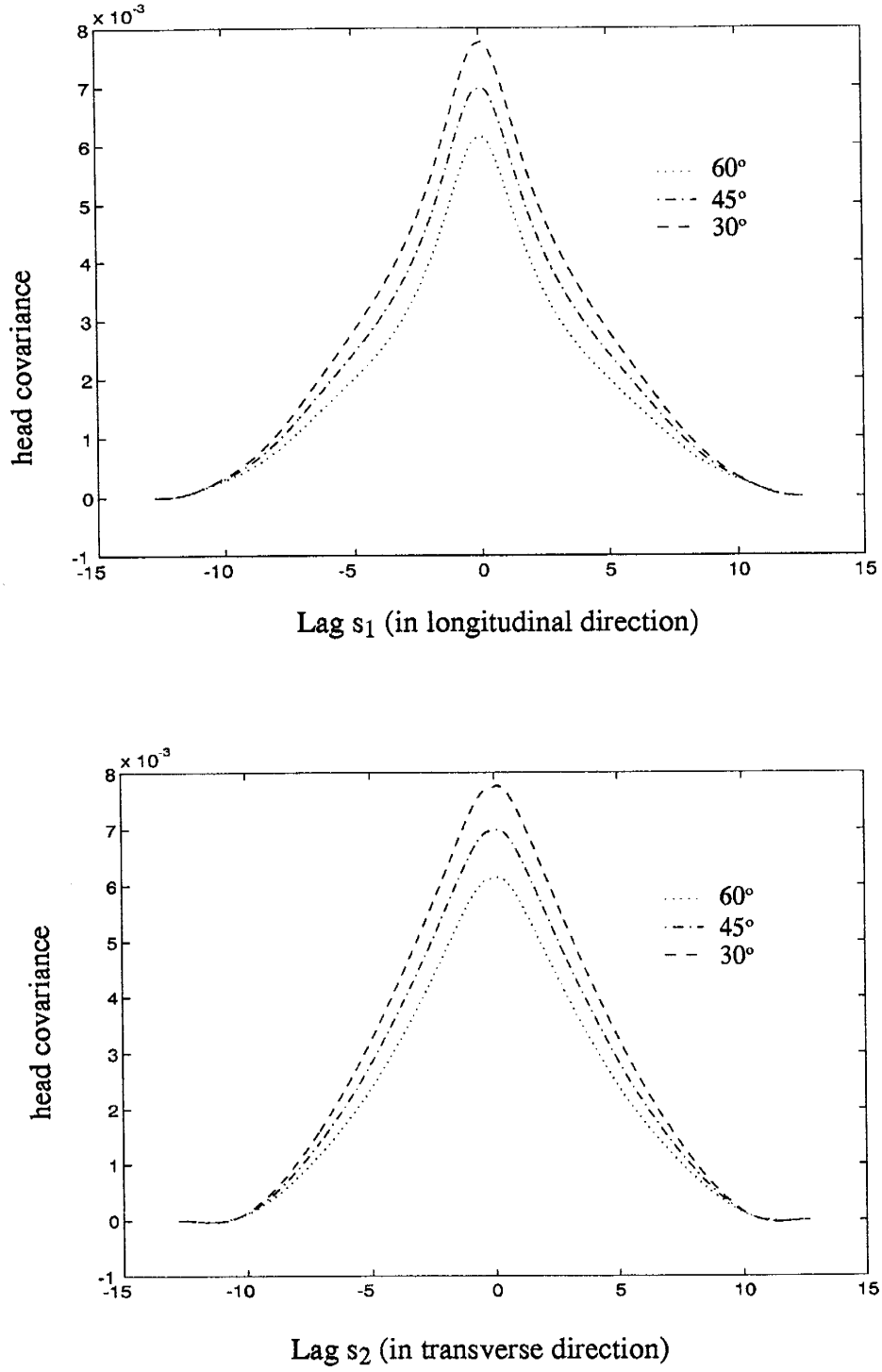

Figure 2-12: The comparison of the head covariances for different θ where θ is the angle between the trend vector **B** and the head gradient **J**: dot line, $\theta = 60^0$; dash dot line, $\theta = 45^0$; dash line, $\theta = 30^0$.

Monte Carlo Simulation:

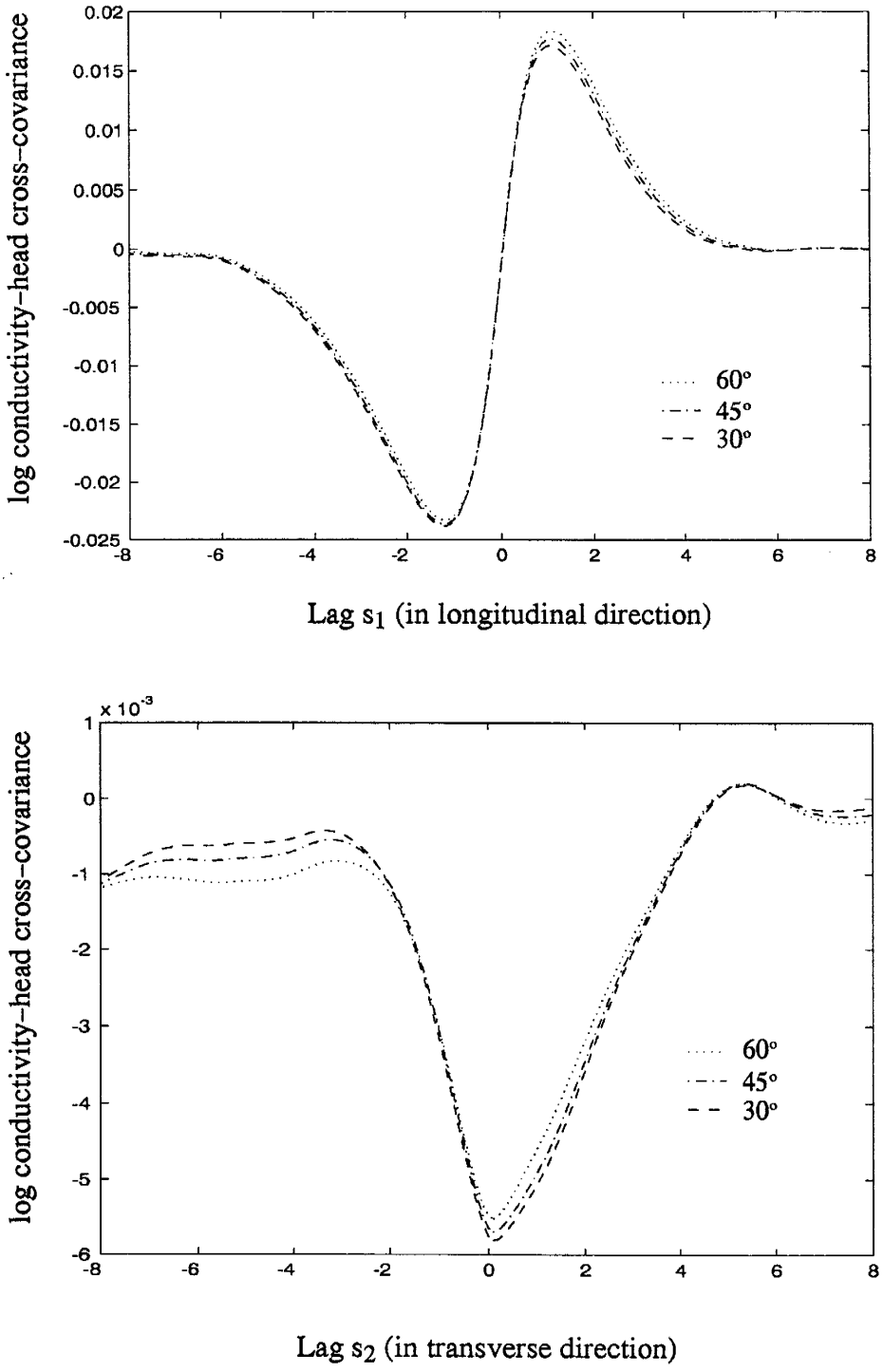

Figure 2-13: The comparison of the log conductivity-head cross-covariances for different θ where θ is the angle between the trend vector **B** and the head gradient **J**: dot line, $\theta = 60^0$; dash dot line, $\theta = 45^0$; dash line, $\theta = 30^0$;

Monte Carlo Simulation:

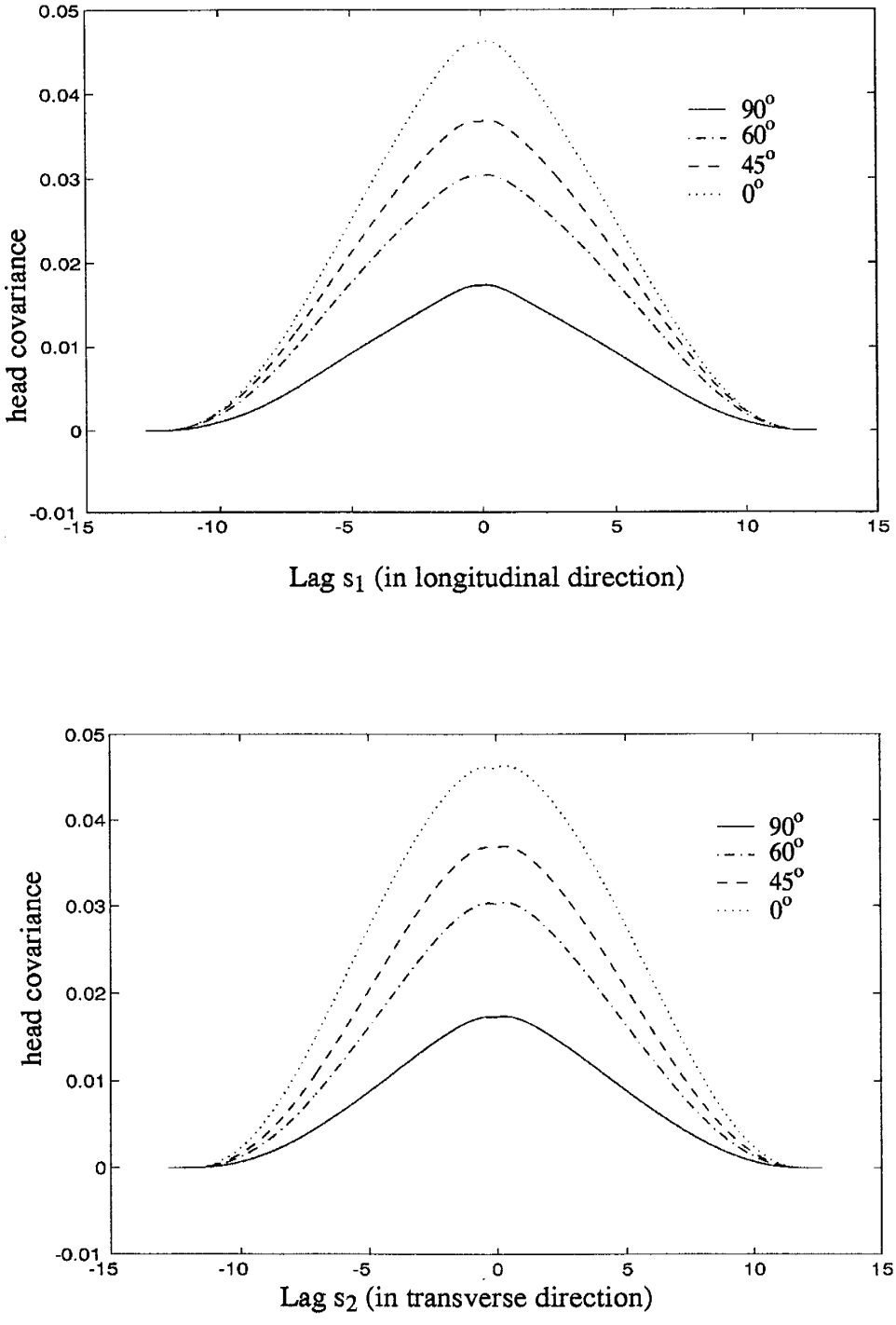

Figure 2-14: The comparison of the head covariances for different θ where θ is the angle between the trend vector **B** (|**B**|=0.5) and the head gradient **J**: solid line, $\theta = 90^0$; dash line, $\theta = 60^0$; dash dot line, $\theta = 45^0$; dot line, $\theta = 0^0$.

Monte Carlo Simulation:

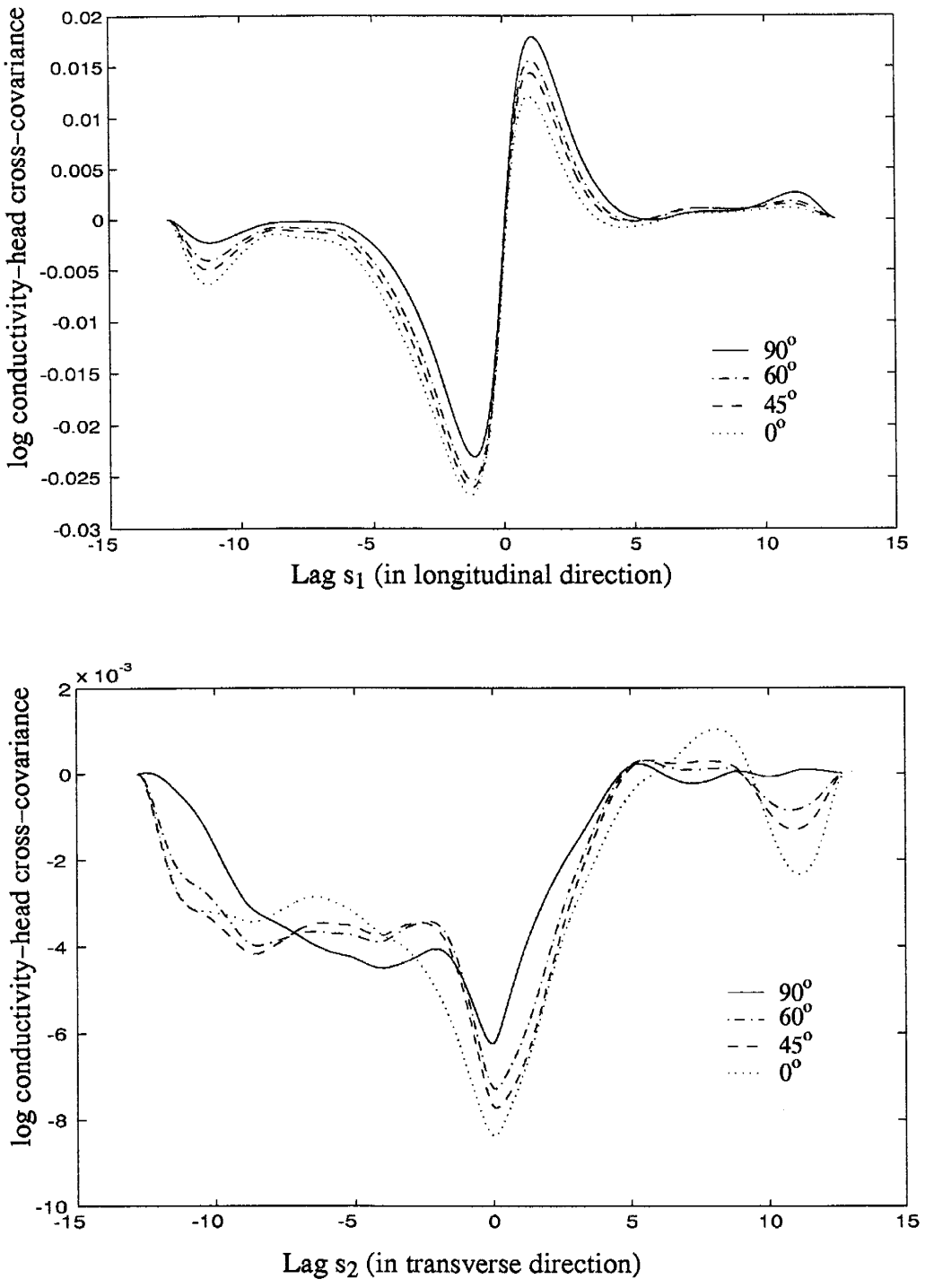

Figure 2-13: The comparison of the log conductivity–head cross–covariances for different θ where θ is the angle between the trend vector **B** (|**B**|=0.5) and the head gradient **J**: solid line, θ = 90^0; dash line, θ = 60^0; dash dot line, θ = 45^0; dot line, θ = 0^0.

Monte Carlo Simulation:

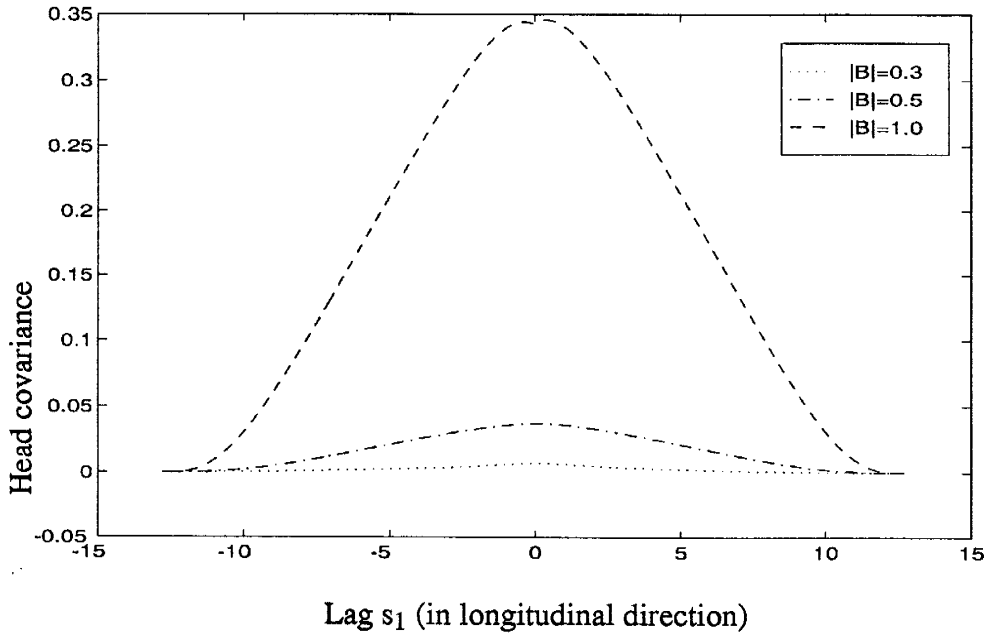

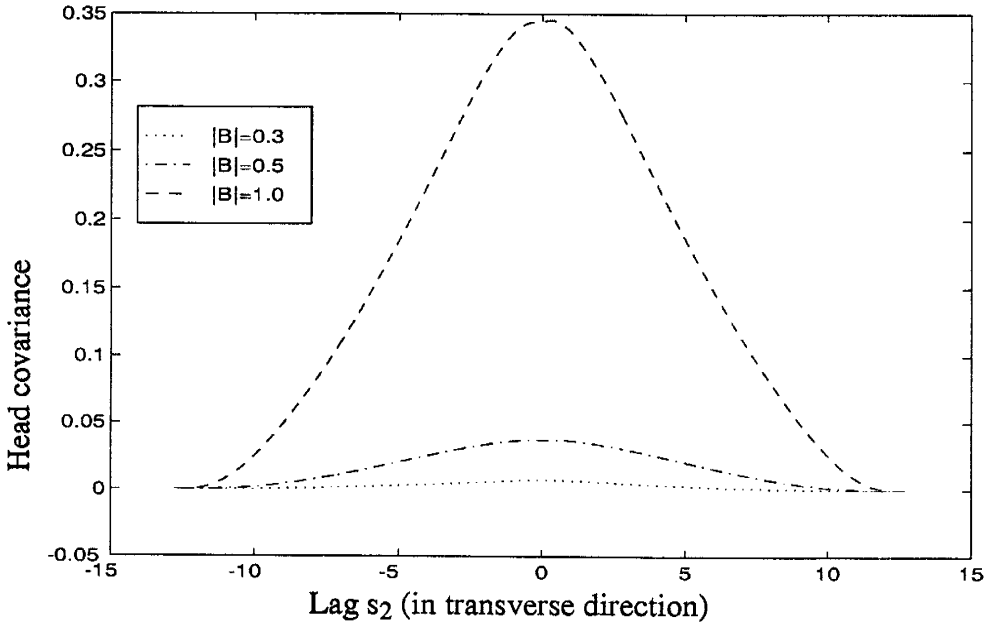

Figure 2-15: The comparison of the head covariances for different value of the trend **B**.

Monte Carlo Simulation:

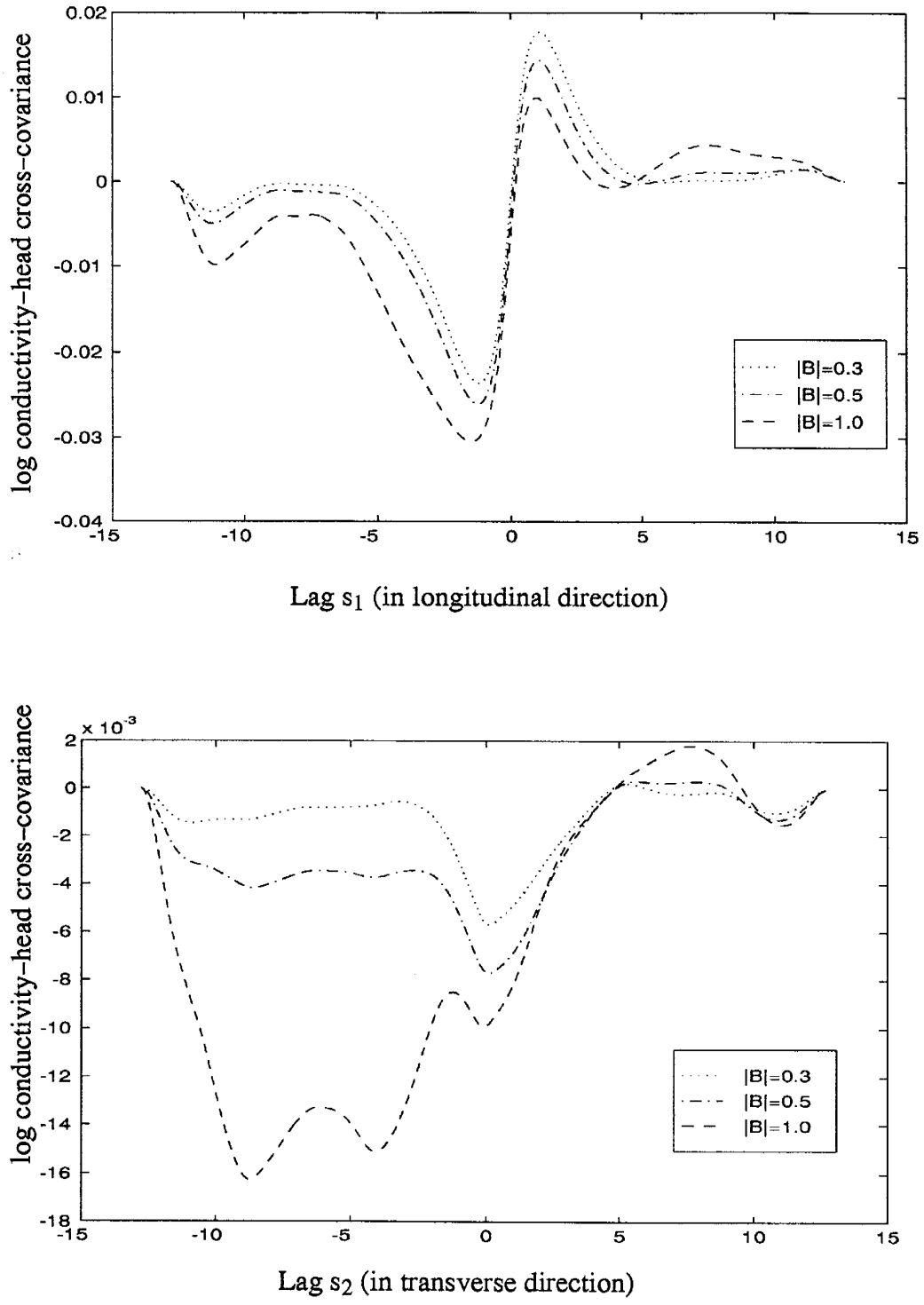

Figure 2–16: The comparison of the log conductivity–head cross–covariances for different value of the trend **B**.

REFERENCE

Bakr, A. A., L. W. Gelhar, A. L. Gutjahr, and J. R. Macmillan, Stochastic analysis of spatial variability subsurface flows, 1. Comparison of one– and three–dimensional flows, *Water Resour. Res.*, 14(2), 263–271, 1978.

Chirlin, G. R., and G. Dagan, Theoretical head variograms for steady flow in satistically homogeneous aquifers, *Water Resour. Res.*, 16(6), 1001–1015, 1980.

Clifton, P. M., and Newuman, S. P., Effects of kriging and inverse modeling on conditional simulation of the Avra Valley aquifer in southern Arizona, *Water Resour. Res.*, 18(4), 1215–1234, 1982.

Harder, T., and T. C. Jim Yeh, An efficient method for simulating steady unsaturated flow in random porous media: Using an analytical perturbation solution as initial guess to a numerical model, *Water Resour. Res.*, 29(12), 4139–4149, 1993.

Dagan, G., Models of groundwater flow in statistically homogeneous porous formations, *Water Resour. Res.*, 15(1), 47–63, 1979.

Dagan, G., Analysis of flow through heterogeneous random aquifers by the method of embedding matrix, 1, Steady state flow, *Water Resour. Res.*, 17(1), 107–121, 1981.

Dagan, G., Stochastic modeling of groundwater flow by unconditional and conditional probabilities, 1, conditional simulation and the direct problem, *Water Resour. Res.* 18 (4), 813–834, 1982.

Dagan, G., Statistical theory of groundwater flow and transport: Pore to laboratory, laboratory to formation and formation to regional scale:, *Water Resour. Res.* 22(9), 120–134, 1986.

Dagan, G., Theory of solute transport by groundwater, *Ann, Rev. Fluid Mech.*, 19, 183–215, 1987.

Dikow, C., Stochastic analysis of groundwater flow in a bounded domain by spectral methods, *Transp. Porous Media,* 3, 173–184, 1988.

Freeze, R. A., and J. A. Cherry, Groundwater, Prentice–Hall, Englewood Cliffs, N. J., 1993.

Freeze, R. A., A stochastic–conceptual Analysis of one–dimensional groundwater flow in nonuniform homogeneous media, *Water Resour. Res.* 11(5), 725–741, 1975.

Gelhar, L. G., *Stochastic Groundwater Hydrology*, Prentice–Hall Englewood Cliffs, N. J., 1993.

Gelhar, L. G., Stochastic subsurface hydrology from theory to applications, *Water Resour. Res.* 22(9), 135S–145S, 1986.

Gelhar, L. W., and C. L. Axness, Three–dimensional stochastic analysis of macrodispersion in a stratified aquifer, *Water Resour. Res.*, 19(1), 161–180, 1983.

Gelhar, L. W., Stochastic analysis of phreatic aquifers, *Water Resour. Res.*, 10(3), 539–545, 1974.

Gradshtein, I. S., and Ryzhik, I. M., *Table of integrals, series, and products*, New York, Academic Press, 1980.

Graham, W., and D. Mclaughlin, Stochastic analysis of non–stationary subsurface solute transport, 1, Unconditional moments, Water Resour. Res., 25(2), 215–232, 1989a.

Graham, W., and D. Mclaughlin, Stochastic analysis of non–stationary subsurface solute transport, 2, Conditional moments, Water Resour. Res., 25(10), 215–232, 1989b.

Graham, W., and D. Mclaughlin, Stochastic analysis of non–stationary subsurface solute transport, 2, Conditional moments, 25(11), 2331–2355, 1989.

Gutjahr, A. L., B., Bullard, S., Hatch, and L., Hughson, Joint conditional simulations and the spectral approach for flow modeling, *Stochastic Hydrology and hydraulics*, March, 1994.

Gutjahr, A. L., S. Hatch, B., Bullard, and L., Hughson, Conditional simulations and contaminant flow modeling: Effects of linearization, Technical Completion Report WERC 91–08, NMIMT, 1993.

Gutjahr, A., L., Q., Bai and S.,Hatch, Conditional simulation applied to contaminant flow modeling, Technical Conpletion Report WERC 91–38, NMIMT, 1992.

Gutjahr, A. L., Fast Fourier transform for random field generation, Project Report for Los Alamos Grant to the New Mexico Institute of Mining and Technology, Contract No. 4–58–2690R, 1989.

Gutjahr, A. L., and L. W. Gelhar, Stochastic models of subsurface flow: Infinite versus finite domain and stationarity, *Water Resour. Res.*, 17(2), 337–350, 1981.

Gutjahr, A. L., L. W. Gelhar, A. A. Bakr, and J. R. Macmillan, Stochastic analysis of spatial variability in subsurface flows, 2, Evaluation and applications, *Water Resour. Res.*, 14(5), 953–959, 1978.

Kitanidis, P. K., and R. W. Lane, Maximum likelihood parameter estimation of hydrologic spatial processes by the Gauss–Newton method, *J. Hydrol.*, 79, 53–71, 1985.

Li, S. G., and D. Mclaughlin, A nonstationary spectral method for solving stochastic groundwater problems: Unconditional analysis, *Water Resour. Res.*, 27(7), 1589–1605, 1991.

Li, S. G., and D. Mclaughlin, Using the nonstationary spectral method to analyze flow through heterogeneous trending media, *Water Resour. Res.*, 31(3), 541–552, 1995.

Loaiciga, H. A., R. B. Leipnik, M. A. Marino, and P. F. Hudak, Stochastic groundwater flow analysis in the presence of trends in heterogeneous hydraulic conductivity fields, *Math. Geol.*, 2592), 161–176, 1993.

Mizell, S. A., A. L. Gutjahr, and L. W. Gelhar, Stochastic analysis of spatial variability in two–dimensional steady groundwater flow assuming stationary and non–stationary heads, *Water Resour. Res.* 18(4), 1053–1067, 1982.

Priestley, M. B., *Multivariate Series, Prediction and Control, Part B, Vol. 2, Spectral Analysis and Time Series*, Academic, San Diego, Calif., 1981.

Rajaram, H., and D. Mclaughlin, Identification of large–scale spatial trends in hydrologic data, *Water, Resour., Res.*, 26(10), 2411–2423, 1990.

Rehfeldt, K. R., J. M. Boggs, and L. W. gelhar, field study of dispersion in a heterogeneous aquifer, 3, Geostatistical analysis of hydraulic conductivity, *Water, Resour., Res.*, 28(12), 3325–3336, 1992.

Robin, M. J. L., Gutjahr, A. L., Sudicky, E. A., and J. L. Wilson, Cross–correlated random field generation with the direct Fourier transform method, *Water, Resour., Res.*, 29(7), 2385–2397, 1993.

Rubin, Y., and K. Seong, Investigation of flow and transport in certain cases of nonstationary conductivity fields, *Water, Resour., Res.*, 30(11), 2901–2911, 1994.

Rubin, Y., and G. Dagan, A note on head and velocity covariances in three–dimensional flow through heterogeneous anisotropic porous media, *Water Resour. Res.*, 28(5), 1463–1470, 1992.

Rubin, Y., and J. J. Gomez–Hernandez, A stochastic approach to the problem of upscaling of conductivity in disordered media: Theory and unconditional numerical simulations, *Water Resour. Res.*,

26 (4), 691–701, 1990.

Rubin, Y., Stochastic modeling of macrodispersion in heterogeneous porous media, *Water Resour. Res.*, 26 (1), 133–141, 1990.

Rubin, Y., and Dagan, Stochastic modeling of boundary effects on head spatial variability in heterogeneous aquifers, 2, Impervious boundary, *Water Resour. Res.*, 25, 707–712, 1989.

Sagar, B., Solution of linearized Boussinesq equation with stochastic boundaries and recharge, *Water Resour. Res.*, 15(3), 618–624, 1979.

Smith, L. and R. A. Freeze, Stochastic analysis of steady state groundwater flow in a bounded domain, 1, One–dimensional simulations, *Water Resour. Res.*, 15(3) 521–528, 1979a.

Smith, L. and R. A. Freeze, Stochastic analysis of steady state groundwater flow in a bounded domain, 2, Two–dimensional simulations, *Water Resour. Res.*, 15(6) 1543–1559, 1979b.

Woodbury, A.D., and E. A. Sudick, The geostatistical characteristics of the Borden aquifer, *Water Resour. Res.*, 27(4), 533–546, 1991.

Zauderer Erich, *Partial differential Equations of applied Mathematics*, Wiely, New York, 1989.